Update of the GMD3 Groundwater Flow Model
High Plains Aquifer Modeling Maintenance Project

Funded by the

Kansas Water Office (Contract 22-111)

and

Southwest Kansas Groundwater Management District No. 3

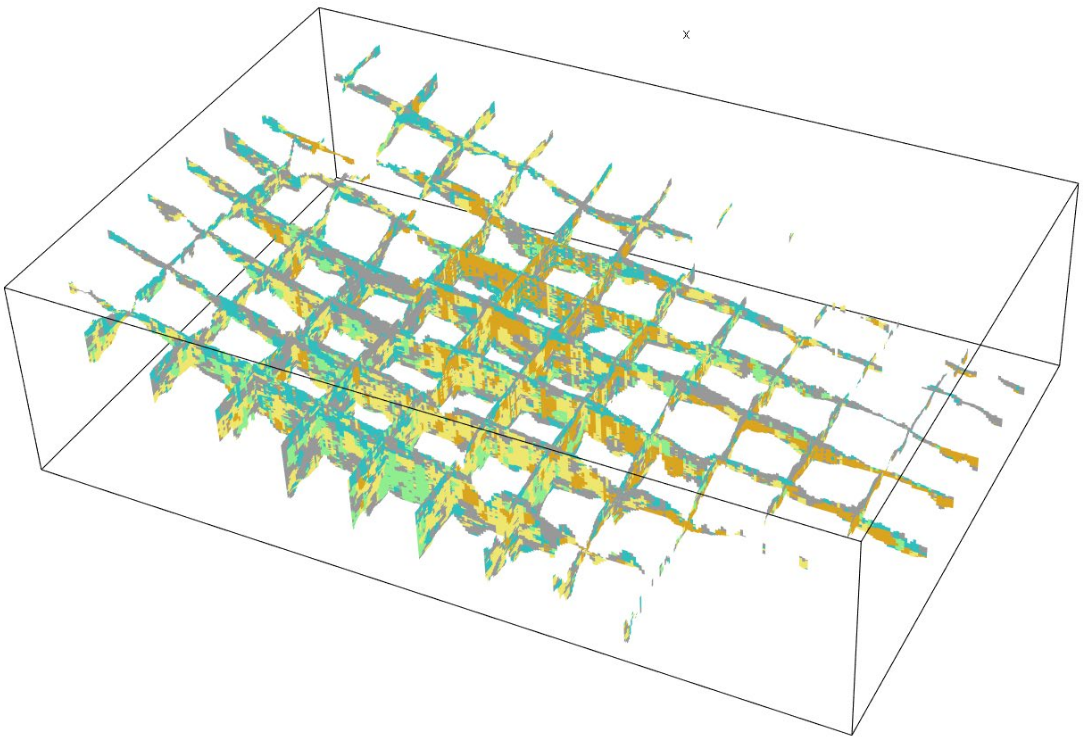

B. B. Wilson, G. Liu, G. C. Bohling, and J. J. Butler, Jr.

Kansas Geological Survey Open-File Report 2024-14

GEOHYDROLOGY

KANSAS GEOLOGICAL SURVEY
The University of Kansas

Update of the GMD3 Groundwater Flow Model
High Plains Aquifer Modeling Maintenance Project

This project was funded by the

Kansas Water Office (Contract 22-111)
and
Southwest Kansas Groundwater Management District No. 3

Kansas Geological Survey Open-File Report 2024-14

Kansas Geological Survey, Geohydrology Section
University of Kansas, 1930 Constant Avenue,
Lawrence, KS 66047
http://www.kgs.ku.edu/

TABLE OF CONTENTS

INTRODUCTION

Southwest Kansas Groundwater Management District No. 3 (GMD3) was formally established on February 24, 1976, and is the third of five districts in Kansas authorized under the Groundwater Management District Act of 1972. The district was organized for the management and conservation of groundwater, to provide local input into the use and management of the aquifer, to garner social and economic benefits from the use of water, and to support research and educational efforts while working with federal, state, and local units of governments. It is one of the largest governing units of its kind in the country, overlying all or parts of 12 counties in southwest Kansas.

Historically and today, southwest Kansas has some of the largest and most diverse groundwater resources in the state, ranging from shallow alluvial systems to the extensive Ogallala portion of the High Plains aquifer (HPA) to the underlying and less understood Dakota aquifer system. The combination of being in the driest region of the state along with the ready availability of groundwater has led to varying stages of declining water levels.

The Kansas Water Office (KWO) and GMD3 contracted with the Kansas Geological Survey (KGS) in the fall of 2021 to update the numerical groundwater model first developed by the KGS for GMD3 in 2008 (Liu et al., 2010). The primary objective of the project is to better understand aquifer conditions in the district and simulate future water use and management scenarios. The project funding period was October 2021 through the winter of 2023. As the model was being developed, the KGS provided progress reports at several GMD3 board meetings.

DESCRIPTION OF STUDY AREA AND GENERAL MODEL SETUP

The study area includes GMD3 in southwest Kansas and extends beyond the district boundaries 6 to 7 miles in all directions (fig. 1). The model domain extends into Colorado and Oklahoma to reduce the impacts of those boundaries on model results in the district. The total area covered by the model is 161,500 square miles. Groundwater-based irrigation represents the largest use of water (about 96%), although groundwater is also the source of supply for municipal, stockwater, industrial, recreational, and domestic uses. The district also encompasses an extensive canal network where surface water is diverted from the Arkansas River for irrigation, primarily in Finney and Kearny counties. GMD3 is divided into two regional advisory committees (RAC) for the Kansas Water Office with the Upper Arkansas RAC to the north and the Cimarron RAC to the south.

Previous Geohydrologic Studies

Several 1940s vintage KGS bulletins report on the geology and groundwater resources of the model area, including Byrne and Mclaughlin (1948) (Seward County), Frye (1942) (Meade County), Latta (1941, 1944) (Stanton, Finney, and Gray counties), Waite (Ford County), and McLaughlin (1942, 1943, and 1946) (Morton, Hamilton, Kearny, Grant, Haskell, and Stevens counties). In addition to characterizing the groundwater conditions in the region at that time, these bulletins provide well records and lithologic logs that have been used to construct and calibrate the model.

More recently, the KGS has conducted a series of studies of the HPA involving GMD3. Whittemore et al. (2016 and 2023) used regional correlations between climatic indices, water-level change, and pumping in each GMD to assess water conservation efforts across western Kansas. Whittemore et al. (2014) reported on the water resources of the Dakota aquifer quantifying the pumping from that system along with mapping the extent and concentrations of various constituents in the groundwater.

Butler et al. (2016 and 2018) applied a data-driven, water-balance approach, which used annual water-level measurements and reported groundwater usage to determine what average level of usage is needed to stabilize water levels in the near term. Liu et al. (2021) combined the water-balance analysis with lithologic logs and developed a new approach for estimating specific yield for use in groundwater models. The methodologies outlined in these publications have been incorporated into the GMD3 model. Wilson et al. (2023) worked with staff from GMD3 and the Finney County Economic Development group to provide customized reports to irrigators in GMD3 comparing their usage to similar wells in their area. The reports also provided information about aquifer conditions and the estimated pumping reductions needed to stabilize water levels.

This GMD3 modeling project is part of the KGS long-term aquifer modeling maintenance program. Since the late 2000s, the KGS has developed groundwater models for the HPA in GMD1 through GMD4 (Liu et al., 2010; Wilson et al., 2015, 2021), as well as the alluvial aquifer below Kannapolis reservoir in the Smoky Hill river valley (Wilson et al., 2008). Although these models were considered to be of the highest quality at the time of construction, they need to be updated periodically as new data on water levels and uses and improved understandings of aquifer properties become available. For example, Whittemore et al. (2023) found the net inflow to the HPA was significantly higher than the estimated precipitation recharge rate in many areas of the aquifer. Butler et al. (2020) and Liu et al. (2021) showed the specific yield values used in many of the previous HPA models were overestimated, leading to inaccurate predictions of aquifer responses to pumping reductions in various conservation efforts.

Physiographic Setting

The vast majority of the active area of the model lies within the High Plains physiographic region intersected by the Arkansas River Lowlands. Much of the High Plains region is characterized by flat to gently rolling, eastward sloping uplands broken by relatively shallow valleys. Shallow depressions/playas are common features. The Arkansas River Lowlands region is a relatively flat, alluvial landscape formed by the river. The northeastern and southeastern portions of the model domain are within the Smoky Hill and Red Hills physiographic regions, respectively, but are outside the district boundaries and largely not incorporated within the active portion of the model.

A land cover classification map was compiled for the area using data from the Kansas Biological Survey (Peterson, 2018) and in Colorado and Nebraska from the U.S. Geological Survey (Homer et al., 2012); this map shows that cropland is the primary land-cover type within the district (fig. 2). Grasslands are typically more prevalent along stream courses and in the Smoky and Red Hills regions, both outside of GMD3. Municipal footprints (and water usage) across the model area are relatively small, with only the county seats, such as Garden City, Dodge City, and Liberal, being visible.

Model Design

This project used MODFLOW, the modeling software developed by the USGS that is based on a finite-difference approximation of the flow equation (Harbaugh et al., 2000). MODFLOW is one of the most widely used groundwater flow models in the world and can be used to simulate the effects of many processes, such as areal recharge, stream-aquifer interactions, drains, evapotranspiration, and pumping. Input files for the MODFLOW model were created with assistance from scripts written in Fortran (https://www.fortran.com/). The model was run by entering the executable file name in a Windows command prompt.

The updated GMD3 model uses the same areal extent as the previous version but with a finer grid composed of uniform and equally spaced square cells, 0.5 x 0.5 miles in size (0.25 mi^2). It contains 200 rows and 300 columns, resulting in 60,000 individual grid cells (fig. 3). The grid maintains its alignment with model cells used in the MODFLOW-based groundwater flow model for GMD1 in west-central Kansas, developed by the KGS (Wilson et al., 2015). The updated GMD3 model divides the model cells into two layers — one for the HPA and a second for the underlying Dakota system. The Dakota model layer is active only where it is unconfined and in direct contact with the HPA.

The streamflow-routing package (SFR in MODFLOW; Prudic et al., 2004) was used to compute stream-aquifer interactions by subdividing streams into a series of segments and reaches. Streams cells were set up for the Arkansas River, Cimarron River, and Crooked Creek.

Time-varying specified-head boundaries are located along the edges of the model where the HPA is present. The head values for these boundaries are determined by a spatial and temporal interpolation of the water-level observations from nearby wells, with some adjustment from model-simulated water-level changes during preliminary model runs. Remaining boundary edges are set to no-flow cells, which prevent flow between active and inactive areas of the model.

The lower vertical boundary of the model is Cretaceous-aged bedrock (mainly shale) for the HPA and the bottom of the Dakota aquifer system where present. These layers have much lower permeability than the aquifer and are thus treated as no-flow boundaries. The upper boundary of the model is the land surface, where water may enter or leave the aquifer through areal recharge, evapotranspiration, and stream-aquifer interactions. Land surface elevations in Kansas are based on bare-earth LiDAR digital elevation models provided by the KGS Data Access and Support Center (DASC); those for Colorado and Oklahoma are based on the USGS National Elevation Dataset.

The modeling work was divided into two main steps. First, we generated a steady-state simulation for the predevelopment period before 1945. Data used for the predevelopment simulation were typically from 1940 to 1950, before large-scale, intensive pumping activities began. Second, we conducted a transient simulation for the period between 1945 and 2021 to replicate the historic evolution of the groundwater system under intensifying pumping. The predevelopment step established the initial conditions for the subsequent transient simulation.

The model takes advantage of detailed information from the KGS HyDRA program (Bohling, 2016), for which the lithologic descriptions from thousands of drillers' logs have been digitally transcribed and categorized into common groups. The lithologic groupings were then spatially interpolated to develop three-dimensional grids of lithologic categories. Next, based on representative hydraulic conductivity (K) and specific yield (Sy) values assigned to each lithologic category, K and Sy for each model cell are computed based on where the water levels intersect the lithologic grid at a specific time. For each lithologic category, K is a calibrated parameter whose value is determined by model calibration, whereas Sy is determined from a water-balance analysis of annual water levels and pumping (Butler et al., 2016, 2018; Liu et al., 2021). Determining Sy using the water-balance analysis approach allows aquifer recharge rates to be estimated much more accurately during model calibration. The GMD3 model domain encompasses 25,500 logs from Kansas, 2,000 from Oklahoma, and 69 from Colorado.

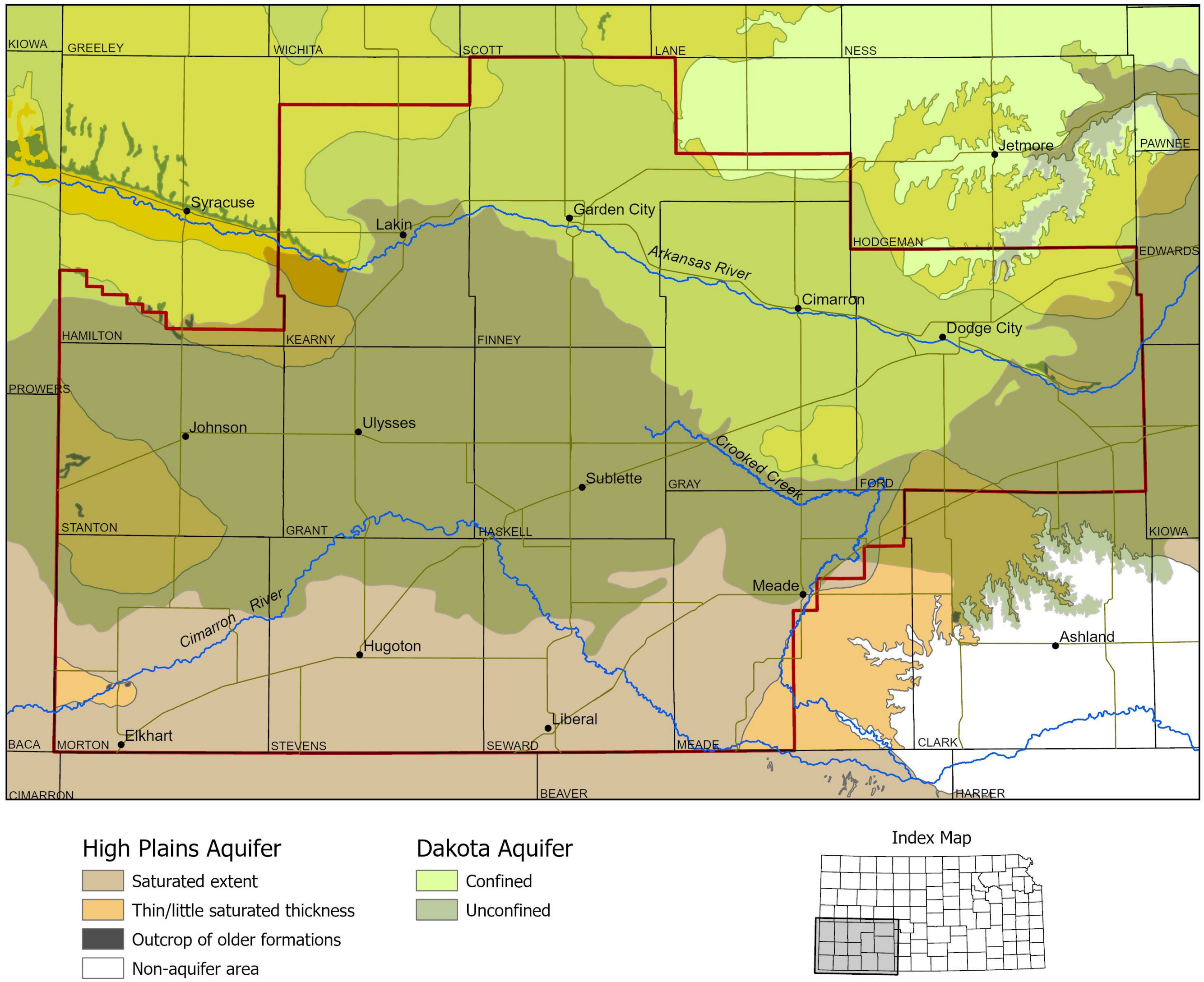

Figure 1. Map of GMD3 model area in Kansas, Colorado, and Oklahoma. The red line indicates the district boundaries of GMD3.

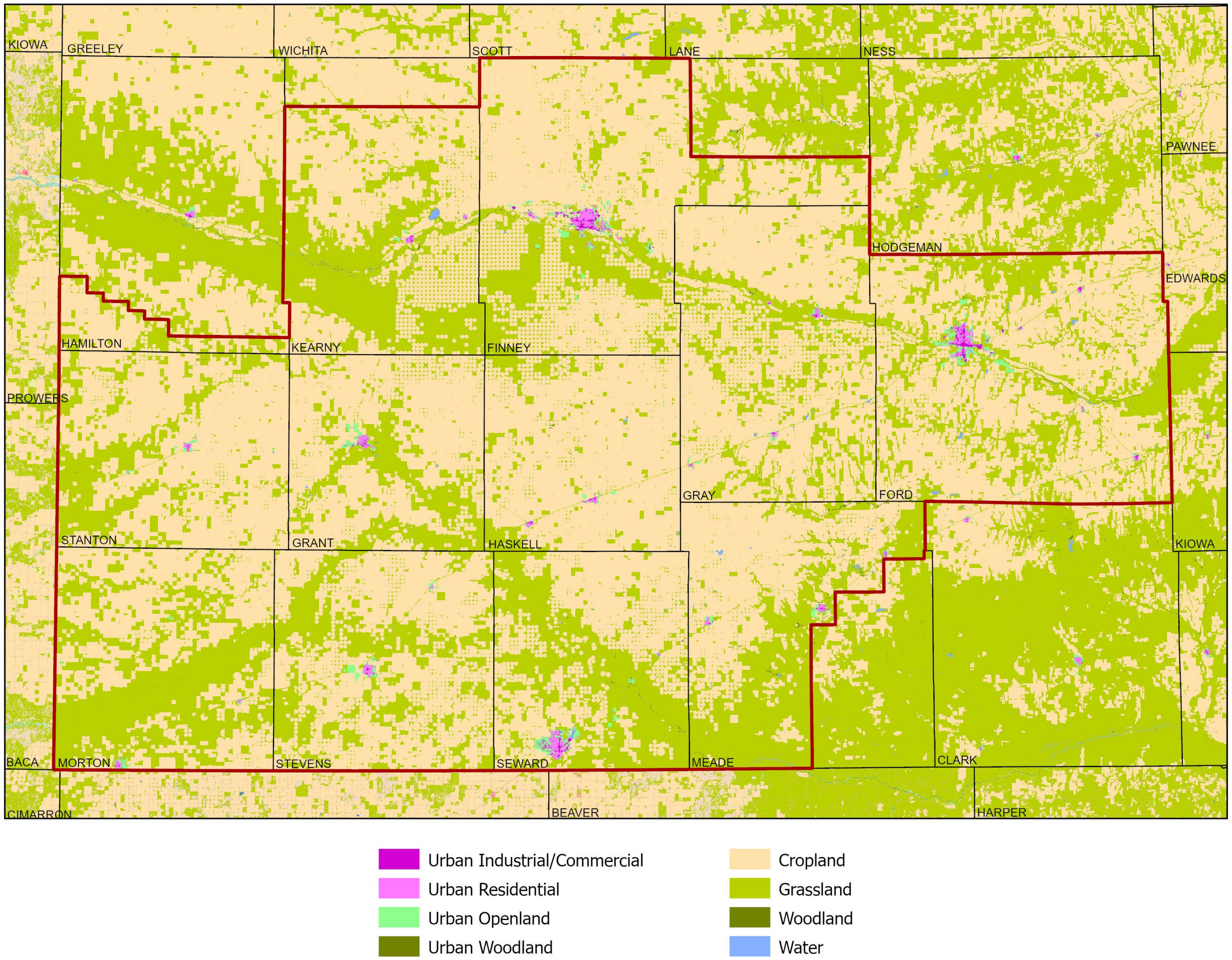

Figure 2. Land use/land cover classifications of the model area, 2015.

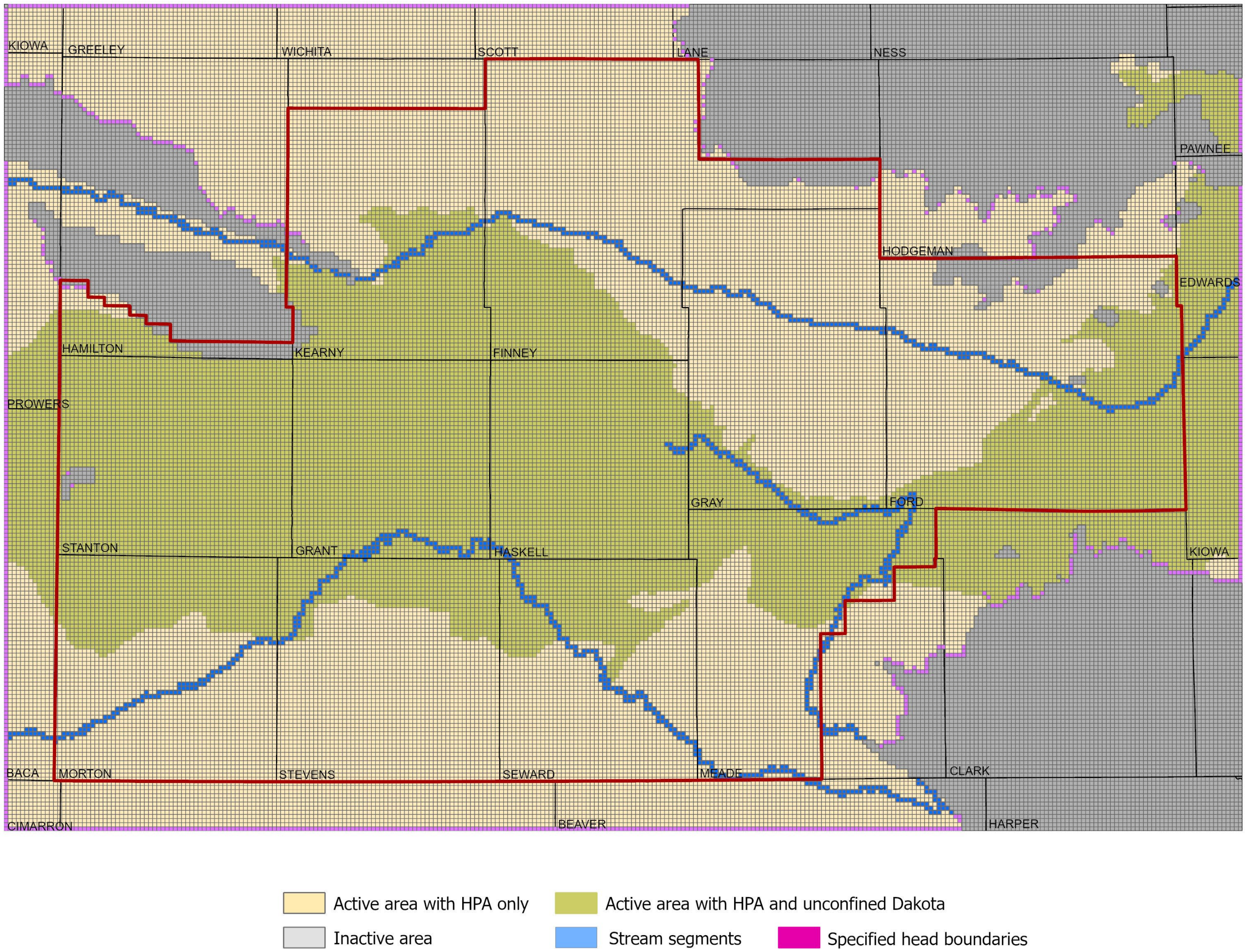

Figure 3. Model boundaries, grid cells, active area, and special model cells.

The model was calibrated to match predevelopment water levels and long-term hydrographs of selected wells, especially the water-level change over time. Stream flows at different USGS gages on the Arkansas River, Cimarron River, and Crooked Creek also were used in the calibration process. Because the model did not consider overland runoff during precipitation events, streamflow calibration was focused on the low flows that are typically observed between January and March. The recharge-precipitation relationship, the parameters controlling the delay between water infiltrating at the land surface and reaching the water table, the lagged release of water from storage in dewatered sediments, and hydraulic conductivity of lithologic categories are all treated as calibration parameters due to their relatively large uncertainties and strong effects on model results.

Active and Inactive Areas

Most groundwater models include “active” and “inactive” areas. The actual groundwater flow calculations are only conducted within the cells in the active area. In this study, the extent of the HPA and unconfined Dakota aquifer in southwest Kansas, including the majority of GMD3, represents the active area. “Inactive” cells are those where the HPA or unconfined Dakota is not present, such as the region that has a substantial area of bedrock outcroppings along the Arkansas River valley in Hamilton County. Additional inactive areas were assigned to cells with very thin aquifer thickness that would routinely go “dry” and cause model convergence errors during preliminary model simulations. The number of active cells in the final model is 47,255, giving a total active model area of 11,800 square miles, a little more than 78% of the model domain (fig. 3).

REVIEW AND SETUP OF DATA PARAMETERS

Precipitation Data

Monthly precipitation data were downloaded from the PRISM Climate Group at Oregon State University (http://prism.oregonstate.edu). PRISM provides raster-based grids (roughly 4 x 4 km) for the entire continental United States, and the data compare very favorably with similar precipitation-based data processing undertaken in past KGS activities (Wilson and Bohling, 2003; Wilson et al., 2008).

The monthly PRISM grids for each year from 1945 to 2021 were processed to compute the annual average, minimum, and maximum precipitation for each year along with averages for the "summer" period (April to September) and the "winter" period (October to March). The "summer" and "winter" periods represent the irrigation and non-irrigation seasons, respectively. The output for each of these processing steps was a new raster-based grid, which was then overlain on the model area and values assigned to each of the model cell centers.

The average summer and winter precipitation over the model area from 1945 to 2021 is 14.54 and 4.93 inches, respectively (fig. 4). The highest summer precipitation year was 1996 followed closely by 2015, with 21.81 and 21.24 inches, respectively, and the lowest period of precipitation was the winters of 1956 and 2002 with only 1.24 and 1.28 inches of precipitation, respectively.

Figure 5 shows spatial patterns in the normal precipitation (average precipitation over the last three full decades, 1991 to 2020) across GMD3. Typically, the area has a pronounced west-to-east gradient with precipitation levels lower along the western and southwestern edges of the model area and increasing eastward to their maximum levels, reflective of the pattern across the state.

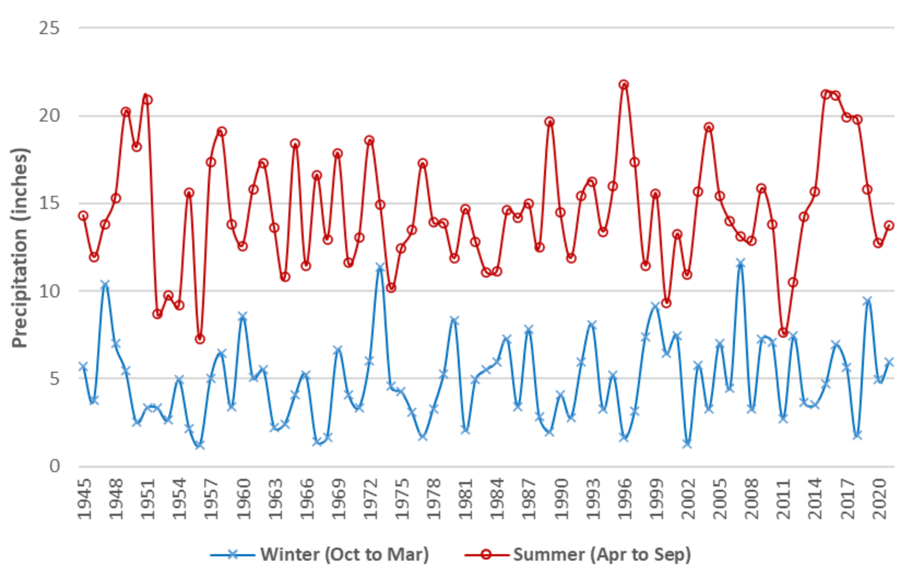

Figure 4. Average "summer" and "winter" precipitation.

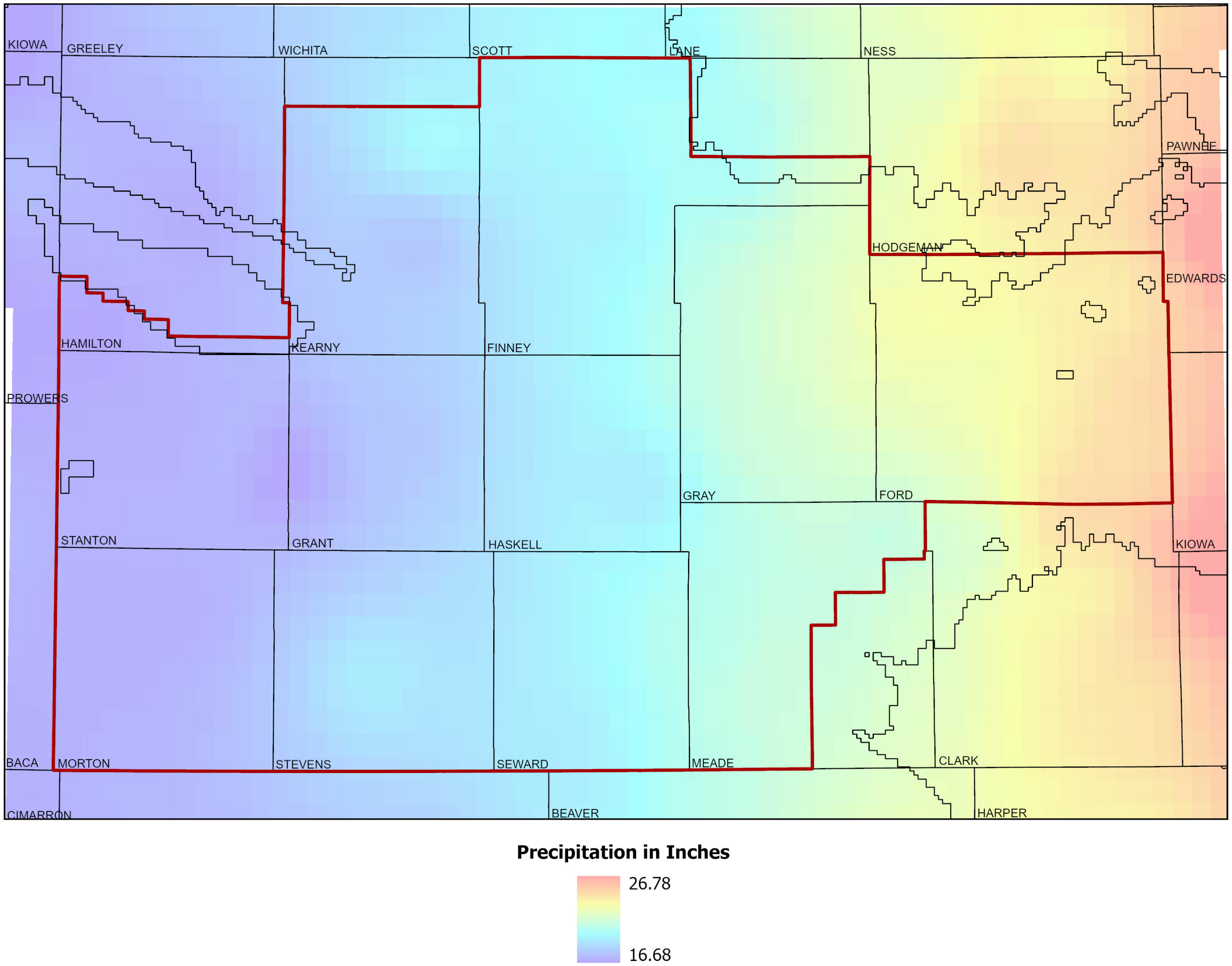

Figure 5. PRISM normal annual precipitation (average for 1991 to 2020). The irregular black line represents the active area of the model.

Geology and Lithology

Geologic formations at or near the surface across GMD3 are sedimentary in nature and are relatively recent in age (geologically speaking). The area is overlain by unconsolidated sediments primarily from the Ogallala Formation of the HPA, belonging to the Neogene System, and undifferentiated Pleistocene deposits, mainly loess and recent alluvial deposits (fig. 6). The Ogallala and undifferentiated Pleistocene deposits, which consist of clay, silt, sand, and gravel, accumulated as an apron of clastic (particulate) sediments that were eroded from the uplifting Rocky Mountains and carried eastward by streams (Ludvigson et al., 2009). Sand hills/dunes are prevalent primarily along the south side of the Arkansas River and Cimarron River. The oldest surface outcrops, ranging in age from Late Cretaceous to Permian are generally found to the northeast and southeast of the model domain, within the inactive portions of the model.

Aquifer Characteristics

The HPA is the principal aquifer in the area and provides water for the majority of uses within the active model area, although the underlying Dakota aquifer is increasingly being looked to as an additional water source. Groundwater also is found in the alluvial deposits of streams, but, except for the Arkansas River, most of these are limited to relatively small yields. The intent of this project is to simulate groundwater conditions in the unconsolidated material and no distinction is made between the HPA and alluvial deposits.

The Cretaceous-aged Dakota aquifer, where it is unconfined and in direct contact with the HPA, is also included in this study. However, the Dakota system is much less understood and given the channelized nature of the sandstone deposits, is highly variable in terms of its viability as a water supply. The interplay between the HPA and Dakota aquifer is represented within the model, but the simulation accuracy needs to be improved in the future as more data are collected from the Dakota system.

The next formation in sequence (found in the inactive northwest corner of the model) is the Niobrara Chalk, which is water bearing but is not considered a principal source because the water typically is found in fractured limestone or in dissolved solution openings and thus can be highly variable in terms of availability. The Graneros Shale, Greenhorn Limestone, and Carlile Shale are found below the Niobrara but are generally of very low permeability and yield little water. In the inactive southeast corner of the model are Permian-aged formations like the Nippewalla Group and Whitehorse formation, which also yield little water.

Water quality in GMD3 is generally suitable for most uses; however, the area does have sites of contamination from both natural and human-induced sources. Surface water high in sulfate and uranium enters Kansas from Colorado and is infiltrating into the alluvial aquifer and HPA, generally in areas along the Arkansas River and associated ditches west of Garden City (Whittemore et al., 2023). In southeast Seward County and southwest Meade County, natural saltwater is intruding from the Permian bedrock into the HPA (Whittemore et al., 2005). In both areas, the lesser groundwater quality affects public, private, agricultural, and industrial groundwater supplies.

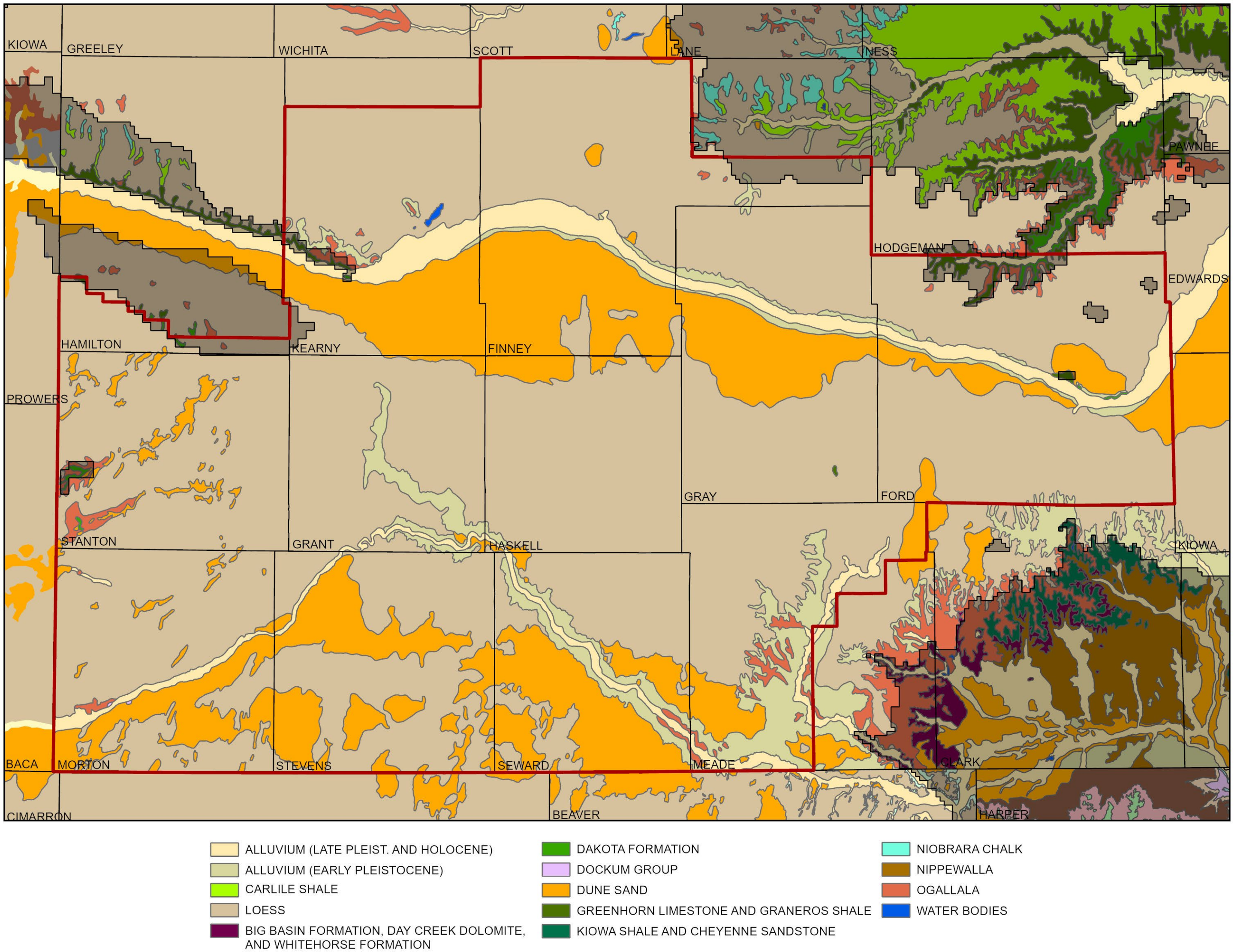

Figure 6. Surficial geology. Gray-shaded areas represent the inactive portions of the model.

Bedrock Surface

Data for the HPA bottom were updated from the 2008 GMD3 model by supplementing the bedrock study of Macfarlane and Wilson (2006) with a similar but unpublished project completed in 2009 for the Kansas GIS Policy Board covering south-central Kansas. Both bedrock projects used lithologic logs obtained from water well completion records, county geologic bulletins, and geophysical logs stored at the KGS, along with additional data from drilling companies and the USGS. For this study, the HPA bedrock elevation isolines were extended slightly into Colorado and Oklahoma and then interpolated to form a continuous raster-based surface. The bottom configuration of the Dakota aquifer, taken from Macfarlane et al. (1995), was used to create a second continuous raster-based surface, clipped to the extent of the unconfined portion of the aquifer. The two raster surfaces were overlain to create the HPA and unconfined Dakota layer elevations. The northern edge of the contact zone between the two raster surfaces was further smoothed to remove the abrupt change in elevation by finding the average elevation in each of the interpolated raster cells using a moving 2-mile circle within a 4-mile buffer along the Dakota edge with the low permeability confining unit. Along the southern contact zone, the deeper of the two bedrock sources was used to represent the overall bottom of the aquifer systems (fig. 7).

The model cells were overlain on the interpolated bedrock surface below the HPA and unconfined Dakota layers. Given its low permeability, the bedrock was treated as a no-flow boundary. Within the active area of the model, the bedrock elevation was manually adjusted to be at least 10 ft below the land surface for 32 cells. These cells were mostly found along stream channels outside of the district where the model's 0.5 x 0.5-mile grid size was too coarse to adequately capture the local interpolated land surface elevation changes.

The bedrock surface elevation follows the same general slope as the land surface, with higher values located along the western edge of the model and lower values to the east. Bedrock highs are found in Hamilton and Morton counties, with the lowest bedrock elevations found in eastern Ford County. A three-dimensional version of the bedrock surface (fig. 8) facilitates visualization of the bedrock topography. Localized areas of bedrock highs, eroded bedrock/stream channels, and the presence of the unconfined Dakota can readily be seen. Within the district, the depth from land surface to bedrock (i.e., the thickness of the sediments of the HPA and Dakota) ranges from near the land surface (the minimum value set to 10 ft) to more than 700 ft along the southern Stevens and Seward county lines for the HPA and more than 900 ft in southern Finney and northern Grant and Haskell counties for the Dakota (fig. 9).

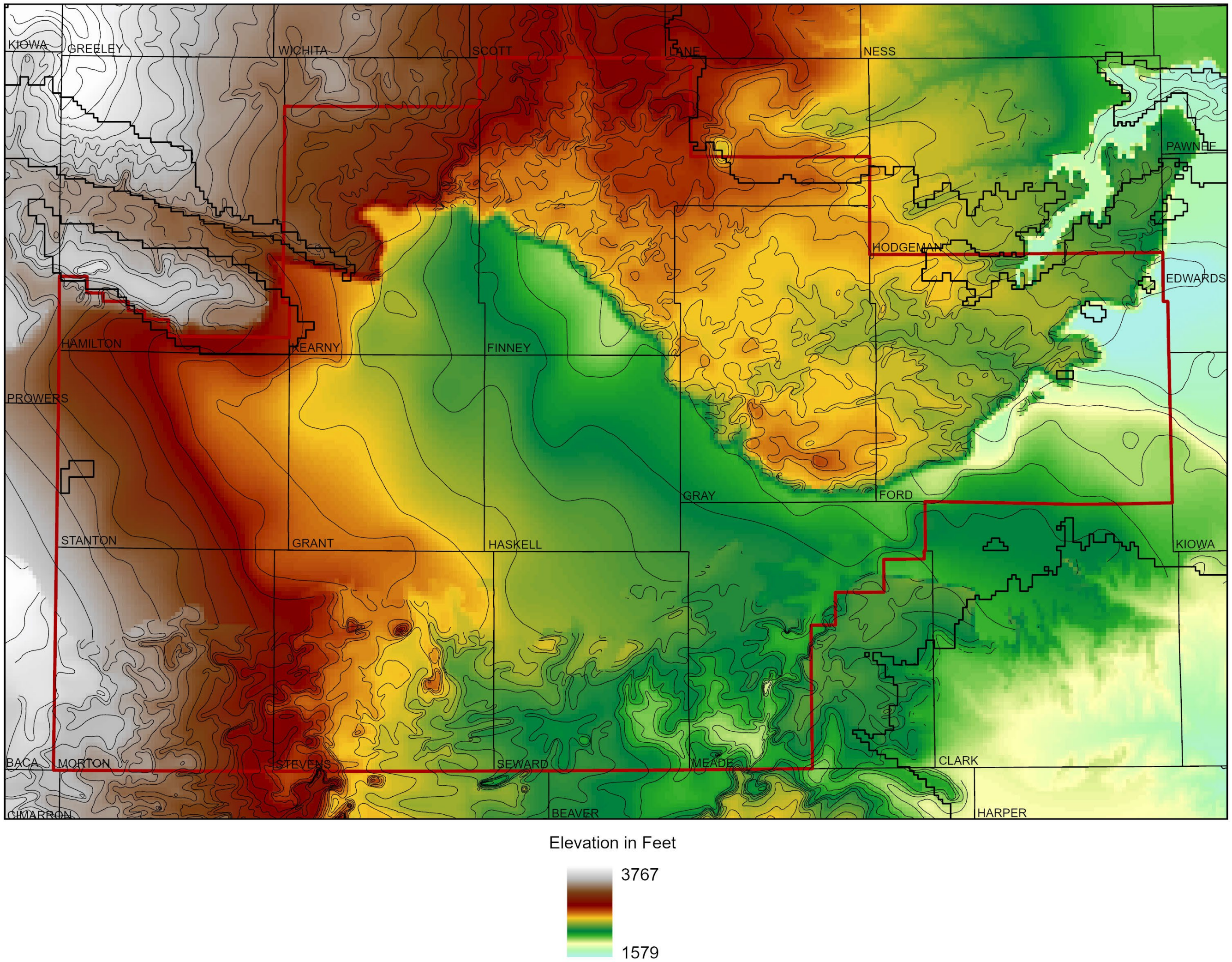

Figure 7. Interpolated bedrock elevations for the HPA and Dakota aquifers. The irregular black line represents the active area of the model. The solid red line represents the GMD#3 boundary.

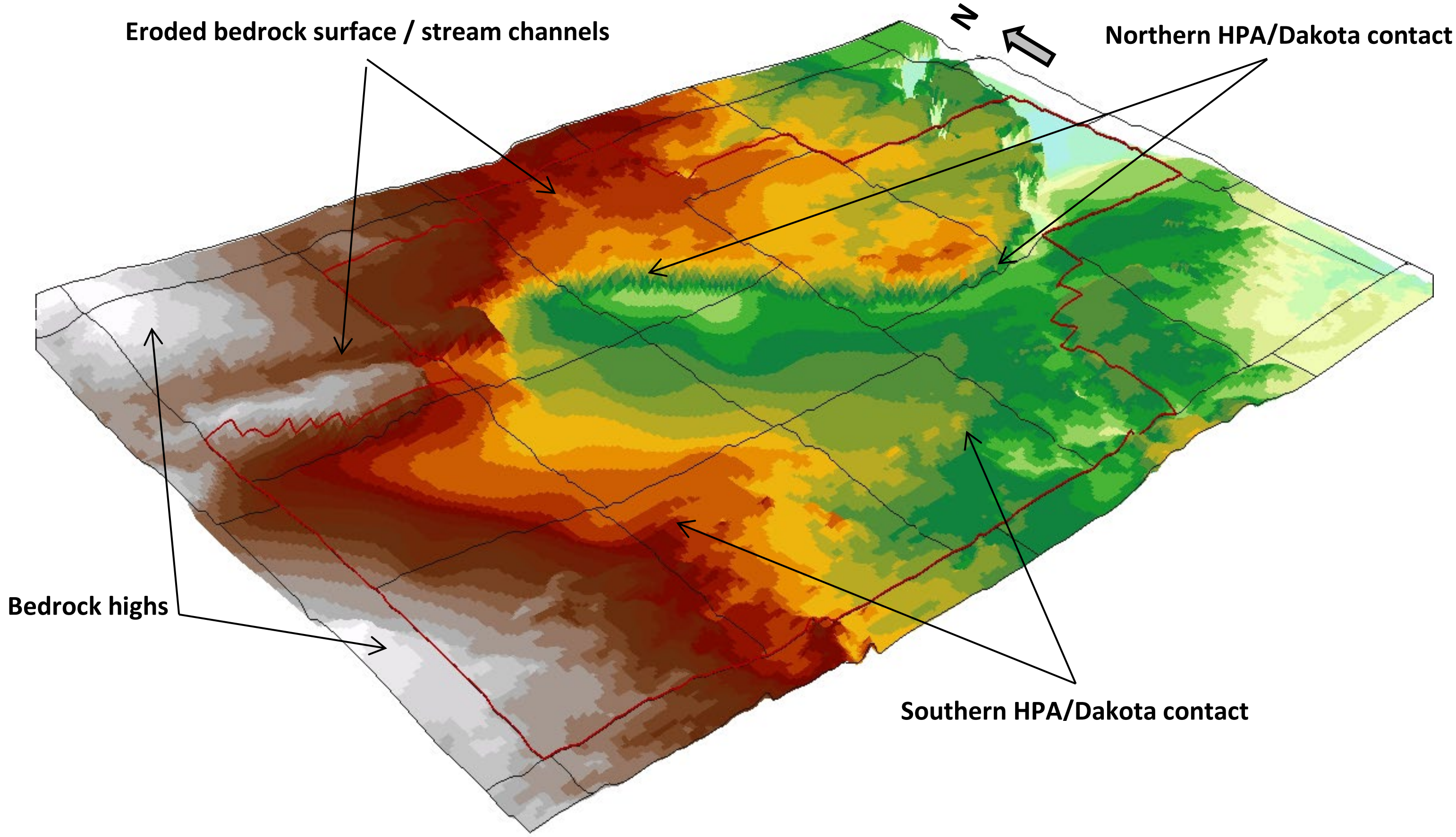

Figure 8. Three-dimensional view of the interpolated bedrock surface, looking northeast (see fig. 7 for color scale).

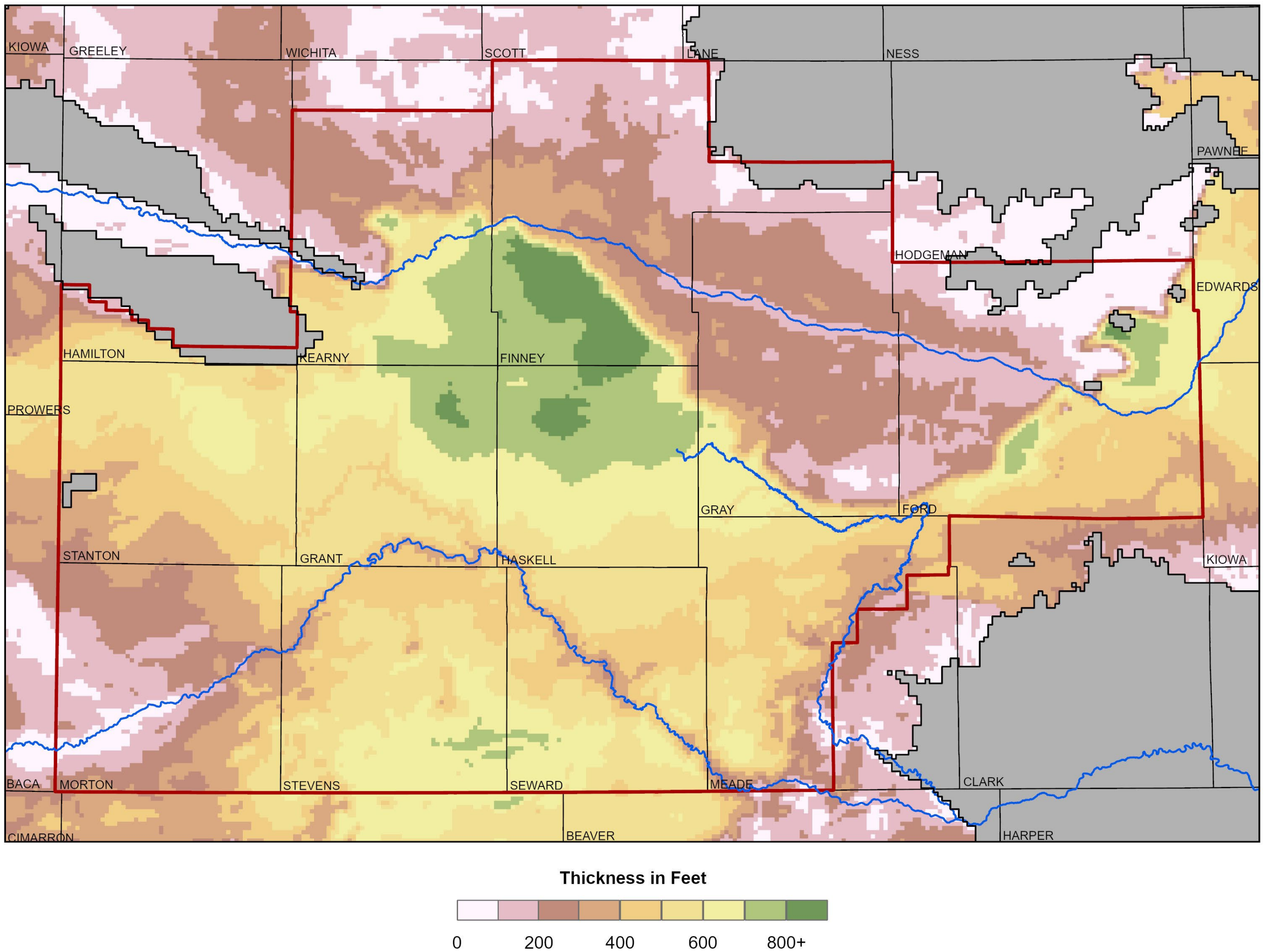

Figure 9. Thickness of the unconsolidated sediments for the HPA and unconfined Dakota aquifer.

Lithologic Classifications

The KGS has established methods to extract and categorize information from drillers' logs with the current version of the process known as the Hydrostratigraphic Drilling Record Assessment (HyDRA) (Bohling, 2016; Bohling et al., 2020). Lithologic descriptions and interval depths have been transcribed and stored in Oracle, an enterprise-level relational database management system, from which they are extracted and categorized into lithologic groupings. The groupings are spatially interpolated to produce a three-dimensional grid, with each grid cell containing the proportions of different groupings. Using representative values for each lithologic group, vertically averaged K is computed for the saturated interval between the predevelopment water table and bedrock surface, and Sy is computed for any water-level interval between two different times.

A little more than 25,000 well logs were used in the HyDRA process (fig. 10). In Kansas, water well completion forms (WWC5) are the source of the lithologic logs; similar records were retrieved from Colorado's Department of Natural Resources' permitted wells database and the Oklahoma Water Resources Board's Groundwater Well Logs geodatabase for the simulated areas in those states. Together, these data sources provide about 298,000 depth intervals for which lithology is described. Of these, roughly 79% matched existing lithology translations, which include 71 standardized lithology codes. Unmatched intervals, roughly 63,000 in this case, are not part of the standardized logs and not used in the interpolation process. The standardized lithologies are further categorized into five groups for the HPA and two groups for the Dakota, each representing a set of lithologies expected to exhibit similar values of K and Sy (table 1).

With the lithologic groupings in place, HyDRA segments each driller's log into 10 ft intervals, starting from the interpolated predevelopment water table (described in the next section) to bedrock. The proportion of each of the lithology categories occurring within each 10 ft interval is estimated based on that driller's log. The category proportions in the 10 ft intervals are then interpolated into a three-dimensional grid across the model's active area, so that each 3-D grid cell contains a set of values representing the category proportions within that cell. Figure 11 shows a summary representation of this information. The authors wrote a special program to intersect MODFLOW-formatted water table and bedrock elevation grids with the three-dimensional proportional grids and then write out the vertically averaged K and Sy values to MODFLOW-formatted grid files, based on the category proportions within the intersected grid cells and the K and Sy values assigned to each category. Specifically, K is calculated as the average value for the entire lithologic interval between the water table and bedrock, while Sy is computed only for the water-level change interval between the start and end of a time interval.

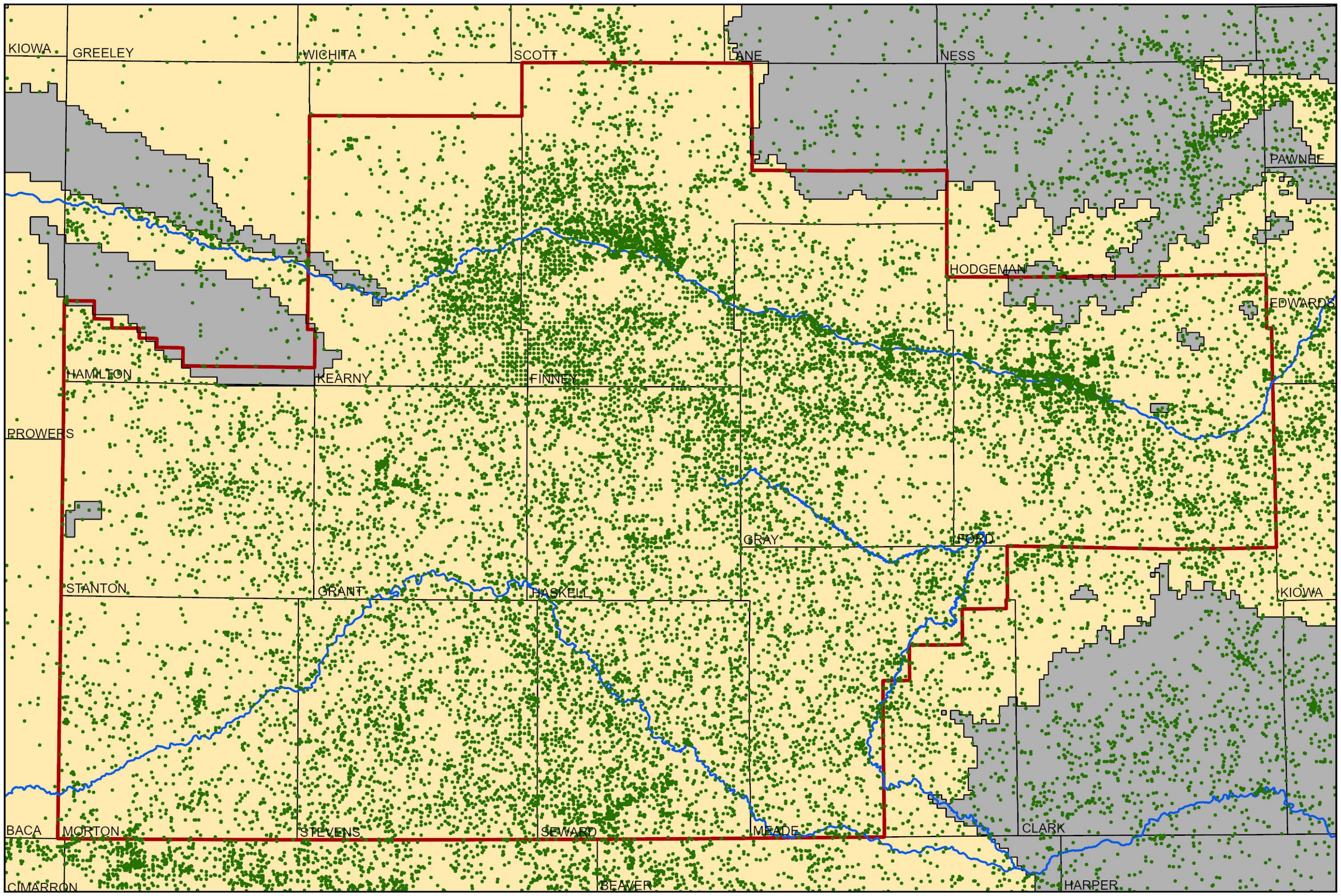

Figure 10. Distribution of lithologic logs used in HyDRA.

<table>
<tr><th colspan="5">Table 1
Standardized lithologies and hydraulic conductivity (K, feet/day) and specific yield (Sy, dimensionless)</th></tr>
<tr><th colspan="5">Ogallala/High Plains Layer</th></tr>
<tr><th>Category 1
K=0.000114 ft/d
Sy= 0.005</th><th>Category 2
K=0.797 ft/d
Sy=0.005</th><th>Category 3
K=49.3 ft/d
Sy= 0.005</th><th>Category 4
K=238 ft/d
Sy=0.11</th><th>Category 5
K=332 ft/d
Sy=0.13</th></tr>
<tr><td>Shale
Clay
Bedrock
Red bed siltstone</td><td>Silty and sandy clays
Silts
Top soil
Marl
Caliche</td><td>Sandy silts
Sandstone
Fine sands</td><td>Medium to coarse sands
Clayey and silty gravels</td><td>Sand and gravel
Fine to coarse gravels</td></tr>
<tr><th colspan="5">Dakota Layer</th></tr>
<tr><th colspan="2">Category 1
$K_{Horizontal}$ = 0.1 ft/d, $K_{Vertical}$ = 0.01 ft/d
S = 10^{-7}</th><th colspan="3">Category 2
$K_{Horizontal}$ = 100 ft/d, $K_{Vertical}$ = 1 ft/d
S = 10^{-5}</th></tr>
<tr><td colspan="2">Shale</td><td colspan="3">Sandstone</td></tr>
</table>

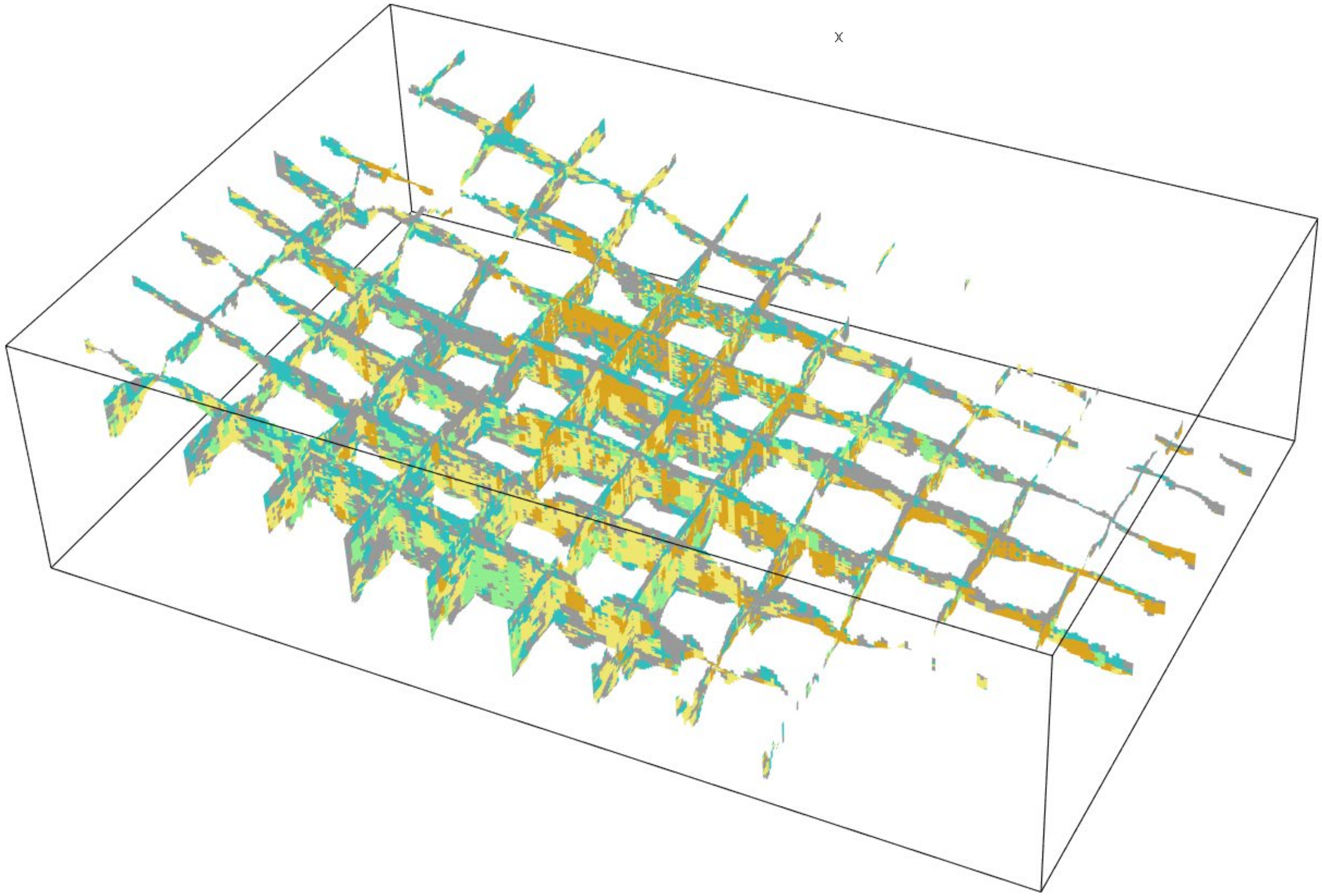

Figure 11. Proportion-weighted average lithology categories in cross sections of the 3-D grid. The gray to blue indicates lower permeability classes and yellow to tan higher permeability classes.

Water Levels

Estimates of the predevelopment water table were similar to the 2008 GMD3 model and compiled primarily from the “Well Records” listing of county-based geologic bulletins. Most of the depth-to-water measurements in GMD3 were taken from 1937 to 1948. Additional predevelopment measurements pre-dating 1945 from the Water Information Storage and Retrieval Database (WIZARD) and the USGS National Water Information System in Colorado and Oklahoma also were included. Predevelopment points and contours from a USGS map product (Becker, 1999) also were used to represent conditions outside the active area lacking observation wells, primarily in Colorado and Clark County, Kansas, to help avoid edge effects associated with surface interpolations. The predevelopment water-table elevations were interpolated to form a continuous 1,000 x 1,000 ft gridded surface (fig. 12). The model cells were overlain on the gridded surface and the average predevelopment water-table elevation within each model cell computed.

Like the bedrock surface, the predevelopment water-table elevation follows the same general slope as the land surface, trending from highs along the western edge of the model to lows in the east. The predevelopment depth-to-water varies across the model’s active area (fig. 13). The depth to water is shallowest along the stream channels, typically within 50 feet of the land surface, with the deepest values found in Haskell County. The predevelopment depth to water in GMD3 averages 104 feet and ranges from near the land surface to 260 feet.

GMD3 has a number of wells with measurement histories going back to the 1970s and 1980s (fig. 14). Depth-to-water measurements for the Kansas portion of the model were obtained from the WIZARD database. The majority of these records from 1996 to present were obtained as part of the annual Kansas Cooperative Water Level Program, operated by the KGS and the Kansas Department of Agriculture, Division of Water Resources (KDA-DWR). Colorado- and Oklahoma-based measurements were downloaded from the USGS National Water Information System and the USGS National Groundwater Monitoring Network (NGWMN).

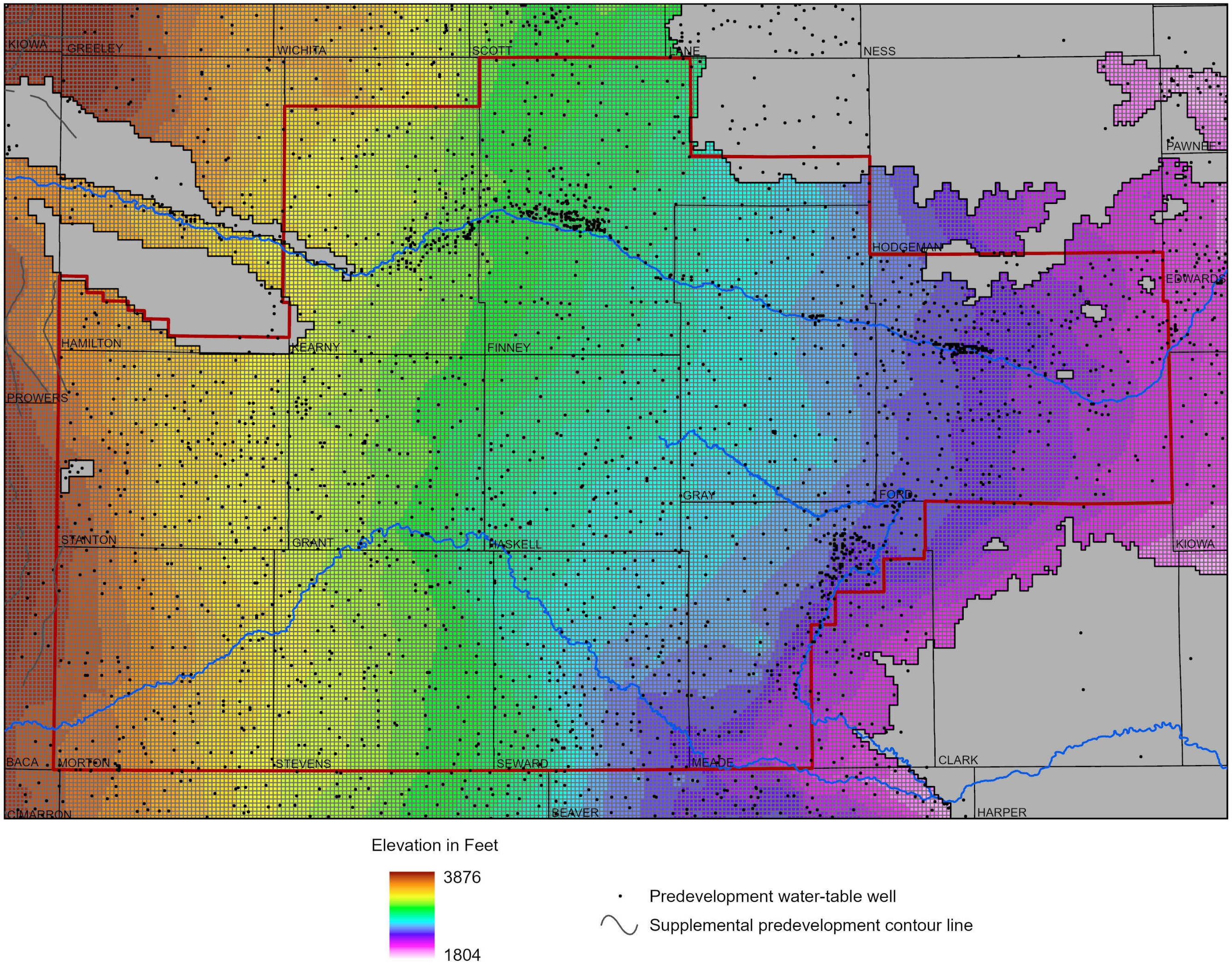

Figure 12. Interpolated predevelopment water table.

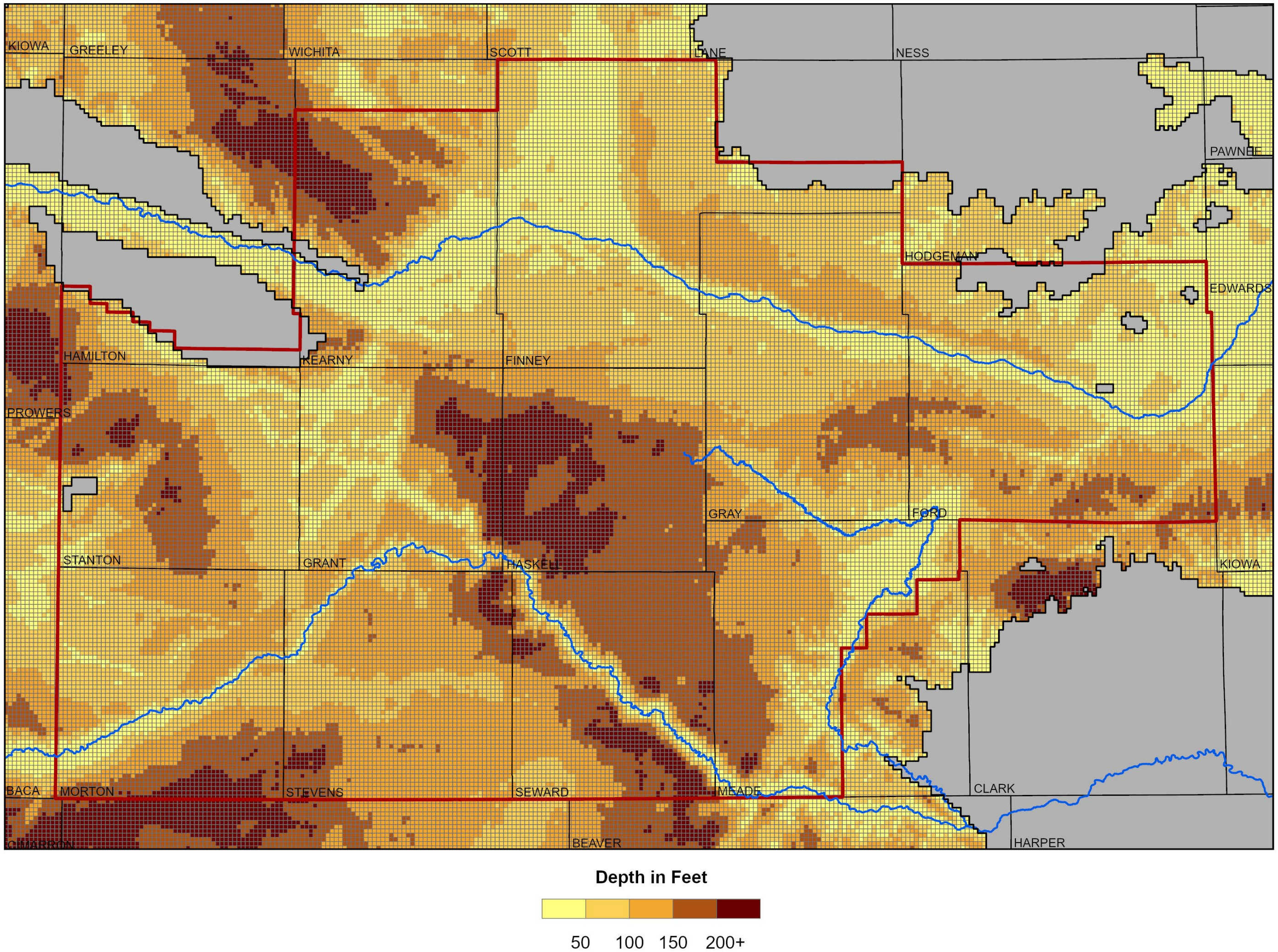

Figure 13. Interpolated predevelopment depth to water.

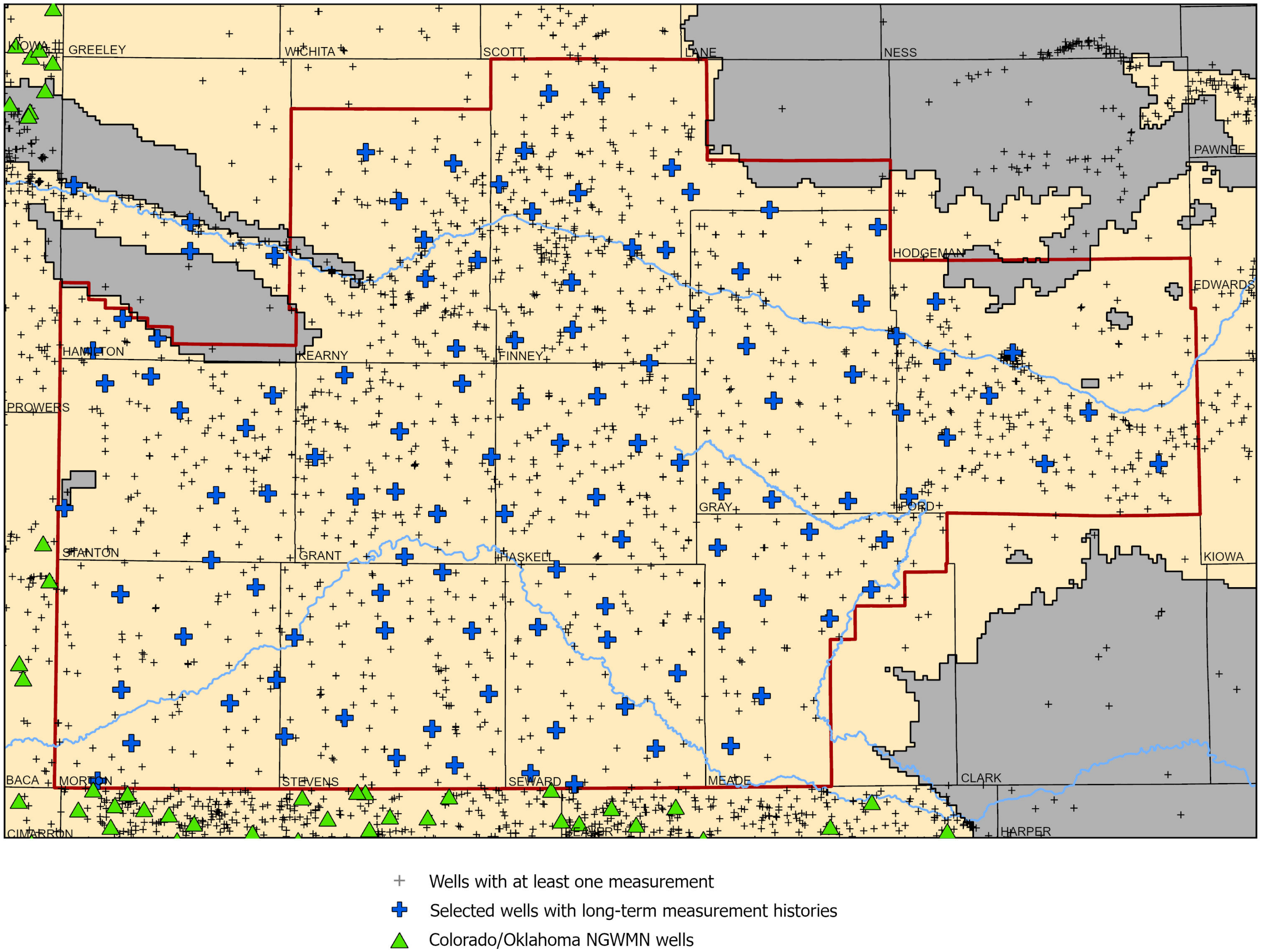

Figure 14. Distribution of water-level measurement wells over the transient period.

Water-level measurements with status codes that indicate the value might not reflect normal conditions (e.g., the well was being pumped) were removed from consideration. “Winter” measurements, those taken between December 1 and April 15, were averaged at each well to obtain a single yearly value for that well. Since 1996 and the start of the state’s annual measurement network, 72% of these measurements have occurred in the month of January. Also, since that time, the number of measured wells has remained fairly static, averaging 421 wells each year, while the number of measurements has a slightly increasing trend (fig. 15).

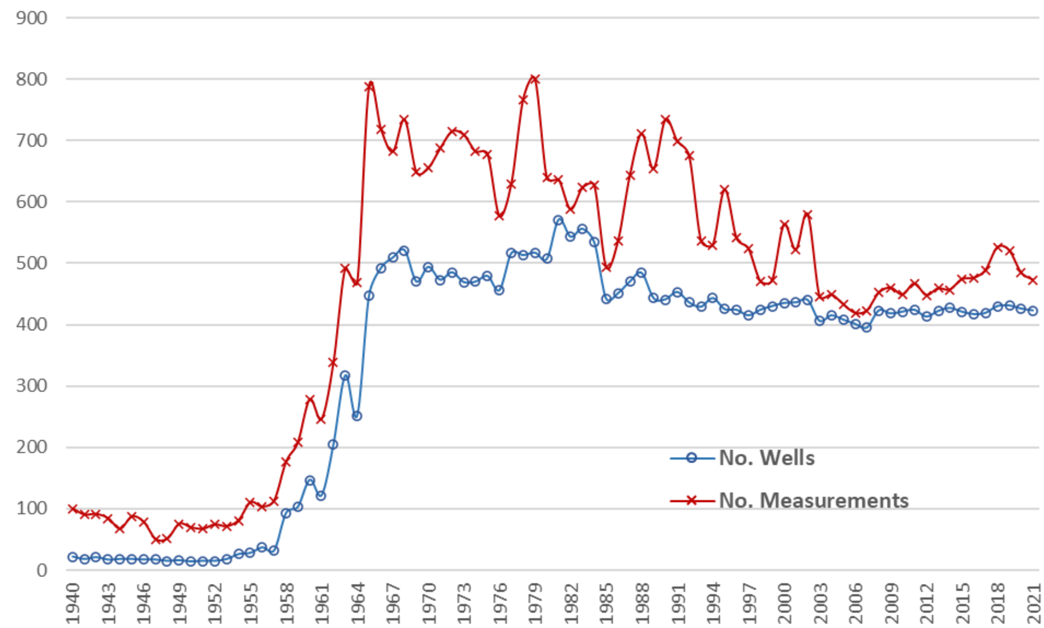

Figure 15. Number of wells in the model domain with “winter” (December 1 to April 15) measurements.

The average predevelopment aquifer thickness of the HPA and unconfined Dakota within the GMD3 boundary and active area of the model is 325 ft and ranges from close to 0 to just more than 800 feet, with the maximum thickness occurring where the HPA and Dakota are in contact in southern Finney County. In comparison, the aquifer thickness averaged 230 ft from 2021 to 2023 with the greatest declines also occurring in the HPA/Dakota contact area in portions of Finney, Grant, and Stanton counties (fig. 16). Many of the fringe areas, the Ark River valley in Hamilton County, southern Morton County, and eastern Ford County have seen relatively small to no changes in water levels due to insignificant pumping. The thickest portions of the present-day HPA and unconfined Dakota can still be found in southern Finney and Kearny counties along with eastern Ford County.

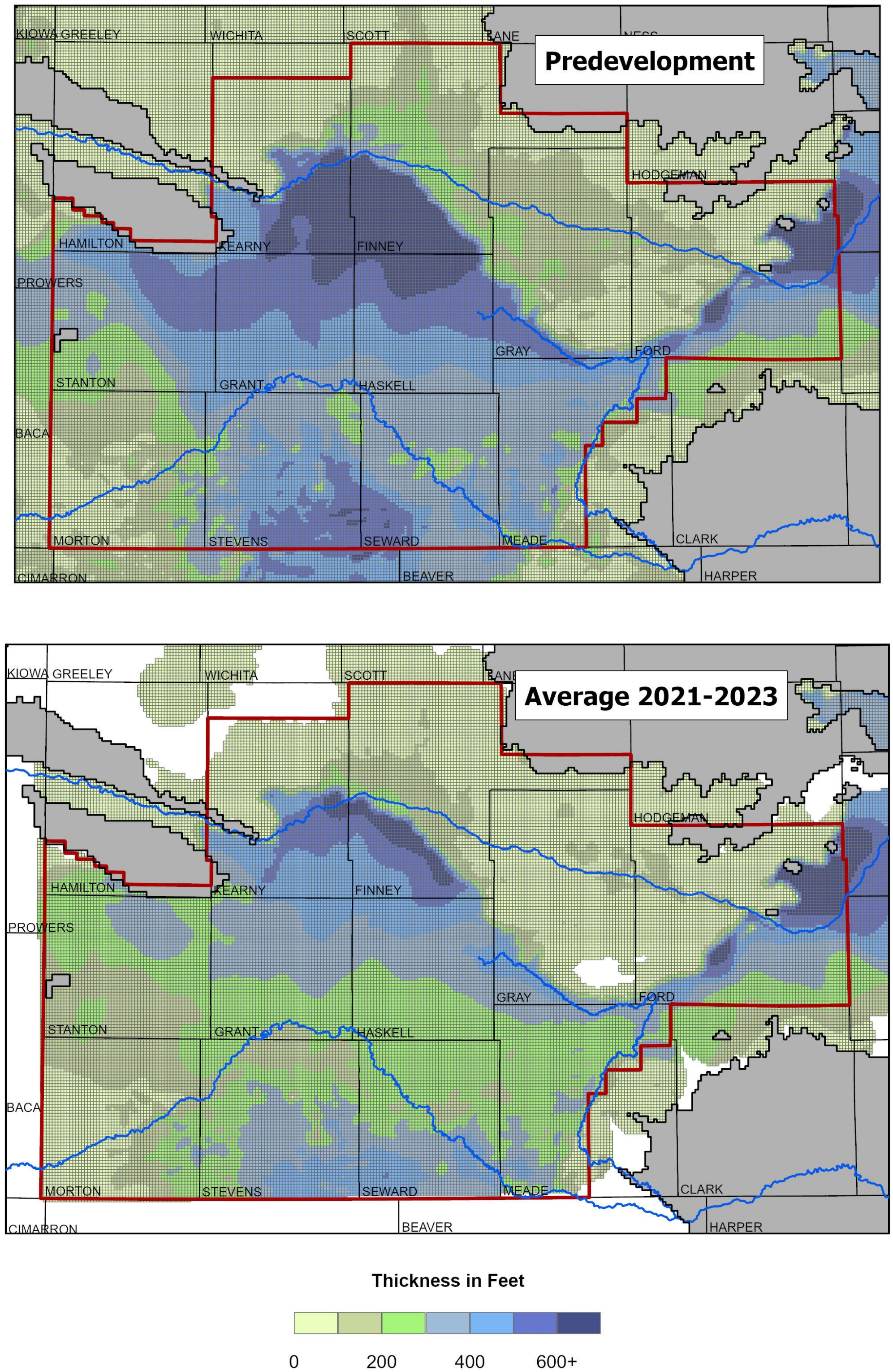

Figure 16. Interpolated predevelopment and average 2021–2023 thickness of the HPA and unconfined Dakota.

Boundary Conditions

The model uses time-varying specified head boundaries along most outer edges of the active areas and a combination of specified heads and no-flow boundaries internally along the inactive area/non-aquifer areas. This allows water to move in and out of the active area and provides control in areas, especially where the aquifer is relatively thin and is bounded by inactive areas. Given that head boundaries in the model are not necessarily located along natural or known hydrologic boundaries, setting appropriate head values is challenging, especially in areas that lack data. Starting with the interpolated predevelopment water levels, each time-varying head cell was reviewed in relation to well measurements taken over the transient period, 1945 to 2021.

There are thousands of well measurements during the transient phase in Colorado and Oklahoma, located along the western and northern edge of the model's domain (fig. 14), although the number of wells containing long, winter-based measurement histories is limited. Colorado, Oklahoma, and Kansas are participants in the USGS National Groundwater Monitoring Network (NGWMN), a network of selected monitoring wells across the country intended to facilitate the planning and management of groundwater resources. These wells meet a set of minimum data requirements and have been selected by each state to represent conditions and trends in various aquifer systems. In Kansas, all of the HPA wells in the annual cooperative water-level network are included in the NGWMN.

In cases where currently measured wells with long-term measurement histories (especially those associated with the NGWMN) are located in or near the head-boundary cells, the water-level trends shown in the measurement histories were applied to the overlapping or closest head-boundary cells. Data gaps in the measurement histories were filled by applying linear projections to existing predevelopment values or applying regional water-level changes from any available nearby wells to provide water-table elevation estimates over the entire transient period. The annual water-level changes from these cells were then applied to adjacent and nearby boundary cells with incomplete records, starting in predevelopment. This process of filling in temporal holes with nearby data works well where data records are present. The process is more subjective in areas with little to no data, such as along the state line in Baca and Prowers counties, Colorado, and the thinly saturated areas of the HPA along the north edge of the active area in Greeley and Wichita counties, Kansas.

Heads were also specified in thinly saturated areas where cell drying was a challenge. In those areas, initial transient model runs generated a significant number of dry cells and caused large computational errors. To overcome the dry cell problem in those areas, time-varying specified heads were assigned to the edges of dry cell pockets. The idea is that precipitation infiltration in those "pockets" would maintain the water level at their edges, although the lateral flow rates across those edges are very small due to relatively small aquifer thickness in those areas.

Stream Characteristics and Flow

The model simulates streams for the Arkansas and Cimarron rivers and Crooked Creek (fig. 17). Mean monthly streamflow records were obtained from the USGS National Water Information System for the gaging stations in the active area of the model. The Coolidge gage, in operation from 1950 to present, was used to represent streamflow into the model for the Arkansas River. Missing records from 1945 to 1950 were estimated based on regressed values in association with the gage at Syracuse. For the Cimarron River, flows at the Kenton gage, Colorado, were used in conjunction with flows at the Elkhart gage to fill in missing records from 1945 to 1973; the distance between the two gages relative to the edge of the model was used to prorate the amount of flow entering the model. The headwaters for Crooked Creek occur within the model (i.e., streamflow at the most upstream reach is zero).

The stream package for MODFLOW requires all surface water courses to be broken down into individual segments and reaches. A “segment” is a longer portion of the stream that has similar properties, such as width, slope, and streambed hydraulic conductivity; a stream segment is further divided into “reaches” that represent each portion of a stream segment within individual model cells. To represent all the streams in fig. 17, the model uses 16 stream segments with 1,496 reaches. Figure 18 shows an example of the stream/reach divisions. Ditch diversions (discussed later in the report) are represented as one-reach segments to allow for the transfer of streamflow into ditch canals.

Streambed elevations were obtained by determining where land surface contours (10 ft intervals) from 7.5-minute USGS topographic maps crossed the stream channel. Roughly 33% of the stream cells had elevation contours crossing the channel. For stream cells without crossing topographic contours, elevations were interpolated between cells with assigned elevations based on the overall change in elevation and length of the particular stream segment.

Depending on how the streams meander over the model’s 0.5 x 0.5 mile grid, the streambed elevations in relation to the bedrock elevations may not be properly represented in the model. This happens when a model cell is designated as a “stream” cell even though the cell is dominated by upland topography. In these cases, the estimated bedrock elevations for this cell are substantially above the streambed, causing computational errors in the model. A total of 145 model stream cells had bedrock elevations estimated to be above the streambed elevations, located primarily in Clark County, outside of GMD3. The bedrock elevations for these cells were lowered to 0.1 ft below the streambed.

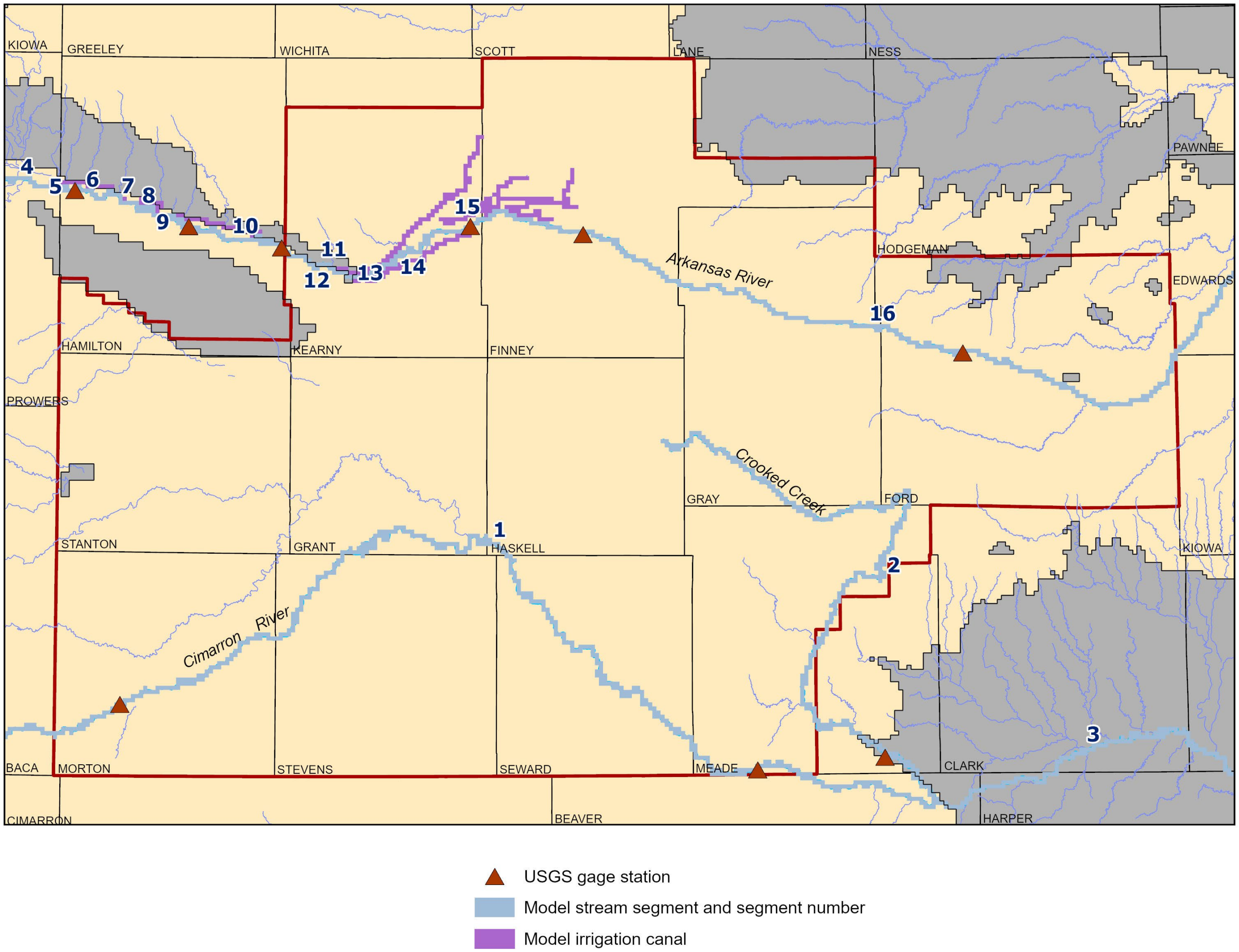

Figure 17. Model stream (labeled by their segment number) and canal cells and USGS stream gaging stations.

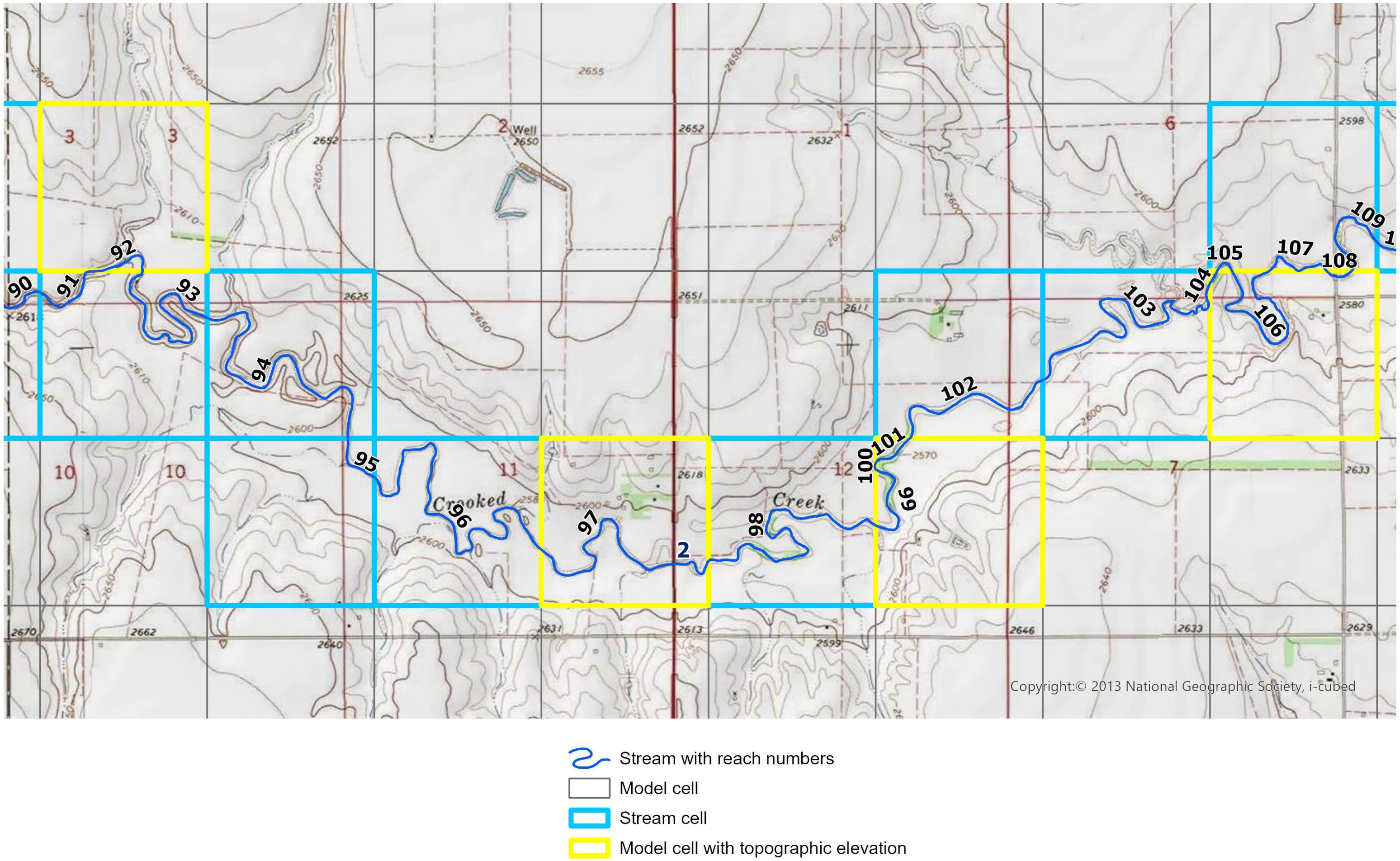

Figure 18. Selected area of the model showing a stream course segmented by reach designations for reach number 2 (Crooked Creek).

Water Right Development

In the United States, regulation of groundwater has traditionally been left to the states. As with Kansas, the states to the immediate north, south, and west follow some version of the prior appropriation doctrine (first in time, first in right) involving water-right permits or certificates. Water rights in Kansas are highly regulated in terms of how much water can be used annually and where that water is applied. Kansas is also one of the few states that maintains a long-standing, self-reporting water-use program. A substantial amount of Kansas water-right data is online. Similar data are available online for Colorado-based permitted wells and Oklahoma-based water rights wells. The KGS has a strong working knowledge of the Kansas water-right system, including the intricacies of the underlying data structure and proper methods to represent the data.

Kansas

Water rights in Kansas are dynamic entities whose characteristics can change over time. The authorized quantities and water-right locations used in the model represent conditions in Kansas as of June 12, 2022. Data were accessed from the Water Information Management and Analysis System (WIMAS) (http://geohdro.kgs.ku.edu/geohydro/wimas/index.cfm). GMD3 encompasses 9,952 unique appropriated and vested water rights and 10,679 active points of diversion. The majority of Kansas water rights in GMD3 are groundwater based (fig. 19), with irrigation making up 96 percent of that total (table 2). The largest surface-water-based appropriations represent the irrigation districts along the Arkansas River in Kearny and Finney counties. Elsewhere, surface-water use within the district is insignificant.

Table 2.
Total authorized quantity, in acre-feet, for appropriated and vested water rights, by use made of water and source of supply for GMD3
Represents conditions as of June 12, 2022

	Domestic	Industrial	Irrigation	Municipal	Recreation	Stockwater	Other	Total
Surface	7	0	153,691	0	1,227	0	0	154,925
Ground	81	44,699	3,461,438	47,603	3,250	55,281	404	3,604,256
Total	88	44,699	3,615,129	47,603	4,477	55,281	404	3,759,181

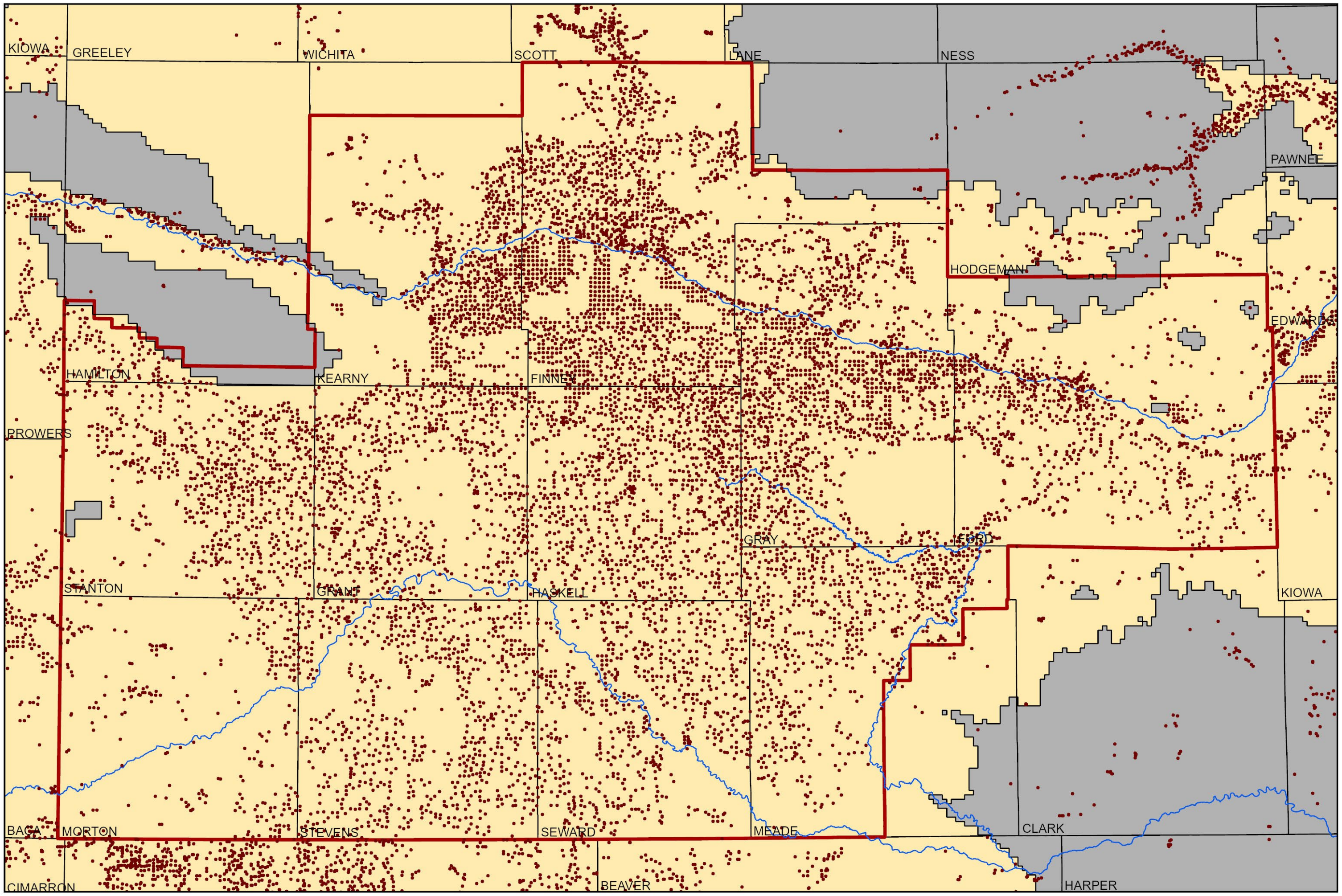

Figure 19. Groundwater-based water rights and permitted wells in Kansas, Colorado, and Oklahoma portions of the model.

The WIMAS database only stores a water right's present authorized quantity. Although quantity values can change as a water right goes through the certification process or by other administration actions (generally becoming less), the historic trends used in the model are based on the appropriated quantity values at the time of the download (June 12, 2022) and in relation to the priority date of the water right.

A common complexity with Kansas water-right quantities is that the annual appropriation can be associated with the water right itself (regardless of how many uses or points of diversion it might have), with the water right's uses of water, or with the water right's multiple points of diversion. Because the points of diversion for a particular water right could be located across multiple model cells, the total annual authorized quantities for water rights that had their appropriations stored by the water right or use made of water were divided equally among the water right's point(s) of diversion. Each point of diversion would then have an associated quantity that when added with the other points of diversion under the water right would equal the total quantity authorized. If the quantity was already stored by the point of diversion, it remained unchanged.

The trend in authorized quantity over time, based on priority dates, in the active portion of the model's area (fig. 20) has similar characteristics to trends elsewhere in the HPA in western Kansas. Kansas water law started with the passage of the 1945 Water Appropriation Act. Water users in place before that time could apply for a "vested" water right. Water rights issued after 1945 are referred to as "appropriated" rights. The authorized quantity, as well as the number of issued water rights, started increasing sharply in the early 1960s and then gradually leveled out around the mid-1970s/early 1980s.

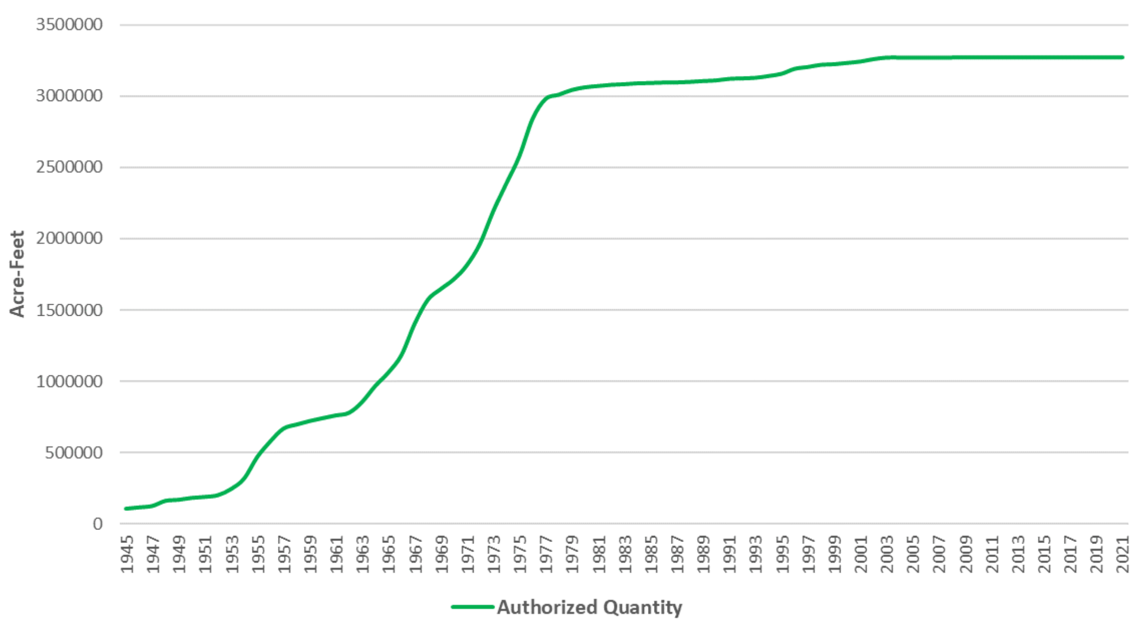

Figure 20. Total authorized quantity of Kansas groundwater-based water rights in the model's active area within GMD3.

Estimation of Historic Water Use

Although Kansas water-use reports go back to 1958, actual water usage as a whole, across large areas, was probably much higher than the early reports indicate, since it wasn't until 1978 that water rights were required to be obtained before diverting water for beneficial use. Even then, it wasn't until the early 1980s that water-right holders were required to submit annual water-use reports and not until 1987 that the KDA-DWR had the regulatory authority to fine water-right holders for lack of submission or knowingly falsifying reports. The Water Use Program of the Kansas Water Office was initiated in 1990. Now operated through the KDA-DWR, this program provides quality control and assurance for the submitted water-use reports. As such, reported water-use records were downloaded only from 1990 to 2021 (at the time of the model development, 2021 was the most recent year available for access as the 2022 water use report was still under review). Points of water diversion known to be drilled in bedrock aquifers, such as the confined Dakota or Permian-age systems, were removed from the HPA data set.

Based on past data analyses and review (Butler et al., 2023), water use from 2005 to present was considered to be of the highest quality and therefore selected for inclusion in the model. To estimate historical pumping levels before 2005, linear regression equations were formulated based on the ratio of water use/authorized quantity versus precipitation between 2005 and 2021, similar to past KGS modeling projects (Wilson et al., 2008; Liu et al., 2010; Wilson et al., 2015; Wilson et al., 2020; and Wilson et al., 2021). Various iterations found the regression of the water use/authorized quantity ratio against summer precipitation (April to September) and winter precipitation (October to March) used in the transient simulation to be statistically significant ($P < 0.00007$ and highly correlated for total groundwater use (R-squared value of 0.75).

Figure 21 shows the results of the regression-based water-use estimates against the authorized quantity and the 1990–2021 reported water use within GMD3. The ratios of water use/authorized quantity for total groundwater use and total irrigation groundwater use are computed for every model cell based on the variations in summer and winter precipitation. The ratios are then multiplied against their respective authorized quantities for a given year to yield an estimate of the actual amount of water used. The transient model uses the regressed water use from predevelopment until 2004, the actual reported water-use data for 2005–2021, and regressed water use for years going forward in future scenarios.

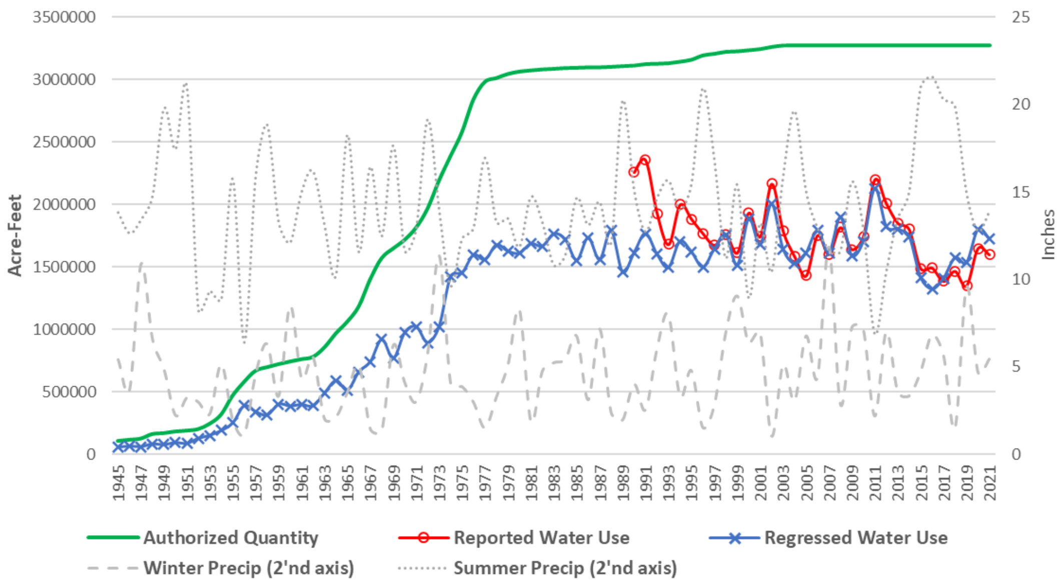

Figure 21. Total authorized quantity, regressed water use, summer precipitation, and reported water use for GMD3.

Colorado and Oklahoma

Estimating water use and groundwater development in other states is challenging as the data are based on complex rules and procedures, much like Kansas water-right data. Consequently, the processing results for water usage outside of Kansas should be viewed with a certain level of caution. For this project, permitted well data from the Colorado Decision Support System (CDSS), developed by the Colorado Water Conservation Board and Colorado Division of Water Resources, and water right records from the Oklahoma Water Resources Board (OWRB) Open Data portal were used.

The CDSS "Final Permit" database contains information related to permit numbers, annual permitted quantities, use(s) of water, aquifer sources, and priority dates. The data set represents larger uses of water (e.g., non-domestic) with irrigation being the dominant type, accounting for 98% of the records in the model domain. Other listed uses are for commercial, domestic, and unlisted. Similar to Kansas, the database lists the permitted well's priority dates and annual appropriation.

The water rights data from the OWRB is also dominated by irrigation usage, accounting for 93% of the total number of wells, with agriculture, industrial, mining, and public water supply accounting for the other uses. Twenty-seven wells listed as temporary, most located in the inactive areas of the model, were removed from consideration.

Given the lack of accessible, long-term estimates of actual water use in Colorado and Oklahoma (like most western states), the regression equation used to estimate water use in Kansas (based on summer and winter precipitation) was applied to model cells in the bordering states using the listed permitted quantities and priority dates or year the permit was filed (OWRB) (fig. 22).

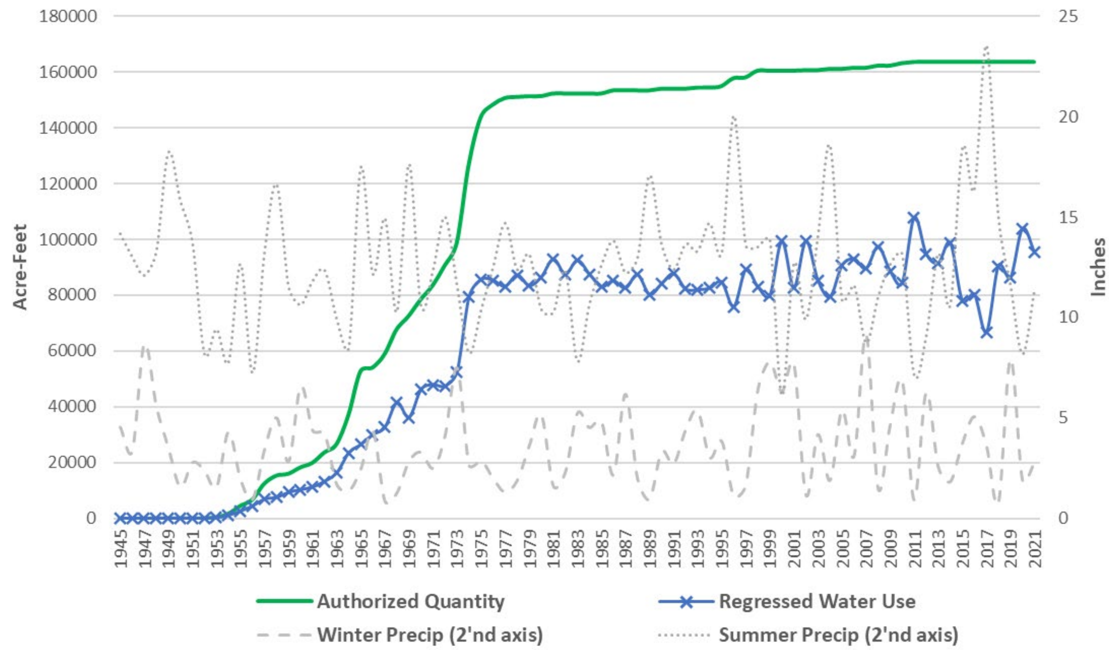

(a) Colorado

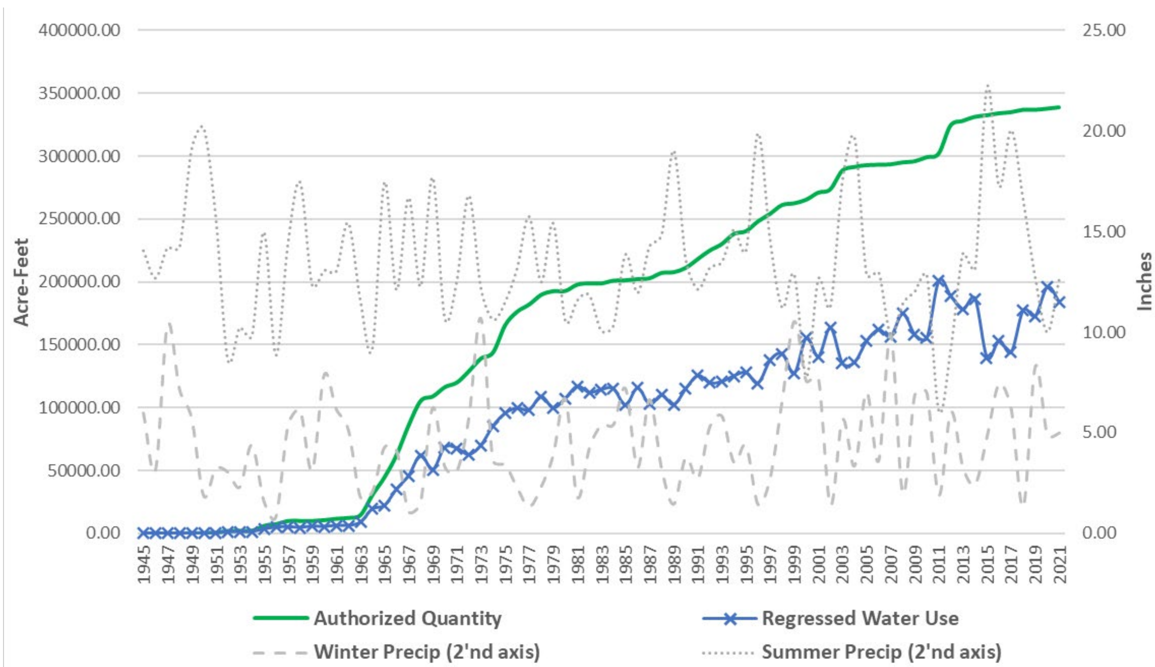

(b) Oklahoma

Figure 22. Total permitted quantity, regressed water use, and summer and winter precipitation, (a) Colorado and (b) Oklahoma.

Dakota Water Use

The updated model uses two layers with the upper layer representing the HPA and the lower representing the underlying unconfined Dakota. This necessitates that model-cell-based pumping values be distributed to the appropriate model layers. In KGS Bulletin 260, Whittemore et al. (2014) reviewed more than 2,000 wells, logs, and water levels to determine how much water was pumped from the Dakota aquifer in 2012. Given the number of records involved, applying the Dakota bulletin's methodology of reviewing wells individually for every year in the model's transient period is impractical; we applied a simpler approach here.

The percentage of usage from the water right records in the Dakota bulletin were assigned to matching well records in the model domain to represent conditions as of 2012. Since the Dakota bulletin was published, an additional 650 wells have been drilled with aquifer codes indicating they are wholly or partially completed in the Dakota. For each of these new site locations, the estimated percentage of pumping from the Dakota was based on the ratio of interpolated 2012 water levels relative to the completed well depth and the base of the HPA (i.e., top of the Dakota). The same process was used to estimate percentages in 1980 (roughly the period at which water right development stabilized) and 2021 (the most current year of available water use data). For each of the assigned years (1980, 2012, and 2021), the Dakota percentage for each well was averaged for each model cell in the unconfined Dakota portion of the model. The Dakota percentage between the years of 1980, 2012, and 2022 was then linearly interpolated between them. The percentage for 1980 was assumed to represent all prior years, going back to 1945. The assigned percentage of Dakota pumping was then multiplied by the cell total water use for each year to represent the total pumping from the Dakota layer of the model.

The estimated percentage of Dakota pumping varies depending on location, with some cells containing zero pumping throughout the transient period while pumping from others was 100%. For those cells with Dakota pumping in the model, the percentages averaged 30% across the transient period, with a range of 26% in 1980 to a high of 45% in 2021. The overall estimated pumping from the Dakota averages 4.9% of all groundwater use over the entire model's transient period (fig. 23).

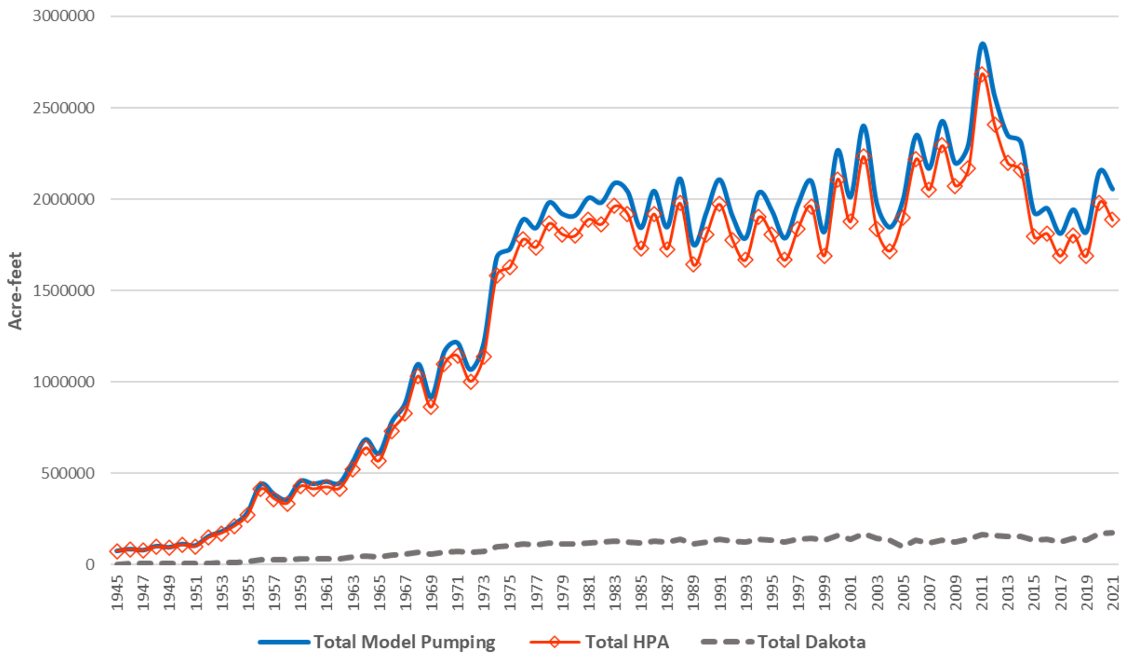

Figure 23. Estimated model pumping from the HPA and Dakota.

Arkansas River Ditch Service Areas

The model used a similar procedure as in Liu et al. (2010) to calculate the infiltration of diverted surface water in the irrigation canals and service areas, located along the Arkansas River, west of Garden City. The primary service areas used in the model are the Amazon, Farmers, Frontier, Garden City, Great Eastern, and the South Side (fig. 24). Some of these diversions have been around since the early 1880s and have undergone changes in shared diversions, different service areas, and transfers of water rights. Data for each diversion were provided by the KDA-DWR in a form suitable for the six-month time steps used in the transient model. In this updated model, the amount of seepage from the main canals is assumed to be roughly 2% of the total diverted water per mile and the amount of irrigation return flows in the service area to be 50%. The ditch infiltration rates are higher than the values used in the previous model (1% along canals and 25% in the service areas; Liu et al., 2010) as the higher infiltration rates are needed to better match the observed water levels in the ditch area. The ditch diversion points are represented as one-reach segments along the Arkansas River (fig. 24).

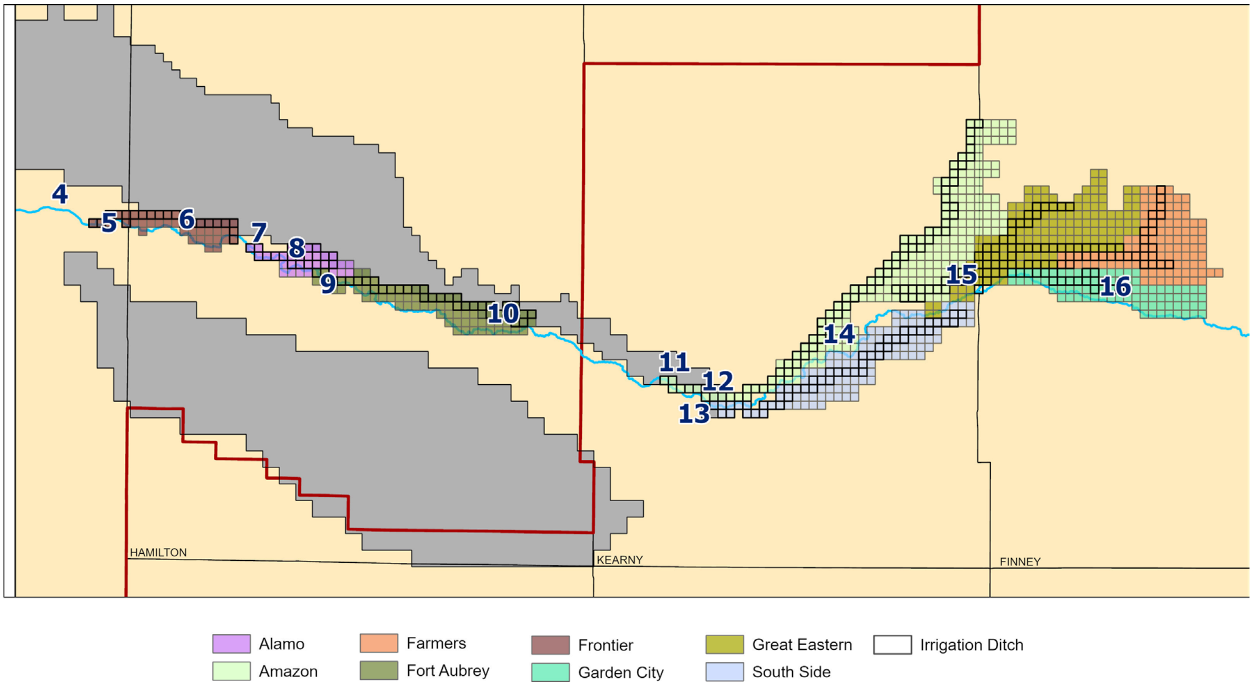

Figure 24. Ditch service areas, canals, and segment numbers along the Arkansas River.

Irrigation Return Flow

A certain amount of water applied by irrigation systems makes its way back to the aquifer in the form of irrigation return flow. The rate of this aquifer recharge is determined by a variety of factors, one of which is the efficiency of the irrigation system. Irrigation system types were added to KDA-DWR water-use reports in 1991. The reported ratio of system types each year was compared across GMD3 using zones that roughly separated areas north and south of the Arkansas and Cimarron rivers while maintaining the presence of the sand hills south of the Arkansas River (fig. 25). The area outside of GMD3 (and the core areas of GMDs 1 and 5) was assigned to its own zone.

The sandier areas of zones 2 and 4 were predominantly center pivot systems that transitioned to more efficient sprinkler systems during the late 1990s and early 2000s, whereas zones 1 and 3, dominated by more loess type deposits, had a much slower transition away from flood systems (fig. 26). Areas outside of GMDs have maintained the highest percentage of flood systems relative to more efficient sprinkler systems since 1991, which is likely the result of both the lack of enhanced GMD-management efforts and the greater presence of river valley systems that are not always suitable for center-pivot systems.

The irrigation return-flow percentages (relative to the total irrigation water pumped) used in past models were assigned to the system types reported in the water-use data. In order of decreasing return-flow percentages, those are the following: flood irrigation, 25%; center pivot and flood, 17%; center pivot, 9%; sprinkler other than center pivot, 9%; center pivot with low energy precision applicators (LEPA), 7%; and subsurface drip (SDI) in combination with other type, 4%. As farming operations have improved with technological advancements, so have irrigation efficiencies, thus reducing the amount of return flow that would infiltrate beyond the plants' roots.

The average percentage of return flow was then computed for each zone in the model from 1991 to 2021 based on the number of each system type and the assigned return-flow percentages for each type. It was assumed that flood irrigation was the only system type in use before 1955. Between 1955 and 1991, a smooth transition from flood to center pivot types for each irrigation system zone was then applied. Water use for each cell is multiplied by the average return-flow percentage to determine the total amount of water returning to the aquifer (fig. 27). Return flows are combined with natural precipitation recharge to form the total recharge at the land surface in the model.

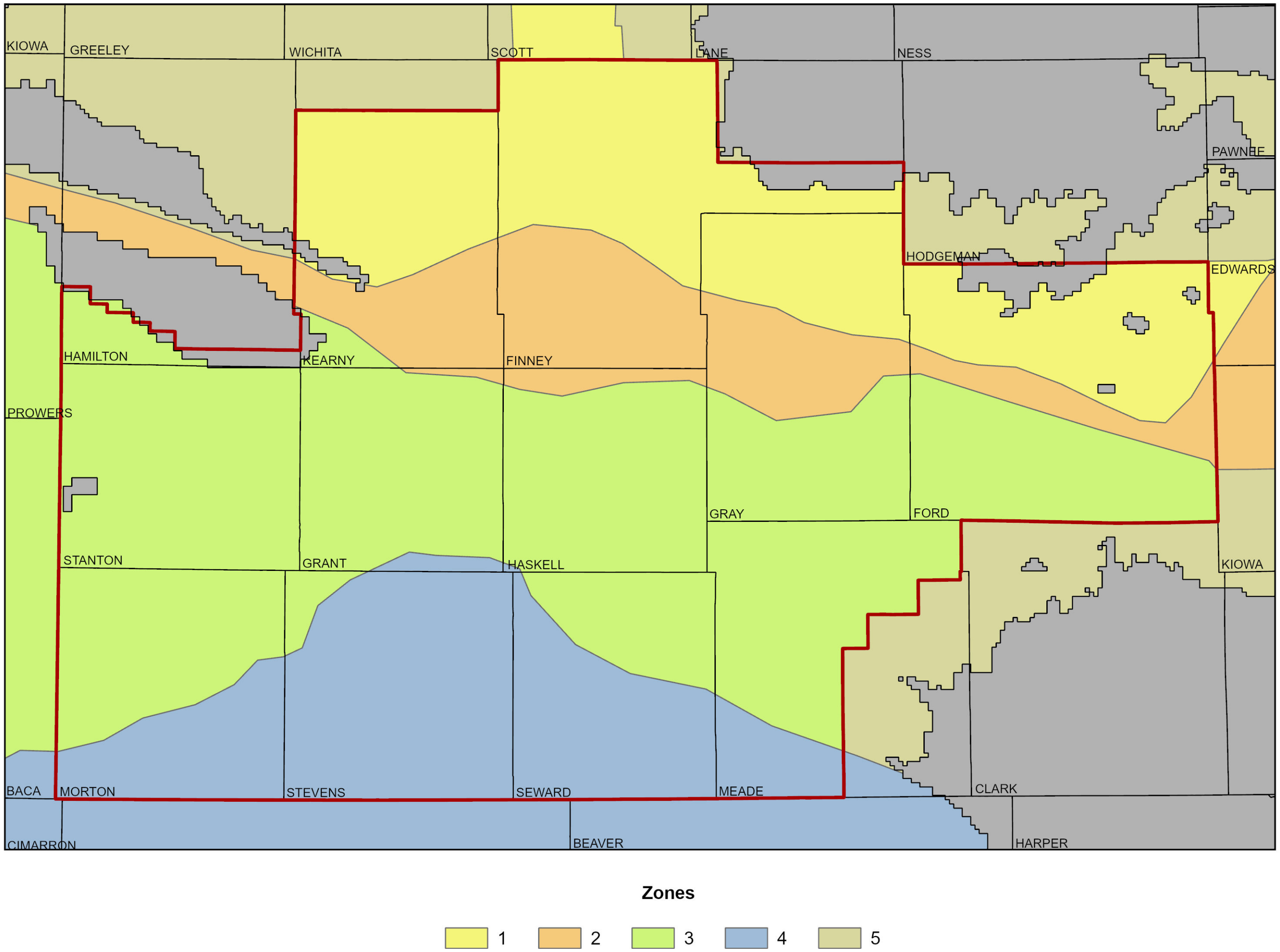

Figure 25. Zones for irrigation system type and return flows calculations.

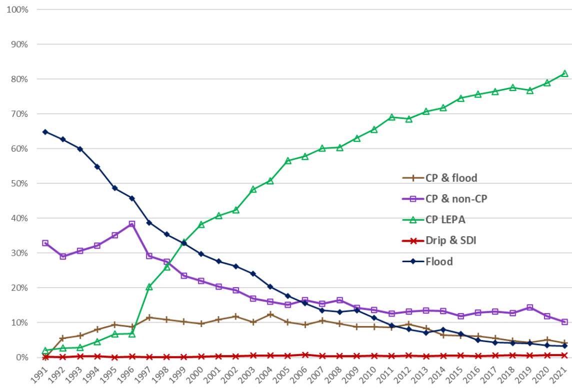

(a) Zone 1 — North of Ark River.

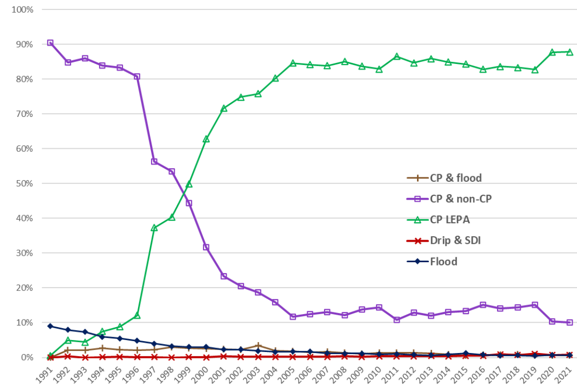

(b) Zone 2 — Sandhills

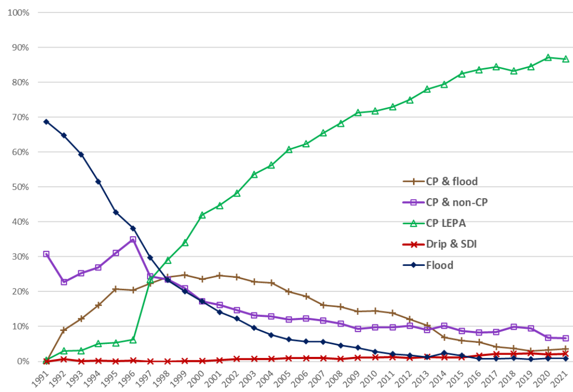

(c) Zone 3 — Between Ark and Cim. R.

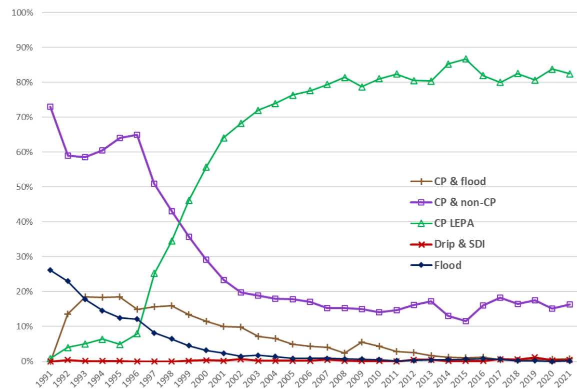

(d) Zone 4 — South of Cim. R.

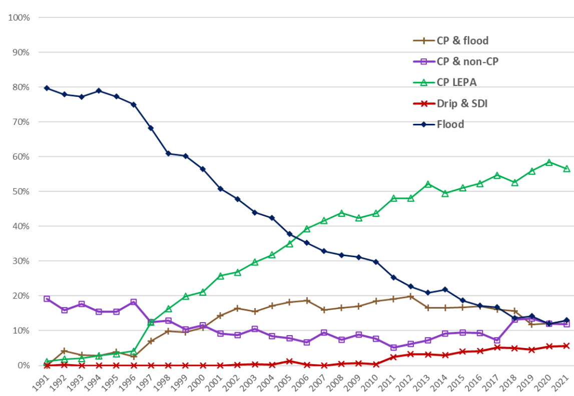

(e) Zone 5 — Areas outside GMDs.

.

Figure 26. Examples of reported irrigation system types by zone, 1991 to 2021. CP = center pivot, LEPA = low energy precision applicators, SDI = subsurface drip.

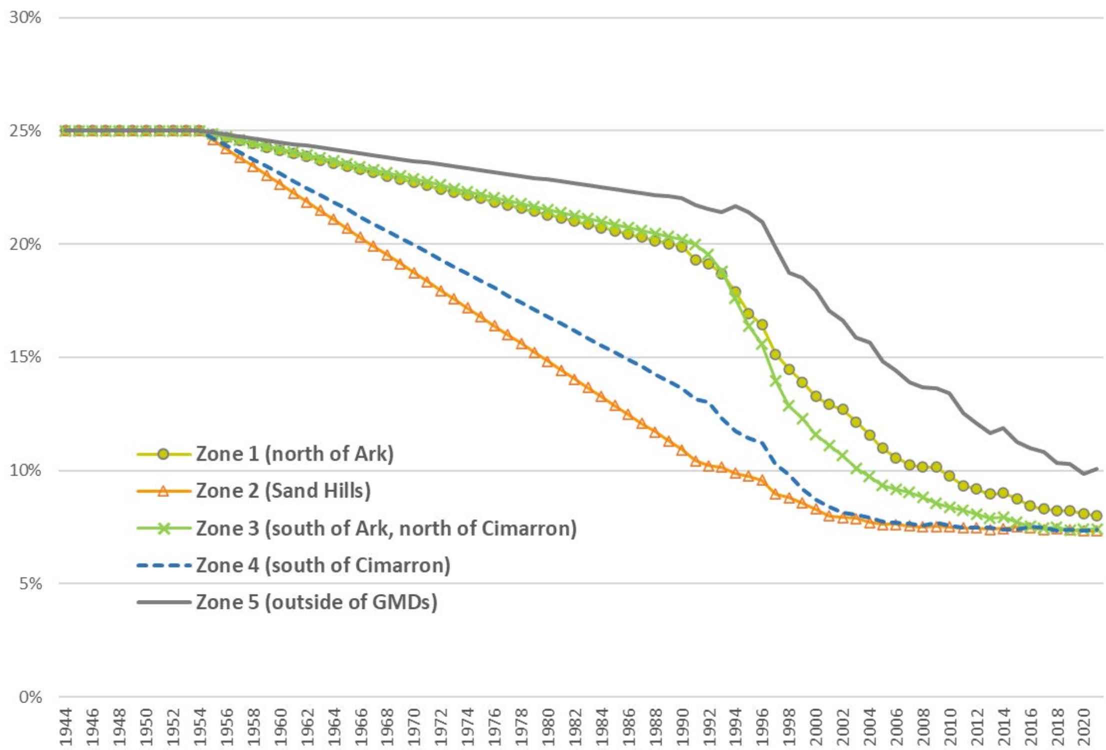

Figure 27. Average percentage of irrigation return flows for GMD3 and areas outside the district, 1945 to 2021.

Irrigated Land Fractions

The rate of precipitation-based recharge is higher for areas under irrigation than adjacent dryland areas, as the soil horizons are at or near saturation during the irrigation season. In all KGS modeling projects, the precipitation-based recharge was adjusted within model cells containing irrigation points of diversion. In practice, irrigation water is applied to field boundaries that can cross into model cells that may not contain pumping wells. To better estimate the irrigation-enhanced precipitation recharge, the irrigated land fraction within each model cell is calculated based on where water is applied, commonly referred to as the place of use.

Although KDA-DWR water-use reports contain information about the total number of acres irrigated each year, the location of the field boundaries is unknown. However, each water right's permit or certificate specifies the authorized place(s) of use and, for irrigation uses, the authorized boundaries are spatially categorized by 40-acre Public Land Survey System (PLSS) tract(s). The total net irrigated (referred to as "additional") acres for each 40-acre tract was summed and joined to a GIS layer representing 40-acre PLSS boundaries to spatially map the authorized places of water use across the model area.

Figure 28 shows the distribution of 40-acre tracts symbolized by the total net acres authorized as of 2020. For a tract with 40 acres (or more), it is assumed the entire tract is irrigated. For tracts with less than 40 acres ("partial" tracts), irrigation is authorized within that tract but the exact location and field boundaries can only be determined by looking at the original water-right permit or certificate on file with the KDA-DWR. For the model, partial tracts of less than 30 acres were deleted and not considered.

A single water right often has multiple places of use, whereas a single place of use can be authorized under multiple water rights. Water rights in the model domain were grouped based on how they overlap each other by point(s) of diversion or place(s) of use. The earliest priority date within the water-right group was assumed to represent the first point in time irrigation water was applied to the 40-acre places of use authorized under the group. It was assumed the senior water right covered all the acres listed under the 40-acre tracts and the junior water rights in the group did not add any additional acreage.

In Colorado, mapped field boundaries representing irrigated lands in 2020 were downloaded from the CDSS for the Division 2 — Arkansas River management area. The data set contained the permit ID number that matched the final permit well data used in the pumping file. The priority date of first use associated with the permitted wells was then assigned to the wells' respective place(s) of use to represent when water was first applied. Subsequent CDSS datasets showing irrigated places of use for 2016, 2015, and 2010 were reviewed to account for any missing fields. Oklahoma's Water Resources Board website provides a GIS layer of irrigated lands associated with water right permits. The date the tract was coded as filed was used to represent the priority date.

The place of use tracts from Kansas, Colorado, and Oklahoma were merged (fig. 28) and overlain with the model grid to calculate the percentage of overlap. The percentage of irrigated tracts within each cell was totaled to estimate the irrigated land fraction each year since the start of use (date of the senior water right for each tract).

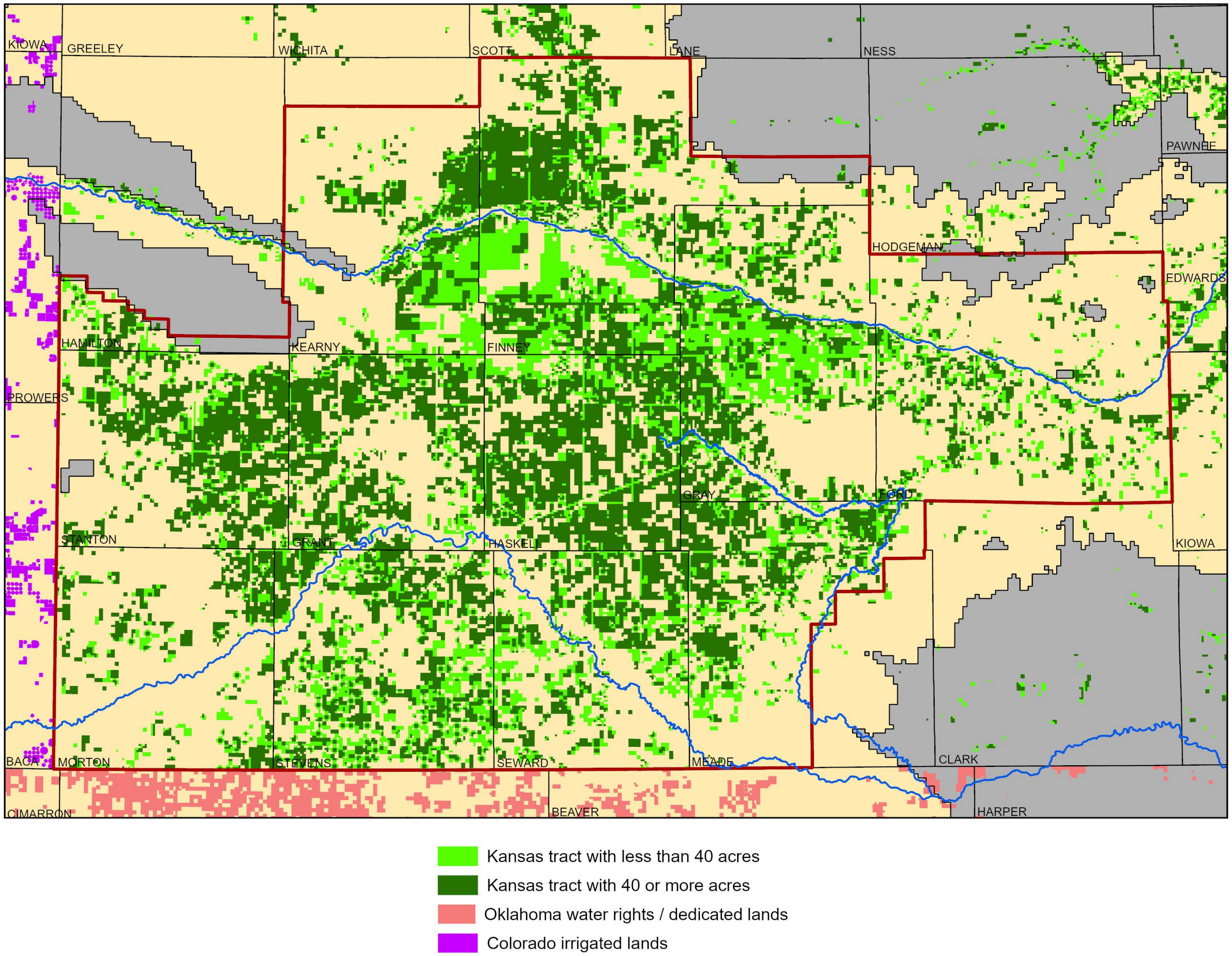

Figure 28. Irrigated places of use in 2020.

MODEL CALIBRATION AND SIMULATION

Like past KGS modeling projects, the updated GMD3 model is divided into two major simulation periods: a steady-state predevelopment period during which water levels remain relatively stable and a transient period during which groundwater development increases and water levels change over time. The predevelopment simulation establishes the conditions from which the subsequent transient model starts.

The major data sources for the predevelopment period are from the years before 1946, although some of the water-level data extends into the early 1950s. Contrary to the implications of the term "predevelopment" (a period of time representing the aquifer before it was extensively developed), the steady-state GMD3 model includes a relatively small amount of pumping, generally clustered around county seats. The transient period simulates groundwater conditions from predevelopment to 2021 (simulation ended in fall 2021 as 2022 water use was not available at the time the model calibration started), during which time groundwater pumping increased. The transient period is based on six-month time steps—a "summer," or growing, season from April to September and a "winter" period representing the months of October to March.

Model Characteristics

Pumping and Irrigation Return Flows

The earlier "Water Right Development" section of the report described how groundwater pumping is determined for the Kansas, Colorado, and Oklahoma portions of the model. The reported and regressed water usages are on an annual basis. For the model's six-month time steps, all irrigation usage was assigned to the "summer" period representing conditions from April to September. All other groundwater usage was proportioned with 56 percent occurring in the summer period and 44 percent occurring during the winter period. Irrigation return flows were added to the overall recharge input file used by the model for the summer period.

Stream Characteristics

All surface water streams are simulated in this project as rectangular channels with an underlying streambed. The streambed widths are set to a representative value of 100 ft for the Cimarron River and Crooked Creek (segments 1 through 3), and to a value of 220 ft for the Arkansas River (segments 4 through 16). The streambed thickness is assumed to be 5 ft for the Cimarron River and Crooked Creek and 3.28 ft for the Arkansas River. The streambed K for most stream segments is estimated to be 0.3 ft/d by model calibration, although some adjustments were made for portions of the Cimarron River and Crooked Creek to improve the simulation of groundwater levels in those areas. Flow data from all available USGS gages on the Arkansas River, the Cimarron River, and Crooked Creek were used in calibrating stream-aquifer interactions (fig. 17).

Evapotranspiration

Evapotranspiration (ET) could be a significant groundwater outflow in stream channels where the water table is close to the land surface. The maximum ET rate at the land surface was set to 1.64 ft/yr in the Arkansas River valley and 3.28 ft/yr in the valleys of the Cimarron River and Crooked Creek. During preliminary model simulations, a higher ET rate was found to improve the simulation of groundwater levels along the Cimarron River valley and Crooked Creek. The extinction depth was set to 10 ft below land surface, at which point the ET rate becomes zero. When the depth to water is between the land surface and extinction depth, the ET rate is linearly interpolated based on the depth to water relative to the extinction depth. In the model cells containing streams, the land surface that controls ET should be that of the stream valley where the depth to water is the shallowest. Therefore, for the stream cells where ET was computed, stream elevations instead of the average land surface elevations of the cells are used for ET calculation. This is considered to be more accurate than the average land surface elevation for a stream cell, which is dominated by the high elevations in the terraces (the width of each model cell is much larger than the stream width).

Time-Varying Specified-Head Boundaries

Time-varying specified-head boundaries are used for active model cells along the borders of the model's active area, as well as portions of the bedrock edges inside the model domain. Time-varying specified heads were established based on a time- and labor-intensive process of reviewing each model cell in relation to any surrounding water-level measurements. Water-level trends shown in the measurement history of wells in the vicinity of head boundaries were applied to the head-boundary cells.

Precipitation Recharge

Precipitation-based recharge was calculated based on the power function used in the original GMD3 model (Liu et al., 2010),

$$R = \begin{cases} 0, & P < P_0 \\ a\left(P - P_0\right)^b, & P \geq P_0 \end{cases},$$

where R is precipitation recharge (infiltration), P is precipitation at a given model cell in each six-month time step, P_0 is threshold precipitation above which groundwater recharge occurs, and a and b are the coefficients of the power function. The precipitation recharge calculated above represents the amount of infiltration through the surface soil of non-irrigated lands. The enhancement to precipitation recharge in irrigated fields is computed as an additional source of recharge water as discussed in the next section.

The model divides the recharge-precipitation power functions into four zones (fig. 29) and two time periods (summer and winter). Recharge in the main aquifer generally averages less than one inch per year, while the stream channels have higher recharge rates, accounting for enhanced recharge that occurs during runoff events. The actual recharge rate varies for each model cell as the precipitation amounts change between different cells and time steps. For the same precipitation, the recharge rate is higher in the non-growing season than in the growing season as surface evapotranspiration is much more significant in the growing season (higher temperature and more consumptive use by plants). The power-function parameters P_0, a, and b are determined by matching observed water levels and streamflows to simulated values during model calibration.

Enhanced Precipitation Recharge from Irrigated Land Fractions

The enhancement of precipitation recharge by irrigation is computed by multiplying the precipitation recharge by a constant factor for the irrigated acreage in each cell over time, based on the priority date of the most senior water right. That factor is set to 1.0 based on the previous model study in southwest Kansas by Liu et al. (2010), which is applied proportionally based on the fraction of the model cell that is irrigated. Because the enhanced precipitation recharge by irrigation is added to precipitation recharge computed using the calibrated precipitation-recharge curve (assuming no irrigation), the total precipitation recharge in the irrigated fields is twice what it would be if the fields were not irrigated.

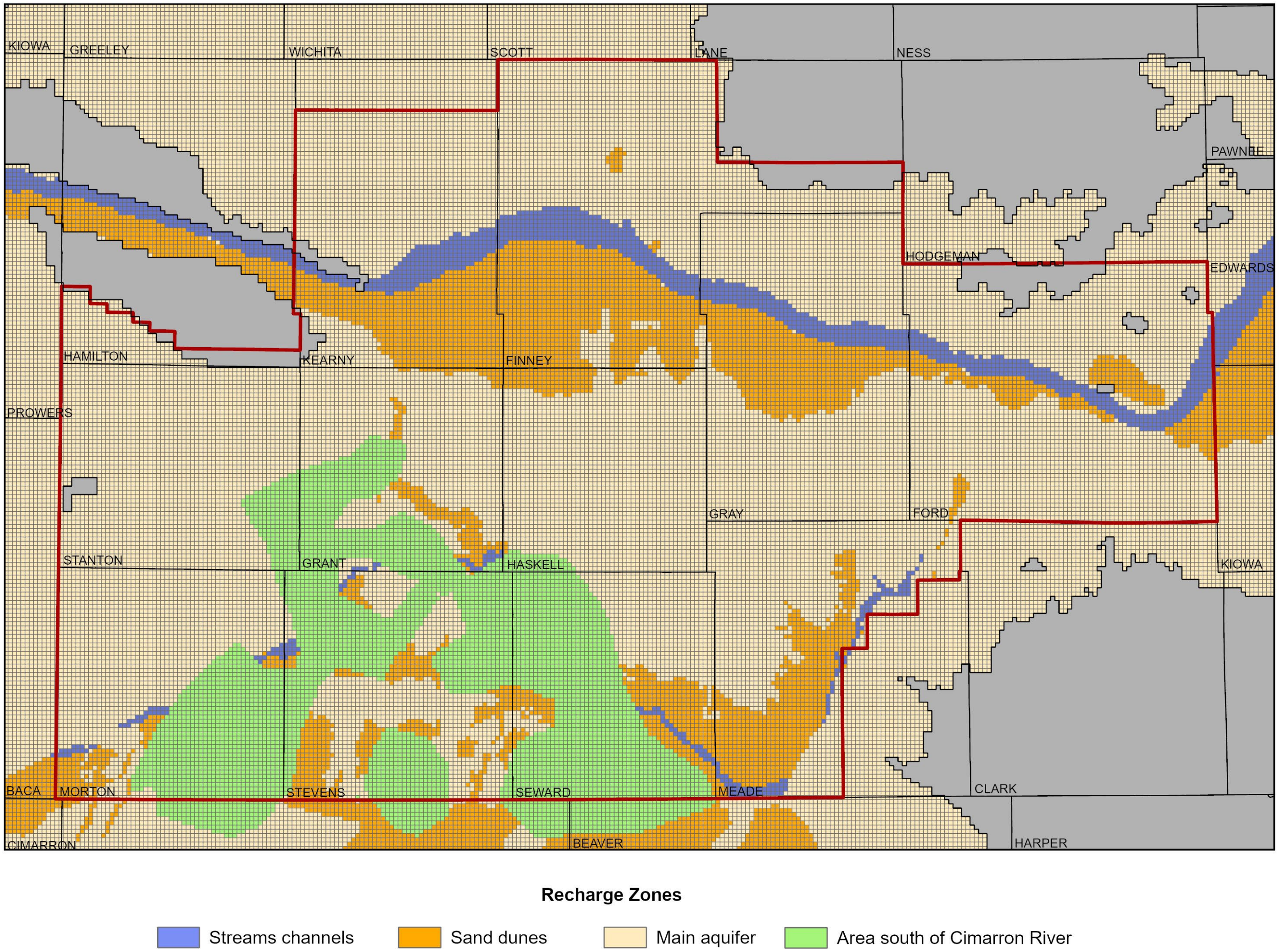

Figure 29. Recharge zones for precipitation-based recharge.

Delayed Recharge

All recharge originating from the land surface is subject to a delay function, first used in the GMD1 model (Wilson et al., 2015), to simulate the vertical distance that surface recharge water must travel in the vadose zone before reaching the water table. To simulate the vertical movement of water through the vadose zone, all surface-based recharge, either from precipitation over a non-irrigated area, enhanced precipitation recharge over irrigated lands, or ditch and irrigation return flows, is assumed to move down through the vadose zone at a constant velocity and diffusivity (diffusivity describes how water molecules spread out at the average velocity and is illustrated in fig. 30). This movement can be expressed by the following function:

$$R(z,t) = \frac{R_0}{2\sqrt{\pi D t}} \exp\left(-\frac{(z-ut)^2}{4Dt}\right),$$

where R(z,t) is the recharge rate (L) at time t and depth z in the vadose zone resulting from a recharge event at the surface R_0 (L). The parameters *u* (L/T) and *D* (L^2/T) are the velocity and diffusivity of water movement in the vadose zone, respectively, both of which are dependent on properties of vadose zone materials. In this work, *u* and D were estimated to be 59 ft/yr and 57 ft^2/yr during preliminary model simulations. R_0 includes precipitation recharge, precipitation recharge enhancement by irrigation in the irrigated lands, and the ditch and irrigation return flows; it is computed for each model cell and six-month time step. For water-table depth L and model time step t_L, the amount of water that has reached the water table from R_0 is calculated as

$$R_T = \int_0^{t_L - t_0} R(L,t)u\,dt\ ,$$

where R_T is water-table recharge from R_0 and t_0 is the time step at which R_0 is computed. To compute the total water-table recharge from the surface at a given time step, the model considers R_0 over all previous time steps that have $R_T > 0.0001R_0$ (i.e., time step t_0 is included in the calculation if greater than 0.01% of surface recharge R_0 reaches the water table). The water that enters the water table from R_0 during a given time step is the difference between the R_T computed at the end of that step and the R_T computed at the beginning of that step.

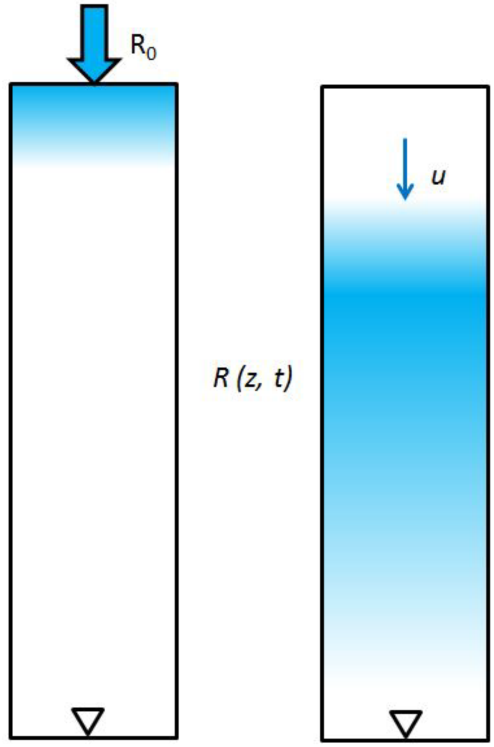

Figure 30. Schematic of the movement of surface recharge in the vadose zone.

Lagged Drainage by Low-Permeability Sediments

As the water table declines, the previously saturated material above a layer of low-permeability sediments might become perched (fig. 31). Some of this water will eventually drain down to the water table with time. The rate of lagged drainage is a function of both the permeability and thickness of the underlying low-permeability barrier.

For this modeling work, the lagged drainage of water after the water table fall is simulated with the following function:

$$W(t) = cd\exp\left(-d(t - t^*)\right), \quad t > t^*$$

where W(t) is the amount of water draining out at time t, t* is the time when the water table fell below the geological unit, c is the total amount of water that is available for delayed drainage per unit volume of dewatered sediment, and d is the exponential decay coefficient (the larger the coefficient, the smaller the amount of drainage). Both c and d are treated as model calibration parameters whose values are determined by matching the simulated water levels to observations.

Figure 31(c) shows the curves of lagged drainage for five different geological units (see table 1 for the detailed information about each categorical unit). The sand unit was estimated to have the most available water for lagged drainage, followed by sands and gravels, silts and sands, clays and silts, and clays. The curves for different lithologic units have the same slope, as it is assumed that a common clay layer with the lowest permeability acts as the barrier for lagged drainage from all lithologic units subject to dewatering.

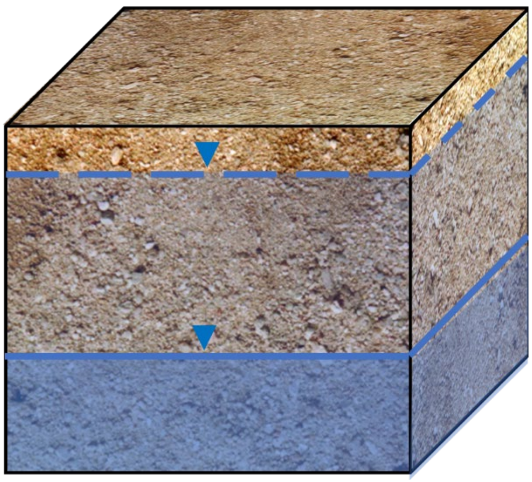

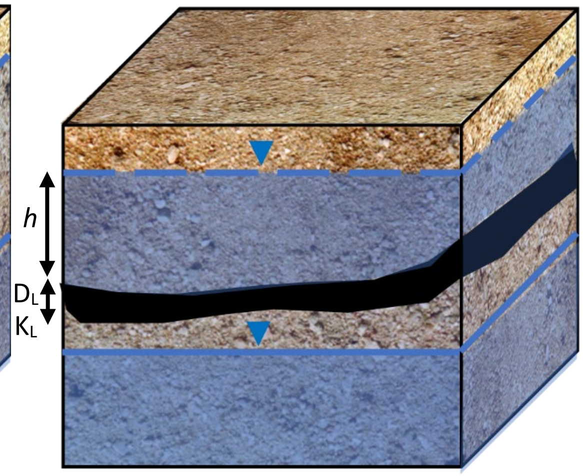

(a) Quick drainage without barriers (b) Drainage delayed by barriers

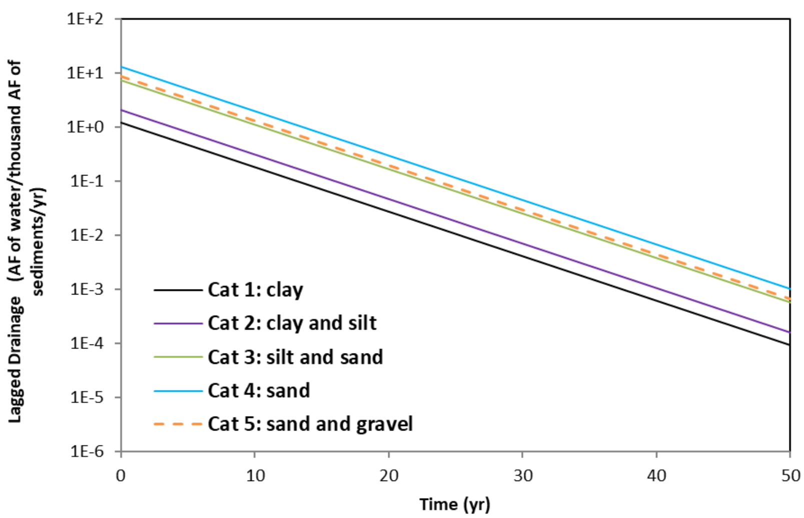

(c) Lagged drainage rate from different lithology units

Figure 31. Lagged drainage by low-permeability sediments: (a) quick drainage without barriers, (b) drainage delayed by barriers, and (c) lagged drainage rate from different lithologic units. In (c), time zero represents the time when a lithologic unit becomes dewatered (water level declines below the unit). The vertical axis represents the amount (AF) of water released from a thousand AF of a lithologic unit after initial dewatering. The slope of curves represents the rate of perched water moving through the low-permeability barrier, which is a function of its permeability and thickness.

Hydraulic Conductivity and Specific Yield

As described earlier, the code developed for the HyDRA project was used to develop a three-dimensional grid describing the proportional distribution of five different categories of the material composing the aquifer throughout the model domain, based on drillers' logs contained in the WWC5 database and other sources in Colorado and Oklahoma. A special program was developed to allow water levels generated for each time step in MODLFOW to intersect with this three-dimensional grid to compute proportion-weighted averages of K and Sy in each cell of the model.

Figure 32 shows the HyDRA lithology-based estimated average K for the interval between the predevelopment water levels and the bedrock surface based on the estimates of K for each of the lithology categories listed in table 1. The average K across the active area in GMD3 in 2020 was approximately 142 ft/day. The highest K estimates occur along the Cimarron River valley in Grant, Haskell, Stevens, and Seward counties, as well as in the southeastern corner of Stanton County. In those areas, K values were manually increased to allow the model to better match observed water levels during the predevelopment period. During the transient portion of the model, two water levels are associated with each model cell, representing the starting and ending water levels for each transient time step. K is computed for the lithological units between the average of the two water levels and bedrock.

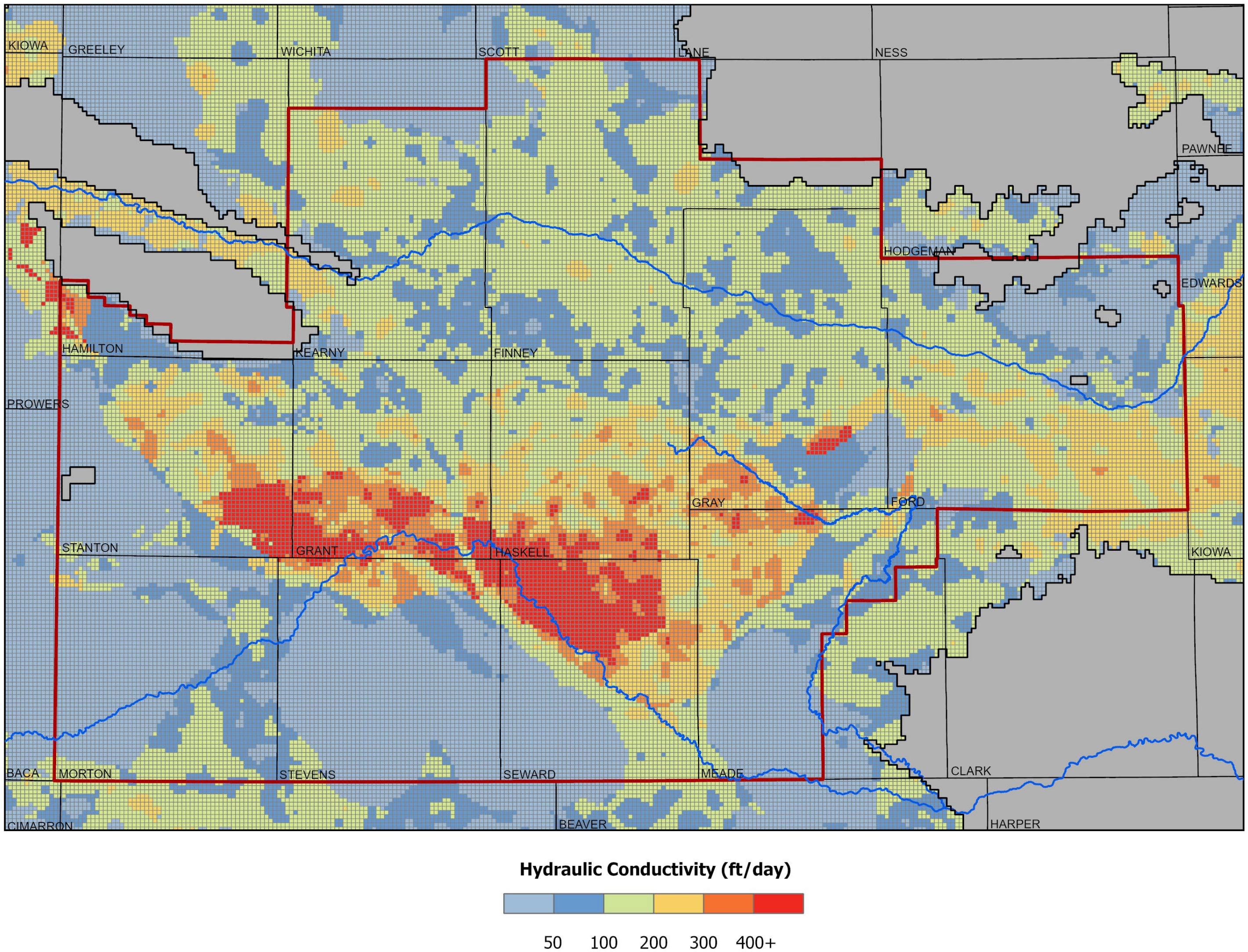

Figure 32. Vertically averaged K based on five calibrated HyDRA lithologic classifications for the interval between the predevelopment water table and the bedrock surface.

Using a method developed from Liu et al. (2021), Sy was estimated from the HyDRA lithology categories combined with a data-driven, water-balance approach developed by Butler et al. (2016) for estimating the average Sy over an area from a linear relationship between annual water use and annual water-level change. Individual water-balance analyses based on data from 2005 to 2021 were conducted for 12 areas representing different county and unique areas (fig. 33a). In each area, an average specific yield value was estimated from the slope of the best-fit line computed by the relationship between groundwater usage and water-level change (fig. 33b). Next, the proportions of five major lithologic categories (table 1) were computed for each of 11 water-balance areas (the thin area was not included due to the lack of significant aquifer thickness). Finally, the specific yield was calculated for each of the five lithologic categories by comparing the lithology-based Sy to the estimated Sy values from water-balance analyses. As a result, the specific yield values for the five lithologic categories were determined as 0.005 for clays, 0.005 for clays and silts, 0.005 for silts and sands, 0.11 for sands, and 0.13 for sands and gravels. Clearly, much of aquifer storage is from the permeable units of sands, and sands and gravels, while the rest of geologic units contribute less than 6% of groundwater pumping.

Using the Sy value estimated for each of the five lithologic units, the Sy for each model cell for any given year can be computed based on the intersection of water levels with the lithology grid at that time. Figure 34 shows the Sy derived from the lithology category–water balance approach from the 2020 water table to the bedrock surface, which averages 0.053 across GMD3. This is substantially less than traditional estimates of Sy for numerical models (Liu et al., 2010) but comparable with the value determined through the water-balance relationships (Whittemore et al., 2023). For the transient portion of the model, the vertically averaged Sy values representing the interval between the upper and lower water levels during each model time step were computed.

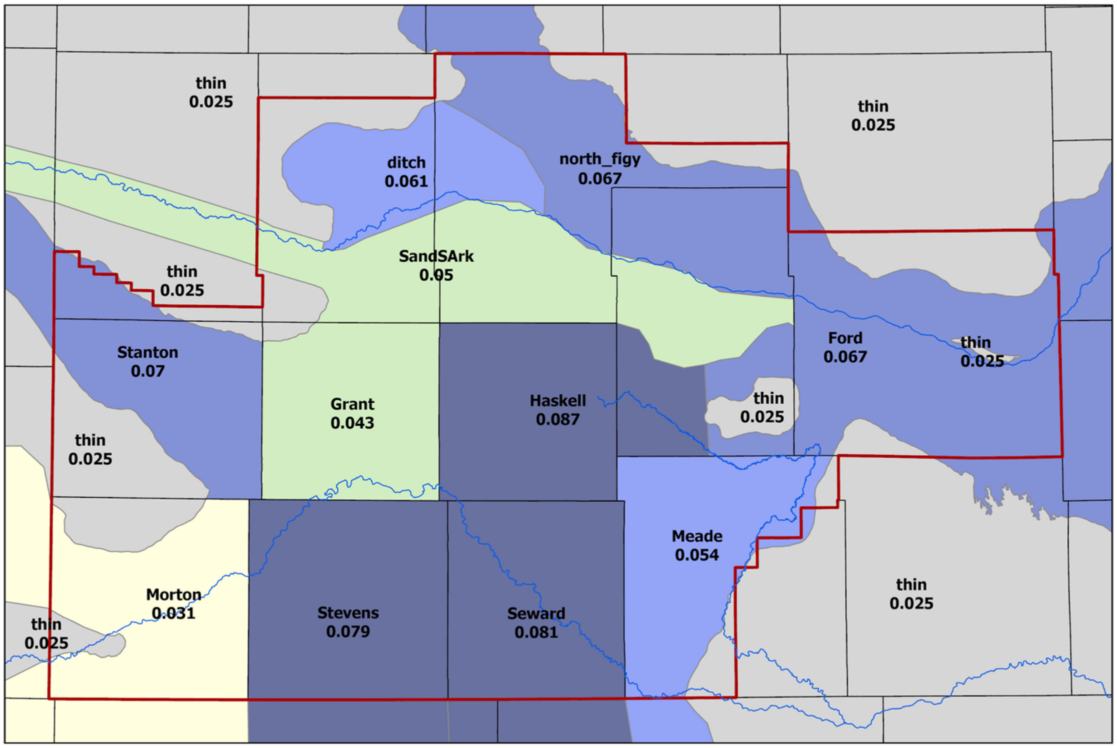

(a)

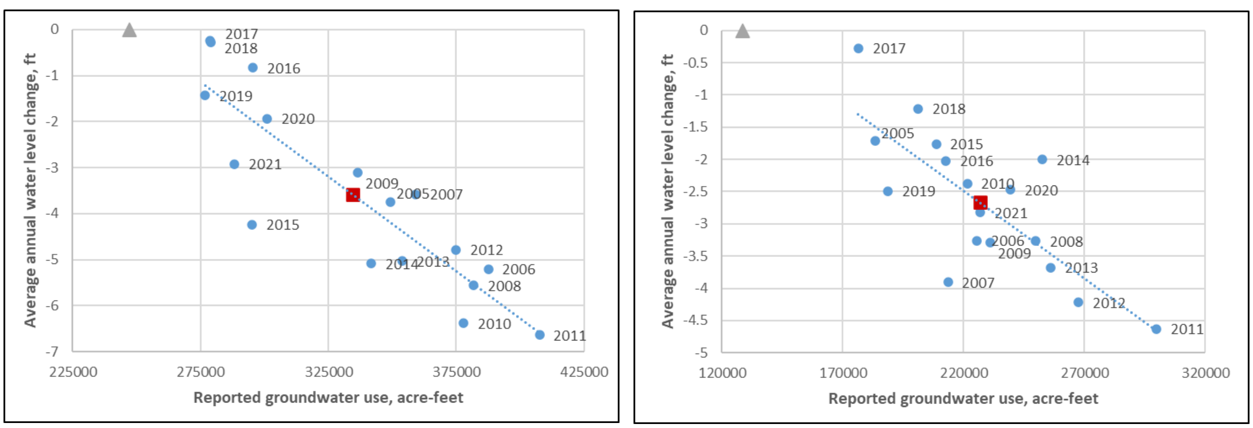

(b)

Figure 33. (a) Map of specific yield estimates from water-balance analyses in 12 sub-areas and (b) average annual water-level change versus annual water use from 2005 to 2021 for Stevens County (left) and the sand hills south of the Arkansas River labeled as "SandSArk" (right) in GMD3. Dashed line is the best-fit line to the plot. Overall average conditions for both water use and water-level change are represented by the maroon squares. The estimated water use under stable water-level conditions is shown by the gray triangle (i.e., net inflow). Sy is calculated from the inverse of the slope of the best-fit line times the area. Total pumping reduction at which stable water levels could be achieved, termed Q-stable, is calculated as the difference between the average reported use and the net inflow.

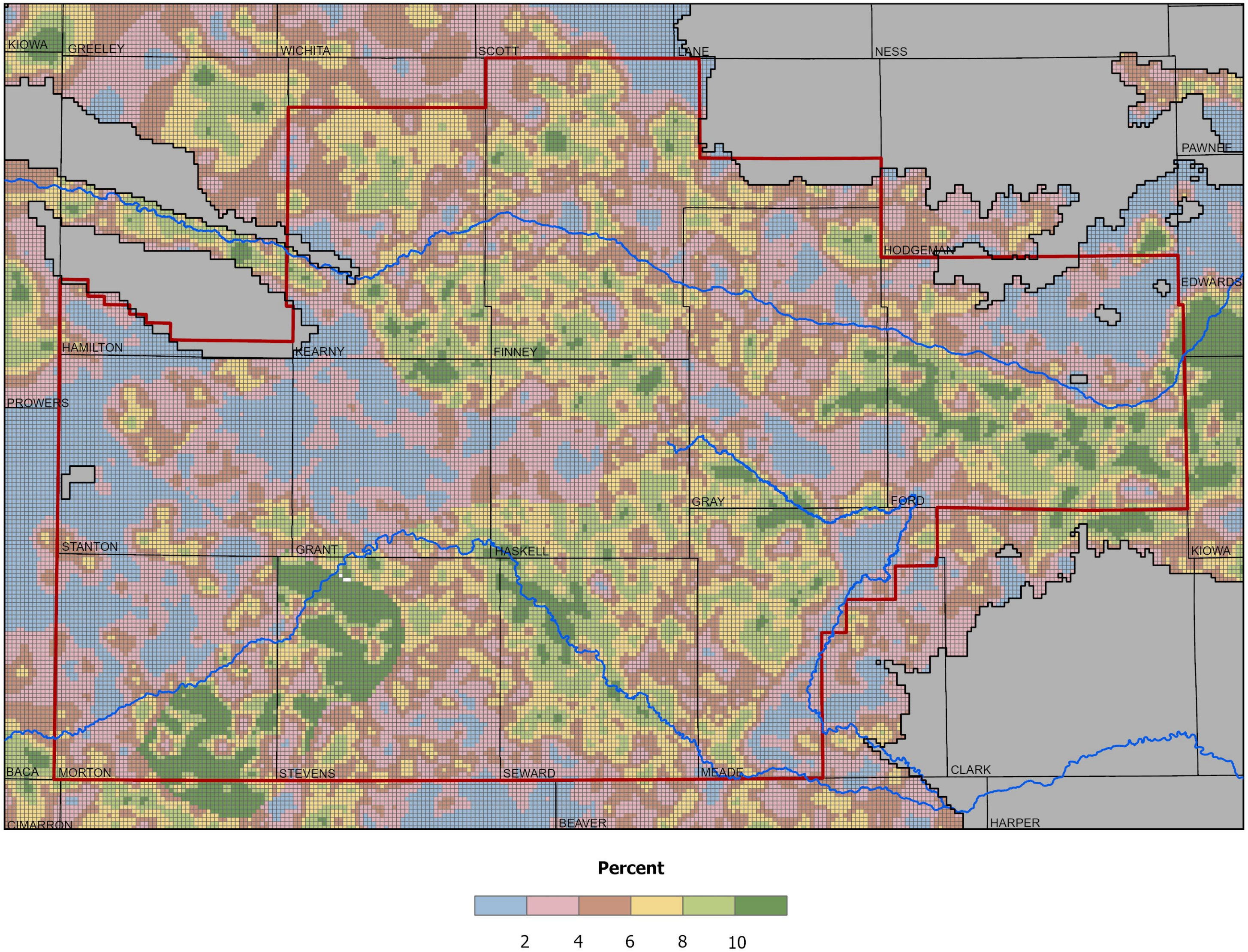

Figure 34. Vertically averaged Sy from HyDRA lithologic classifications and county- and area-based water-balance analyses between the 2020 water table and bedrock.

Model Calibration

Because of our imperfect understanding of the hydrologic conditions in GMD3, some model parameters, especially those that are key contributors to aquifer budget calculations (e.g., K and recharge rate), need to be adjusted so that the simulated results match the observed data to the best extent possible. This process is generally referred to as model calibration. For the GMD3 model calibration, data for comparison with the simulated results include water levels for a number of wells in the active model area from predevelopment to January 2021. For the wells that have multiple water levels during the transient period, the change between consecutive measurements is used. The water-level change provides a more sensitive indicator of aquifer response to different hydrologic processes during the transient simulation.

The model parameters whose values were adjusted during calibration are 1) the threshold precipitation P_0 for recharge and power function coefficients a and b for the four recharge zones, 2) the lagged drainage function coefficient c for all five lithologic categories that describes how much water is available for lagged drainage in each category, 3) the lagged drainage function coefficient d that describes the slow rate at which the perched water moves through the underlying barrier to become water table recharge, 4) the hydraulic conductivity for five lithologic categories, and 5) the streambed hydraulic conductivity. The calibration process was performed with the parameter estimation program PEST (Doherty, 2004).

Figure 35 shows the calibrated precipitation recharge curves for the recharge zones. Note that in the non-growing season, the threshold precipitation at which water starts to infiltrate through the topsoil (i.e., recharge starts) is lower, resulting in a larger recharge rate than that in the growing season for the same precipitation amount. For a given precipitation amount, precipitation recharge is lowest in the main aquifer and much higher in stream channels. Table 1 lists the calibrated values of K for different lithologic categories, and fig. 31c shows the calibrated lagged drainage curves for each of the five lithologic categories. The calibrated value of streambed K is 0.3 ft/d.

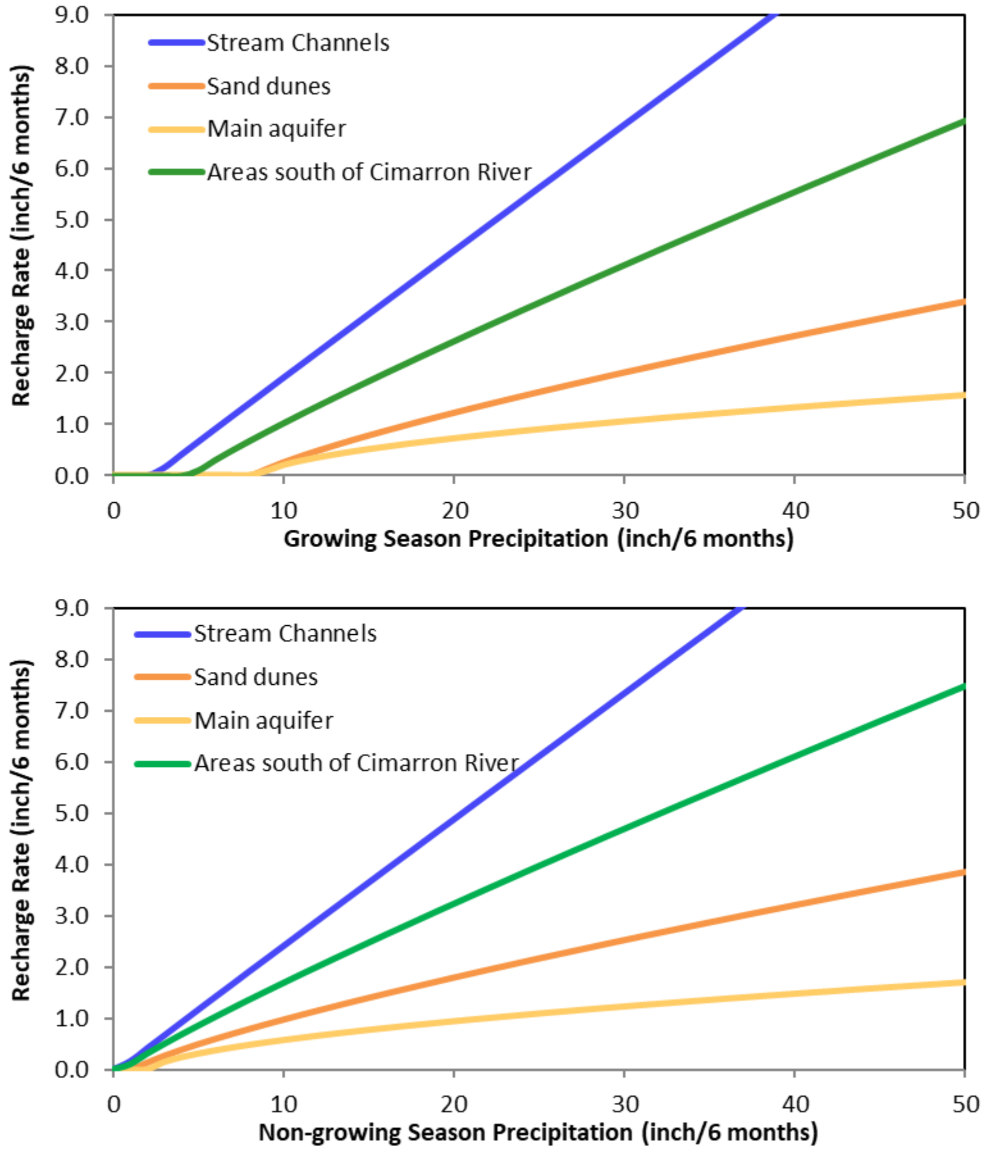

Figure 35. The calibrated precipitation recharge curves for different recharge zones in the growing (top) and non-growing (bottom) seasons.

Figure 36 (top) shows the simulated versus observed predevelopment heads from the PEST calibration. As the figure illustrates, the simulated heads generally align well with the observed values during predevelopment. Figure 36 (bottom) shows the simulated versus observed transient water-level changes from the PEST calibration. Water-level changes were computed by subtracting the later water levels from their corresponding earlier values, so that positive values indicate a decline of water table with time. Figure 37 shows the simulated versus observed streamflows at all USGS gages.

Table 3 lists the mean residual, mean absolute residual, and root mean square of residuals of the PEST calibration data targets. The mean residual is given as the mean of observed minus simulated values, the mean absolute residual is the mean of the absolute values of observed minus simulated values, and the root mean square is the root mean square of observed minus simulated values. The mean residuals for both the water levels and streamflows are small, indicating the calibrated model provides a good overall representation of the observed aquifer responses and stream-aquifer interactions (the hydrograph and streamflow detailed comparisons are presented in "Calibrated Model Results" section). All the different error statistics are comparable to previous KGS models for the other GMDs in western Kansas.

Table 3. Mean residuals, mean absolute residuals, and root mean square of residuals for model calibration targets.

	Number of data	Mean residual	Mean absolute residual	Root mean square (RMS) of residuals
Predevelopment water level (ft)	2,161	-16.0	26.1	37.0
Transient water-level change (ft)	5,412	-0.20	2.55	4.29
Streamflow (ft^3/sec)	977	-1.16	29.1	53.93

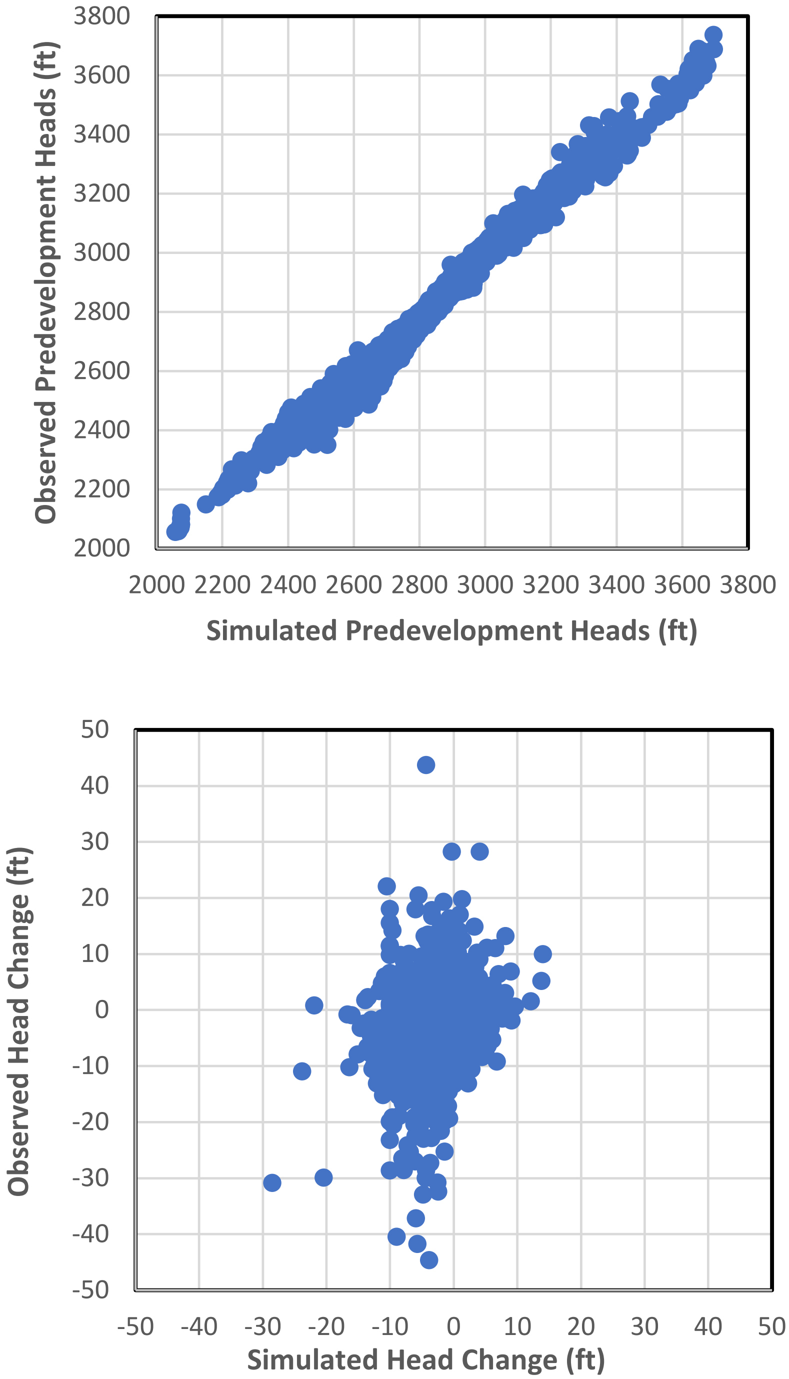

Figure 36. Observed versus simulated heads from the calibrated model: predevelopment water levels at all calibration wells (top) and water-level change at all calibration wells during the transient period (bottom). Transient water-level changes are computed between two adjacent winter water-level measurements (separated by one or more years for each well).

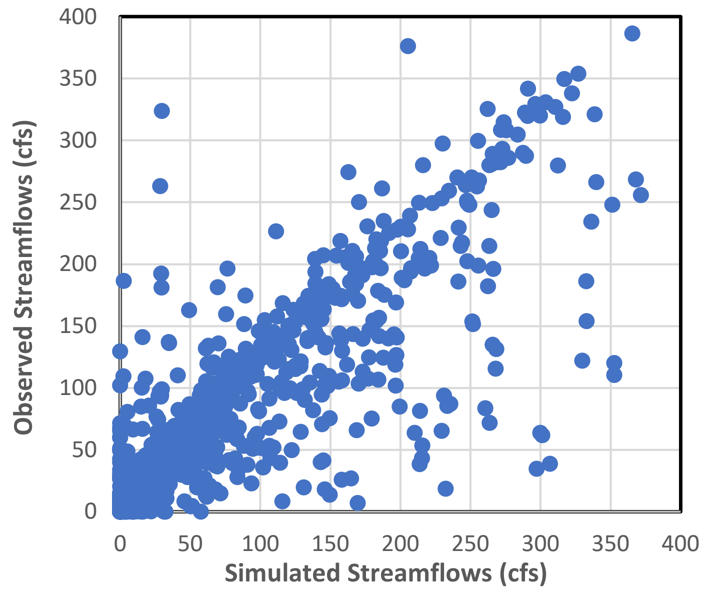

Figure 37. Observed versus simulated streamflows from the calibrated transient model. Plotted values are the average streamflows during the growing (April–September) and non-growing (October–March) seasons.

Sensitivity Analysis

Table 4 lists the sensitivities of simulated responses to different model parameters during calibration. The relative sensitivity of a parameter *p* is computed as (Liu et al., 2010)

$$RS_p = \sqrt{\frac{1}{N}\sum_{i=1}^{N}\left(\frac{\partial d_i}{\partial p/\acute{p}}\right)^2}$$

where ∂p is the small perturbation around the calibrated parameter value $\acute{p}$; ∂d_i is the change in the model-simulated groundwater level or streamflow at observation *i,* and *N* is the total number of observation data points used in the sensitivity calculation. In table 4, p11 and p14 are the threshold precipitation for recharge to start during the growing and non-growing seasons, respectively, in the main aquifer, and p12 and p13 are the precipitation recharge power function coefficients for the main aquifer. Similarly, p21 through p24 are the precipitation recharge parameters defined for the stream channels; p31 through p34 are the precipitation recharge parameters defined for the sand dunes; and p41 through p44 are the precipitation recharge parameters defined for the area near the Cimarron River and to its south. Parameters hy1 through hy5 are the hydraulic conductivity for the first through fifth lithologic categories. Parameters lagc1 through lagc5 are the lagged drainage function coefficient c for the first through fifth lithologic categories, respectively. The parameter lagd is the lagged drainage function coefficient d for all lithologic categories. The parameter strk is the streambed hydraulic conductivity. Compared to other parameters, the hydraulic conductivity of lithologic category 1 (clays) has the lowest sensitivity, indicating its value does not have a significant impact on model calibration. This is expected because the calibrated K value for clays is 0.000114 ft/d and even a 10-time increase would not change the K values calculated for each model cell due to the much higher K values for the other lithologic categories. On the other hand, the hydraulic conductivities of lithologic categories 3 (silts and sands), 4 (sands), and 5 (sands and gravels) have a much higher sensitivity, indicating the calibrated values of those three parameters have a much more significant effect on the match between the simulated and observed heads and streamflows.

Table 4. Relative sensitivities of different model parameters during the PEST calibration.

Parameter	Relative Sensitivity	Parameter	Relative Sensitivity	Parameter	Relative Sensitivity
p11	2.46	p12	3.46	p13	5.17
p14	4.03	p21	1.86	p22	1.71
p23	3.20	p24	12.66	p31	10.43
p32	3.25	p33	2.49	p34	8.63
p41	2.04	p42	2.24	p43	3.24
p44	1.93	hy1	0.00	hy2	4.22
hy3	308.65	hy4	1785.59	hy5	1783.42
lagc1	2.22	lagc2	0.78	lagc3	1.66
lagc4	3.16	lagc5	2.86	lagd	3.52
strk	2.37				

Calibrated Model Results

Water Levels

Figures 38 to 41 show a series of comparisons of the simulated groundwater elevations from the calibrated model to interpolated observed data for predevelopment, 1970, 1980, 1990, 2000, 2010, and 2020. The contour maps (top) are an indication of flow directions and water-level gradients, and the cell-based shaded maps (bottom) show absolute differences between the simulated and observed water levels. The model starts the predevelopment period by underestimating the heads in eastern Stanton County, which progressively grows in expanse over the transient run until the final decade, when the simulated and observed heads converge. In a similar manner, the model overestimates water levels in Morton, Seward, and Meade counties during the predevelopment period. This overestimate is gradually reduced during the transient run; however, another area of overestimation appears in Haskell County. The mismatch in all cases is much smaller than that in the previous model by Liu et al., 2010.

Figures 42 to 45 compare the model's simulated water-level changes between predevelopment and 1970, subsequent 10-year intervals up to 2020, and predevelopment to 2020. At the regional scale, the larger discrepancies in the model simulated changes tend to occur in Stanton and western Grant counties where the Dakota aquifer plays a stronger role in the overall water usage. The model simulates declines observed through the core counties of the district and replicates the inflows to the aquifer from the Arkansas River and ditch systems, especially in the 1980s and 1990s.

Figure 46 plots the location of 116 monitoring wells, labeled by the row and column of the model cell in which each well is located, that were used in the model calibration. The hydrographs for these wells are plotted, by county, in figs. 47 to 63 and show the water levels labeled by the internal ID number of the observation well and the simulated water levels of the cell, labeled by row and column, in which it is located. All hydrographs are plotted to the same scale, using 20-foot intervals over a 200-foot elevation range. In cases where either the simulated or observed water levels exceed this range, the Y axis labels are bolded and dark red in color.

Stream Flows

Figures 64 and 65 show the comparisons between the simulated and observed streamflows at USGS gages on the Arkansas River, Cimarron River, and Crooked Creek. For most of the years, the simulated streamflows match the observed values very well at all the gages. Because no tributary inflows from precipitation events are considered in this model, the simulated streamflows only represent the impacts of stream-aquifer interactions (and ditch diversions on the Arkansas River) as the river water moves downstream. This is particularly the case at both the Forgan and Englewood gages, where the simulated streamflows provide a good representation of the baseflow contributions from the aquifer but do not capture the flow peaks that are likely a result of storm events.

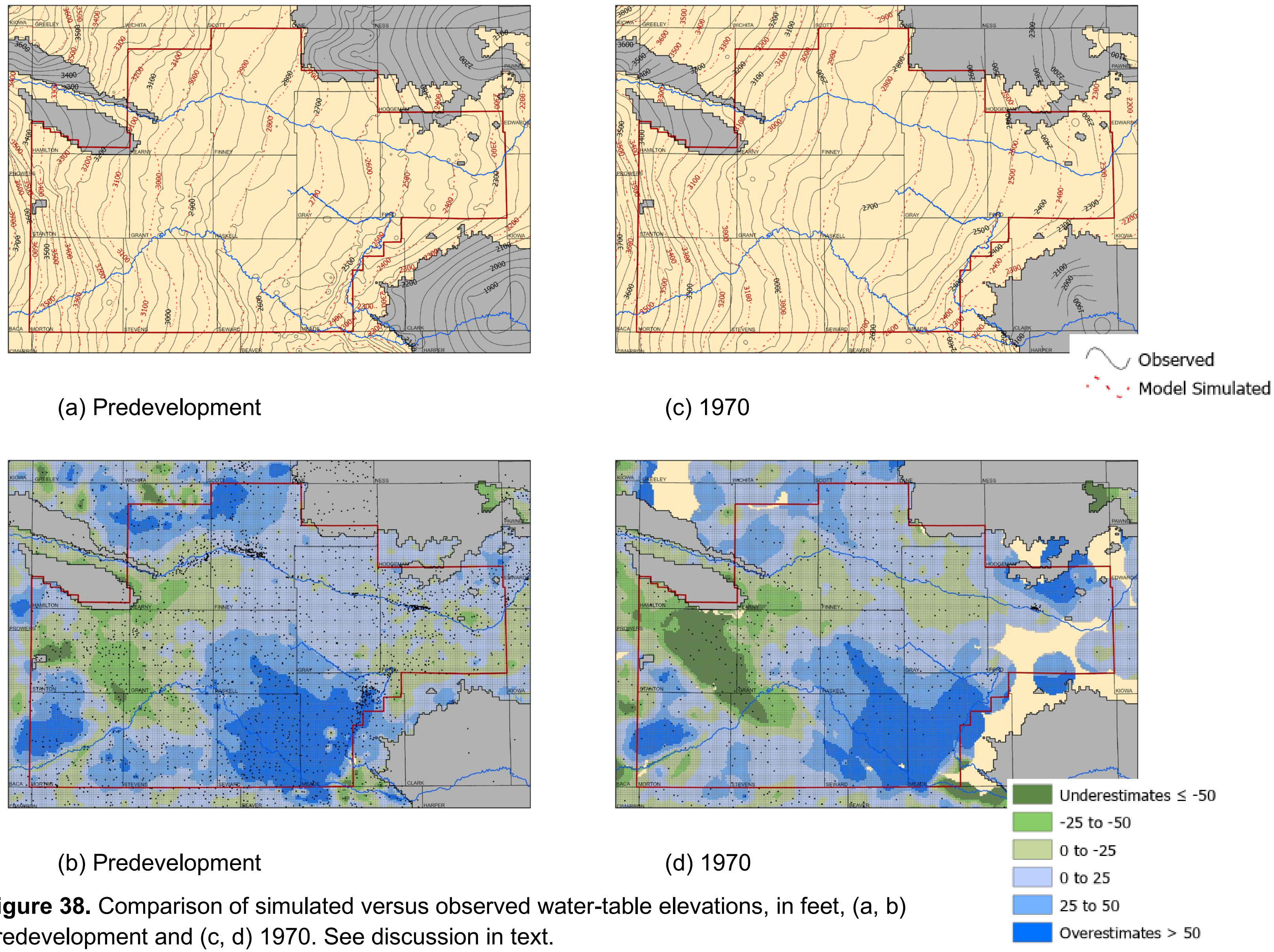

Figure 38. Comparison of simulated versus observed water-table elevations, in feet, (a, b) predevelopment and (c, d) 1970. See discussion in text.

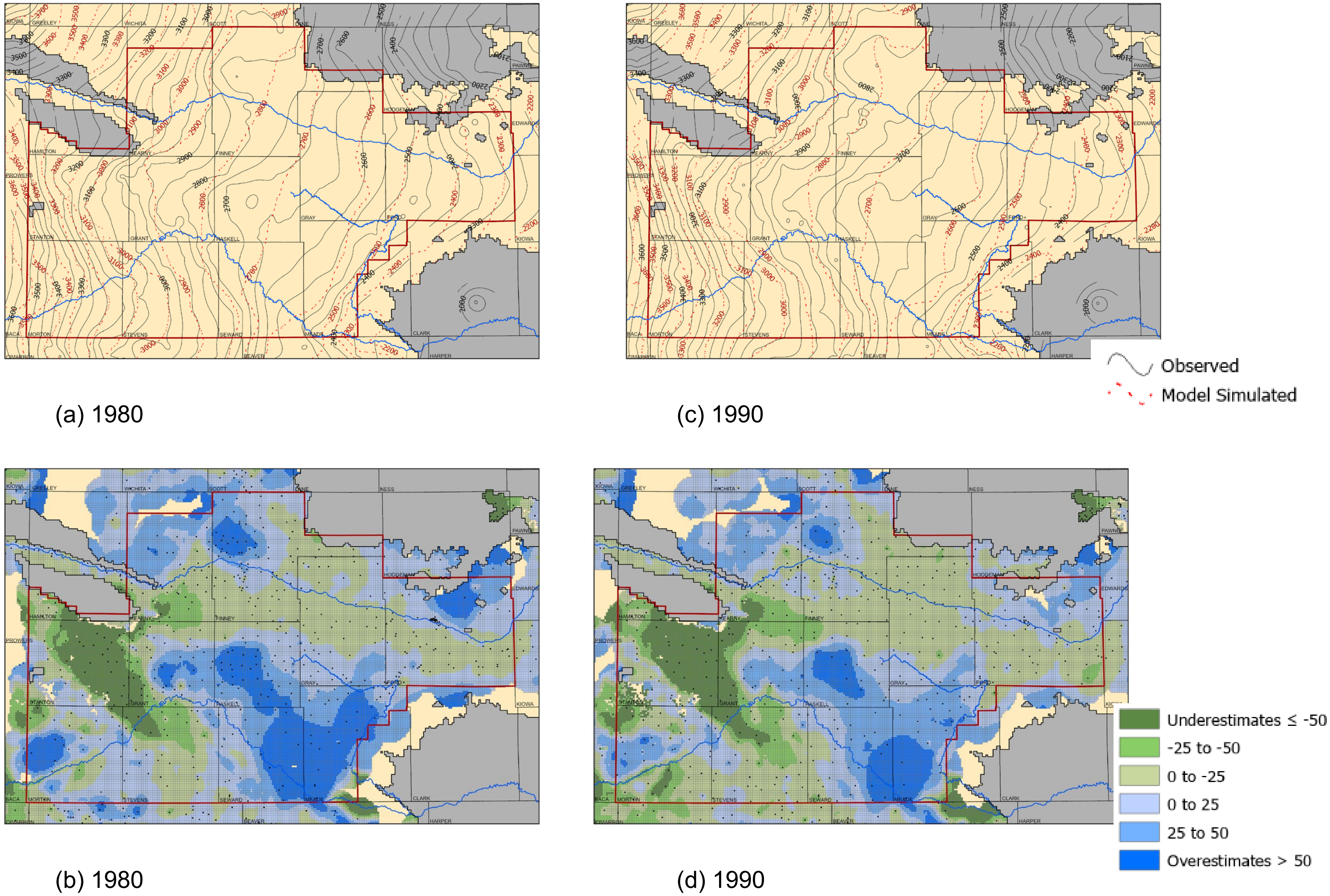

Figure 39. Comparison of simulated versus observed water-table elevations, in feet, (a, b) 1980 and (c, d) 1990. See discussion in text.

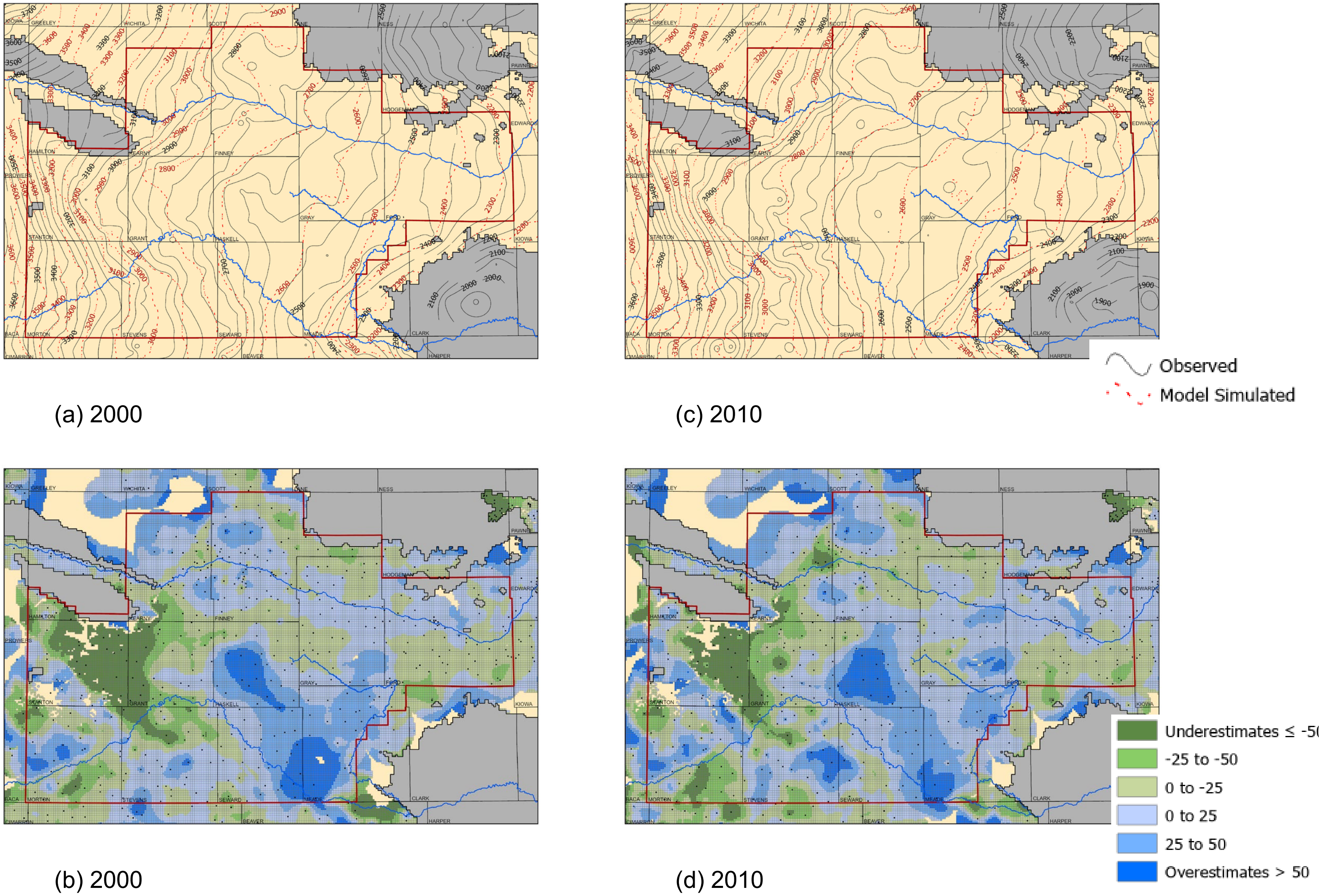

Figure 40. Comparison of simulated versus observed water-table elevations, in feet, (a, b) 2000 and (c, d) 2010. See discussion in text.

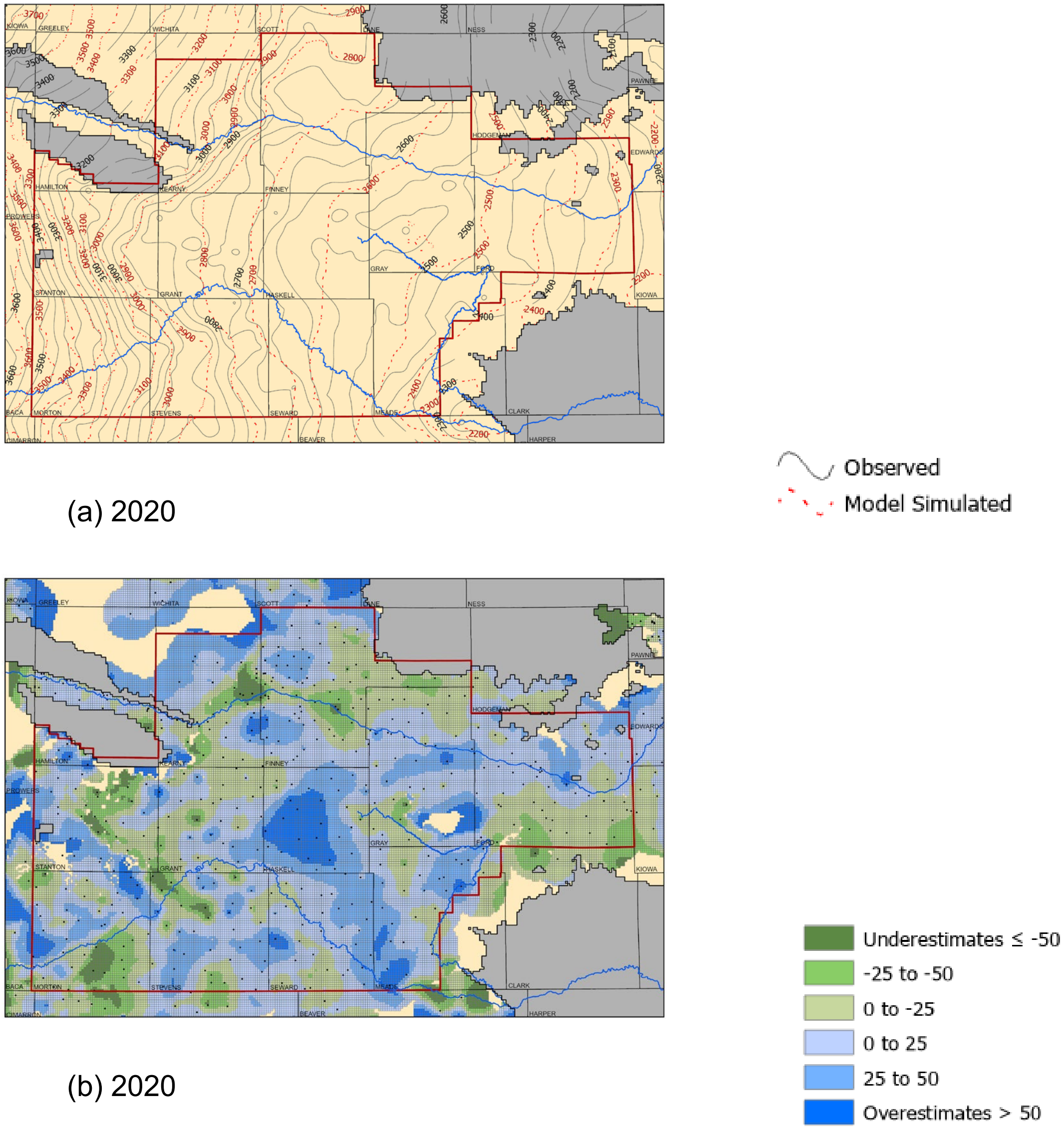

Figure 41. Comparison of simulated versus observed water-table elevations, in feet, 2020. See discussion in text.

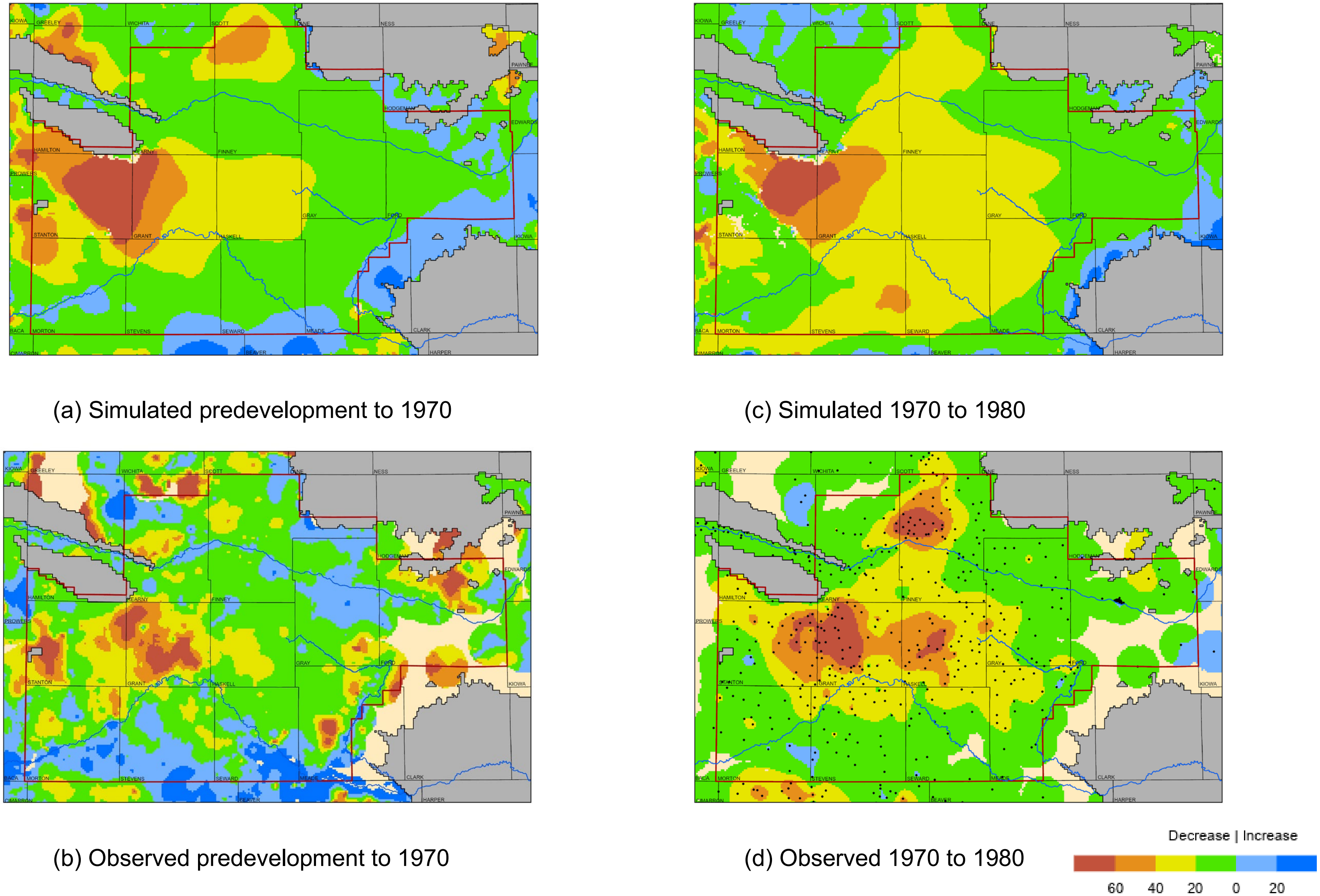

Figure 42. Simulated versus observed water-level changes, in feet, for the intervals (a, b) predev. to 1970 and (c, d) 1970 to 1980.

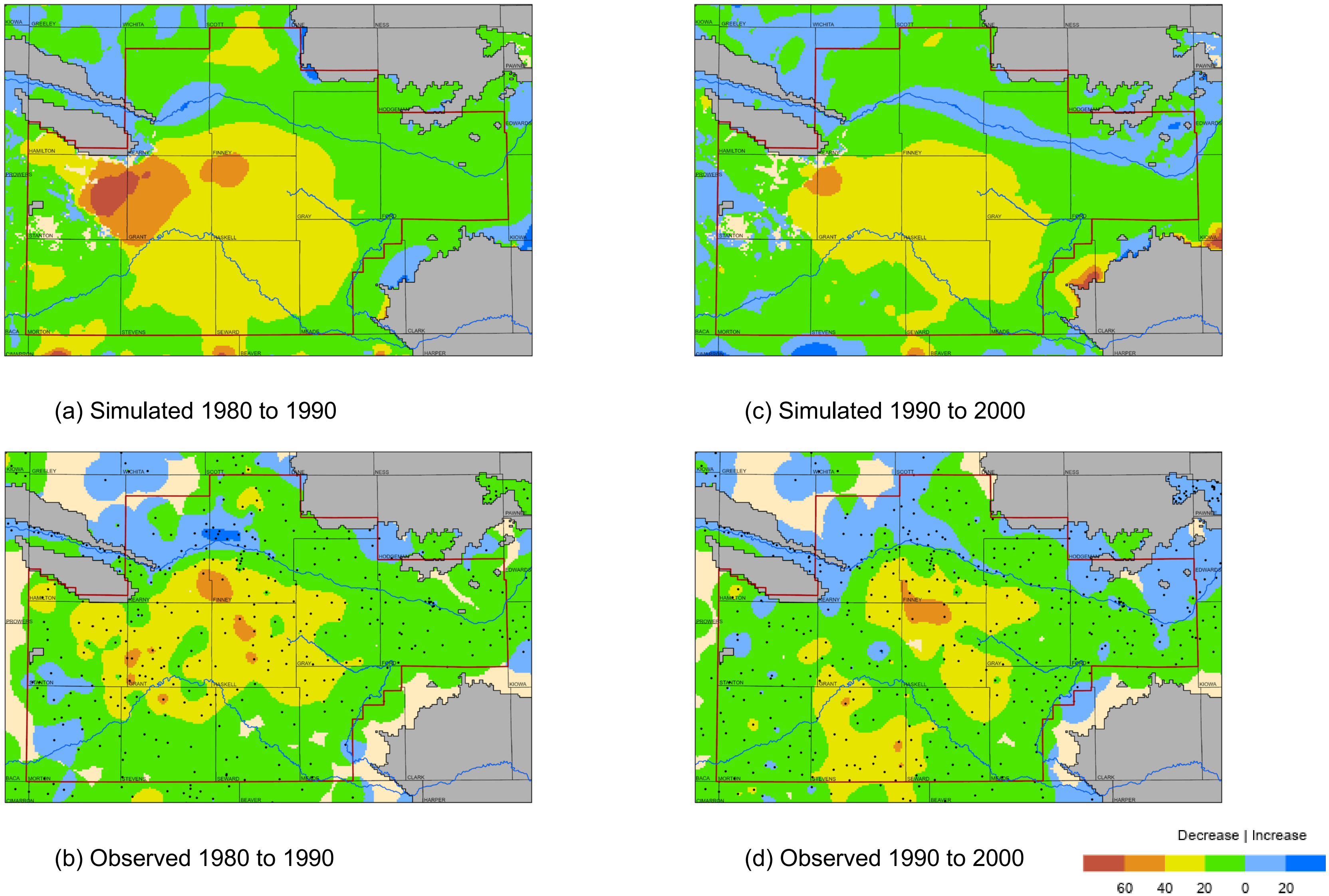

Figure 43. Simulated versus observed water-level changes, in feet, for the intervals (a, b) 1980 to 1990 and (c, d) 1990 to 2000.

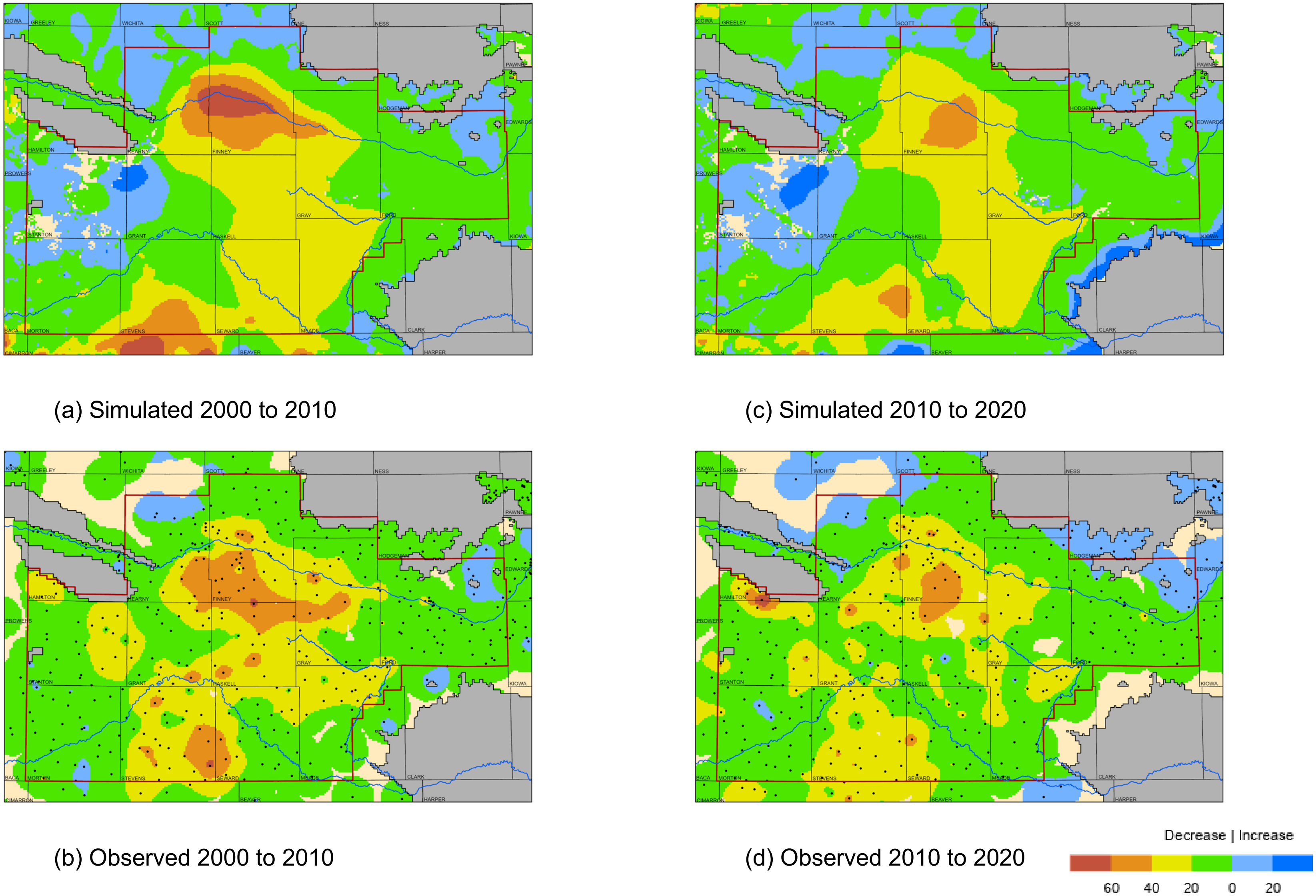

Figure 44. Simulated versus observed water-level changes, in feet, for the intervals (a, b) 2000 to 2010 and (c, d) 2010 to 2020.

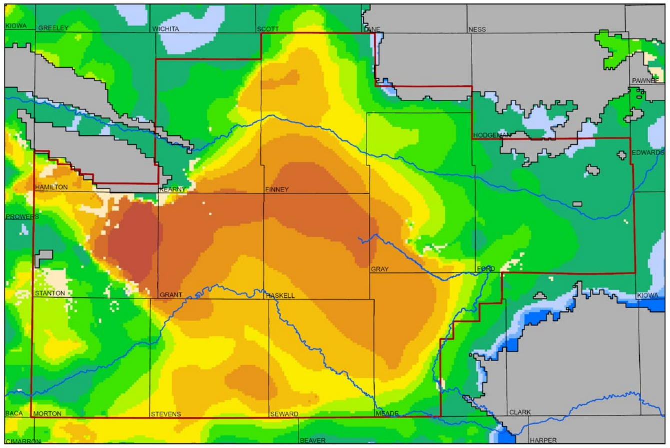

(a) Simulated predevelopment to 2020

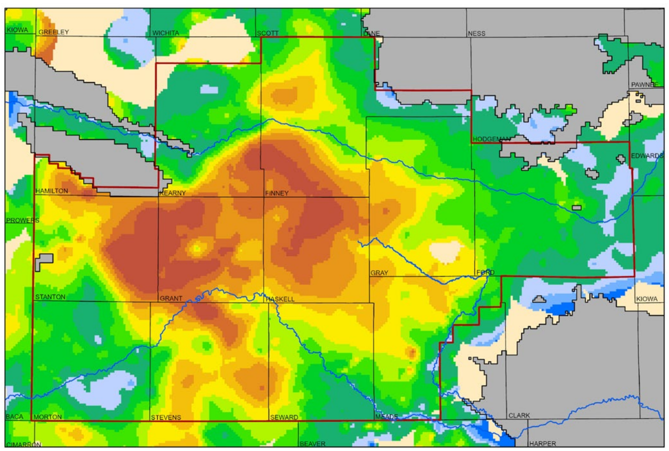

(b) Observed predevelopment to 2020

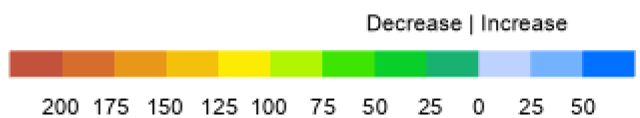

Figure 45. (a) Simulated versus (b) observed water-level changes, in feet, for the interval predevelopment to 2020.

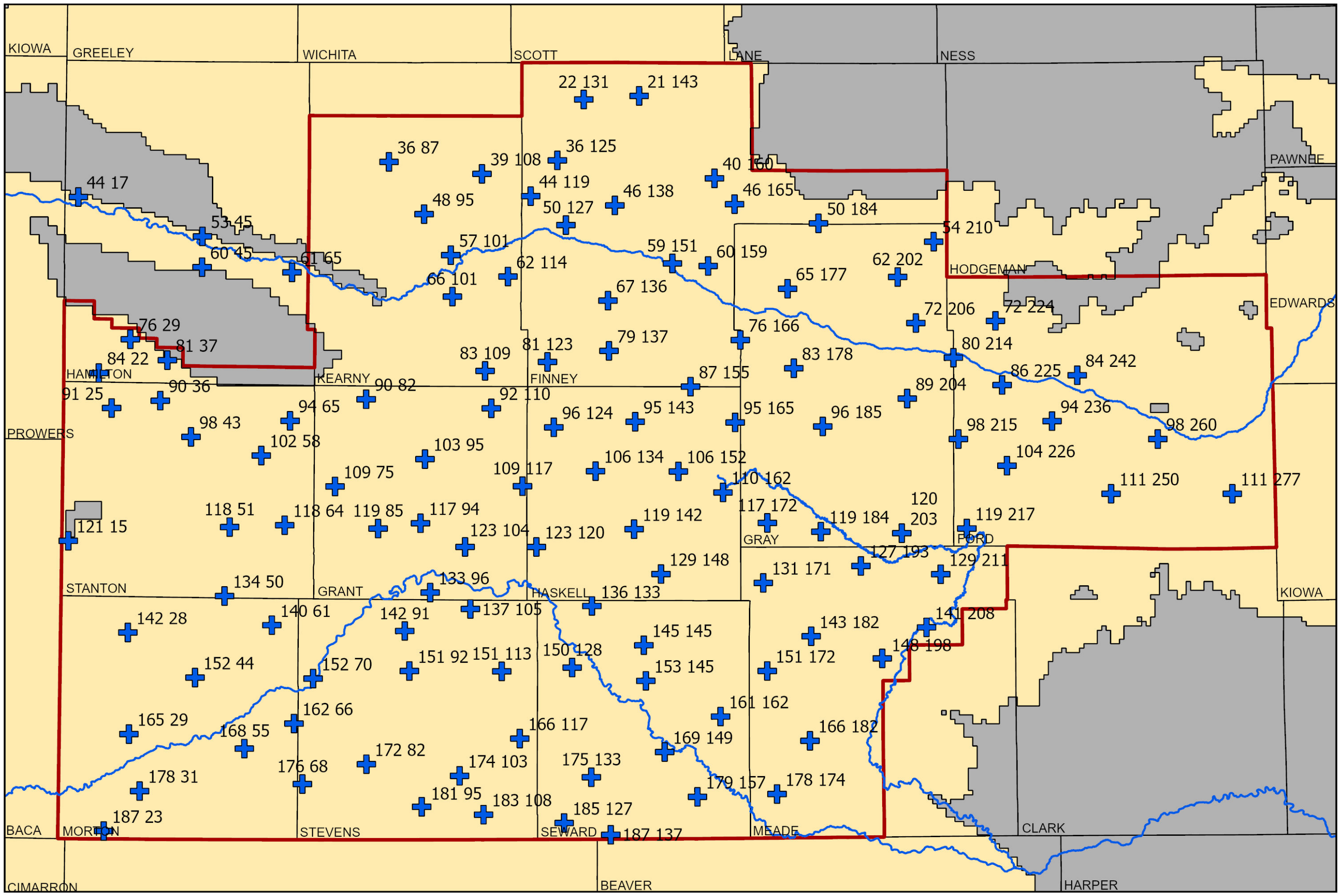

Figure 46. Wells with long-term measurement records used for model calibration, labeled by row and column of the model cell in which each well is located.

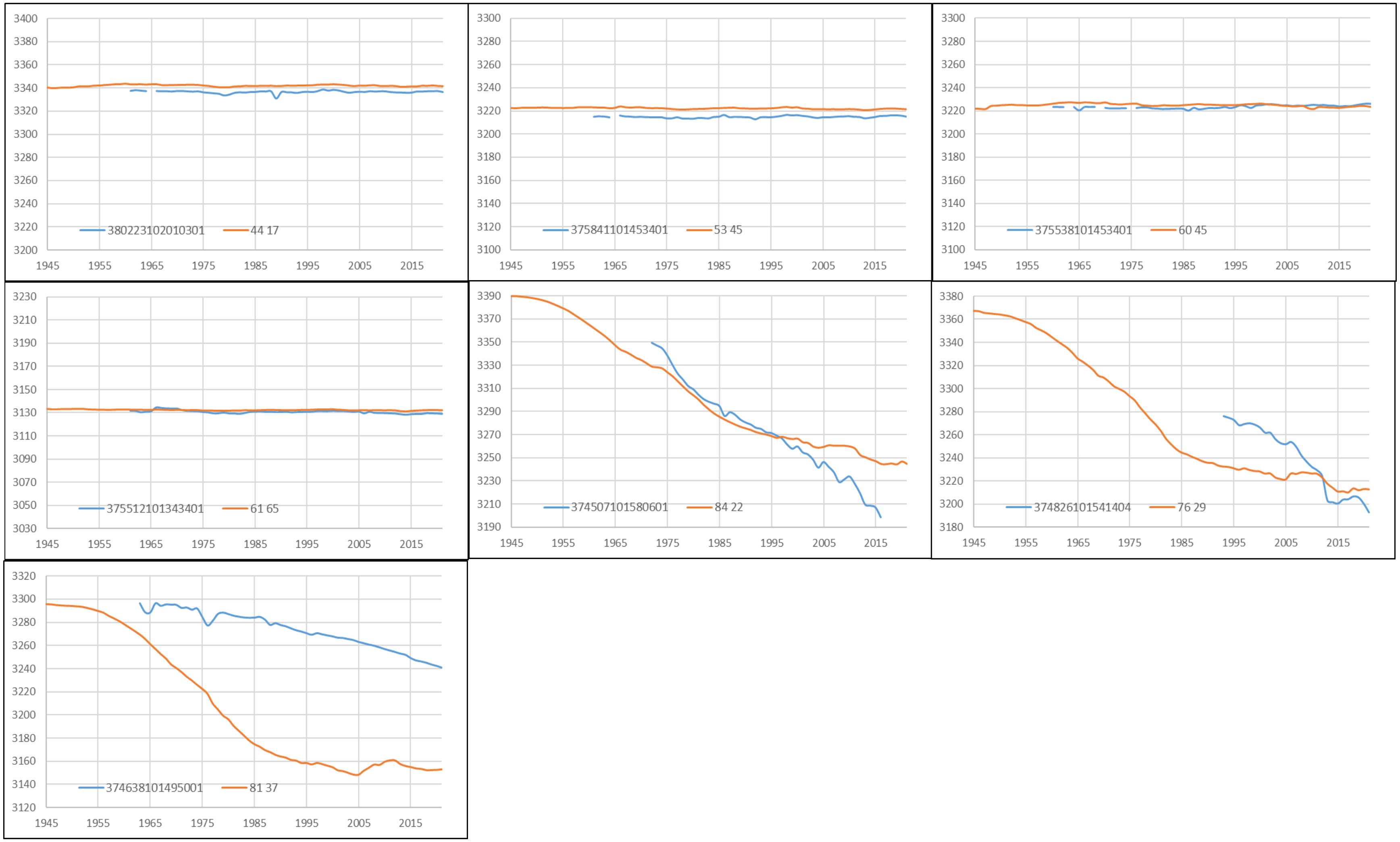

Figure 47. Simulated (orange line) versus observed (blue line) well hydrographs, Hamilton County.

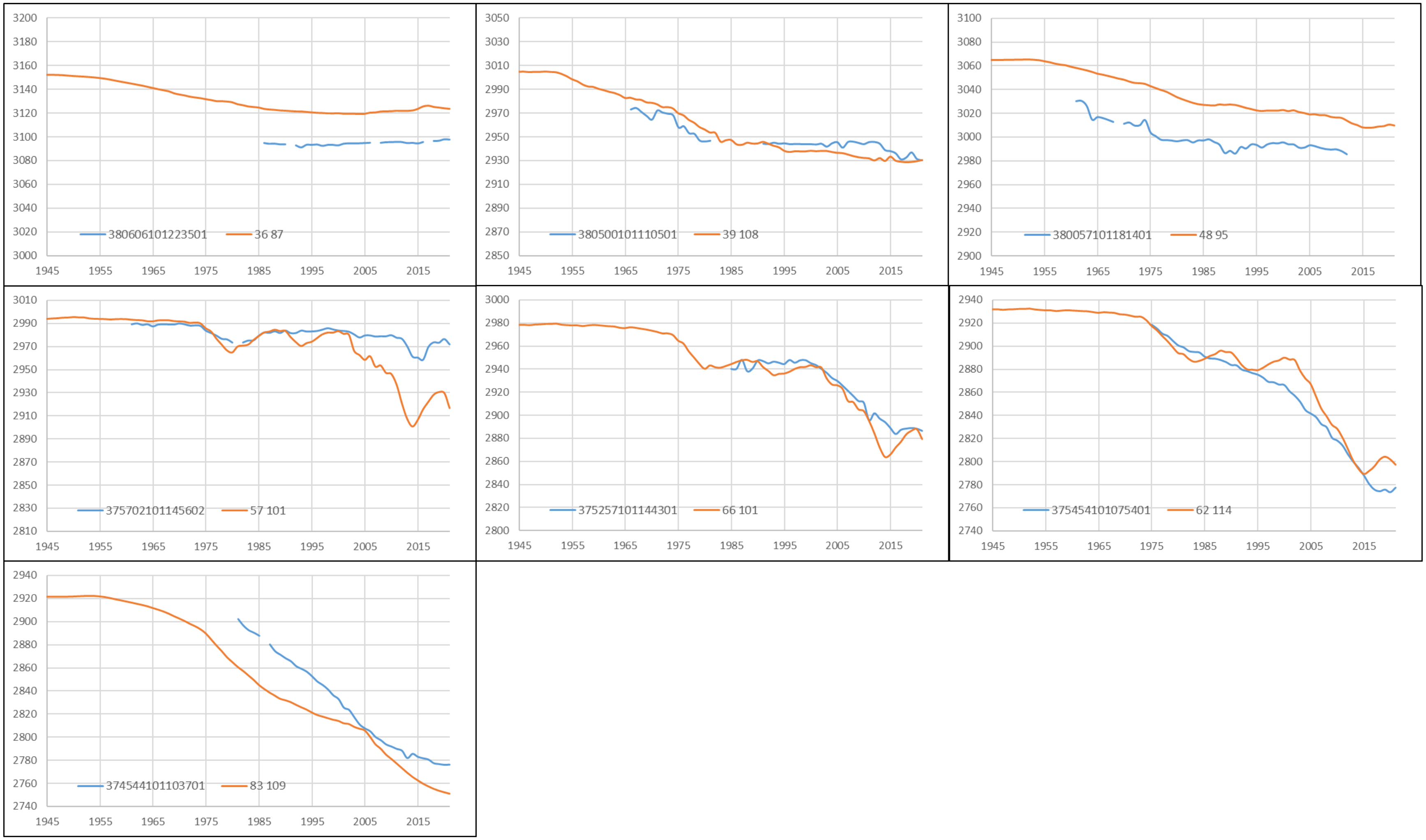

Figure 48. Simulated (orange line) versus observed (blue line) well hydrographs, Kearny County.

Figure 49. Simulated (orange line) versus observed (blue line) well hydrographs, western Finney County. All hydrographs are plotted to the same scale (20 ft intervals over 200-foot range) unless shown in red.

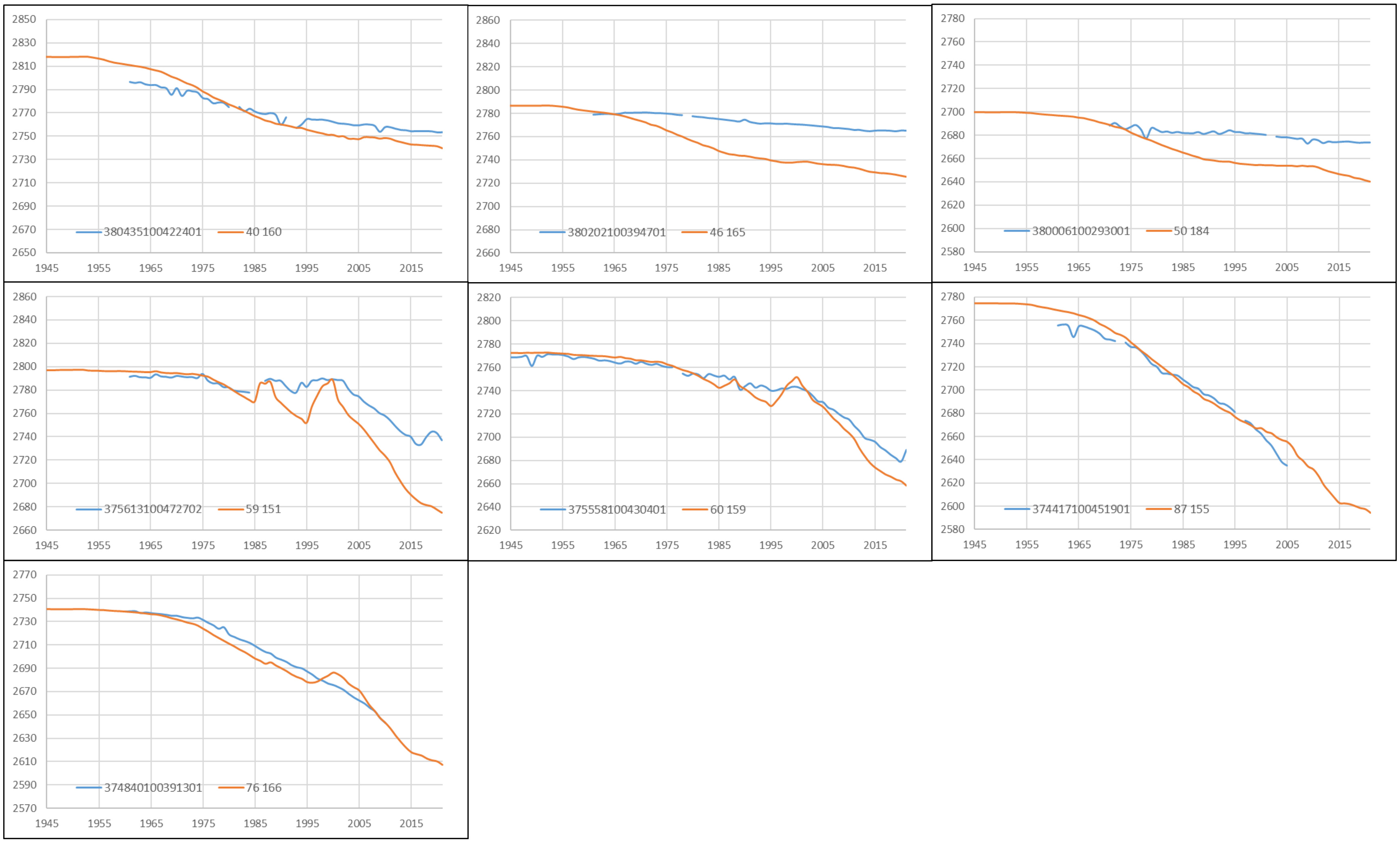

Figure 50. Simulated (orange line) versus observed (blue line) well hydrographs, eastern Finney County.

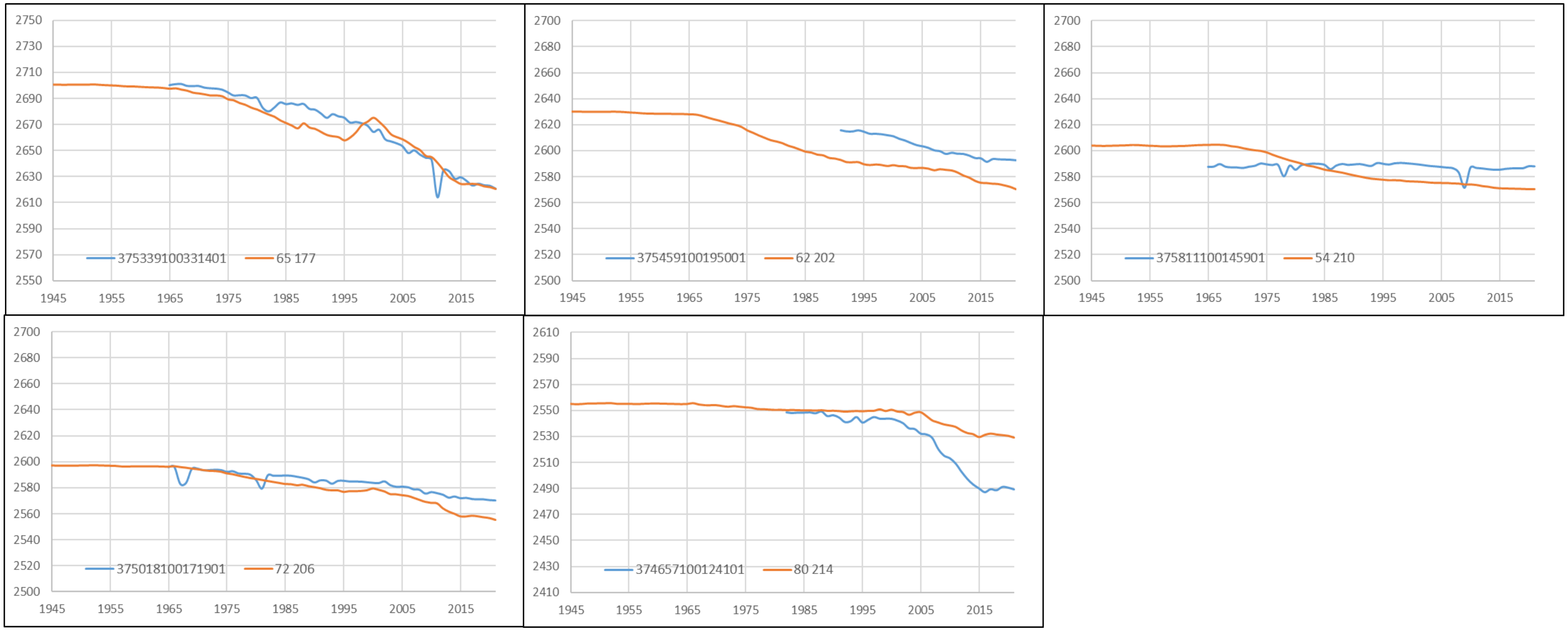

Figure 51. Simulated (orange line) versus observed (blue line) well hydrographs, northern Gray County.

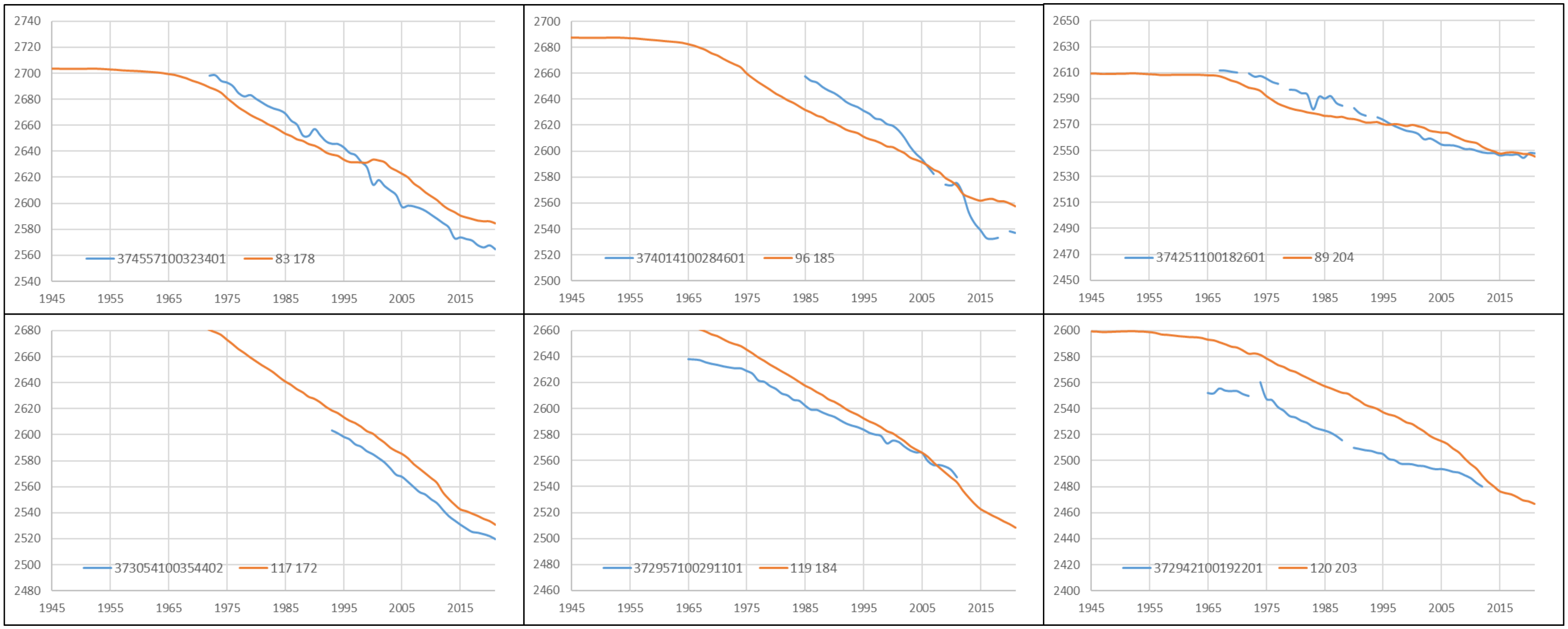

Figure 52. Simulated (orange line) versus observed (blue line) well hydrographs, southern Gray County.

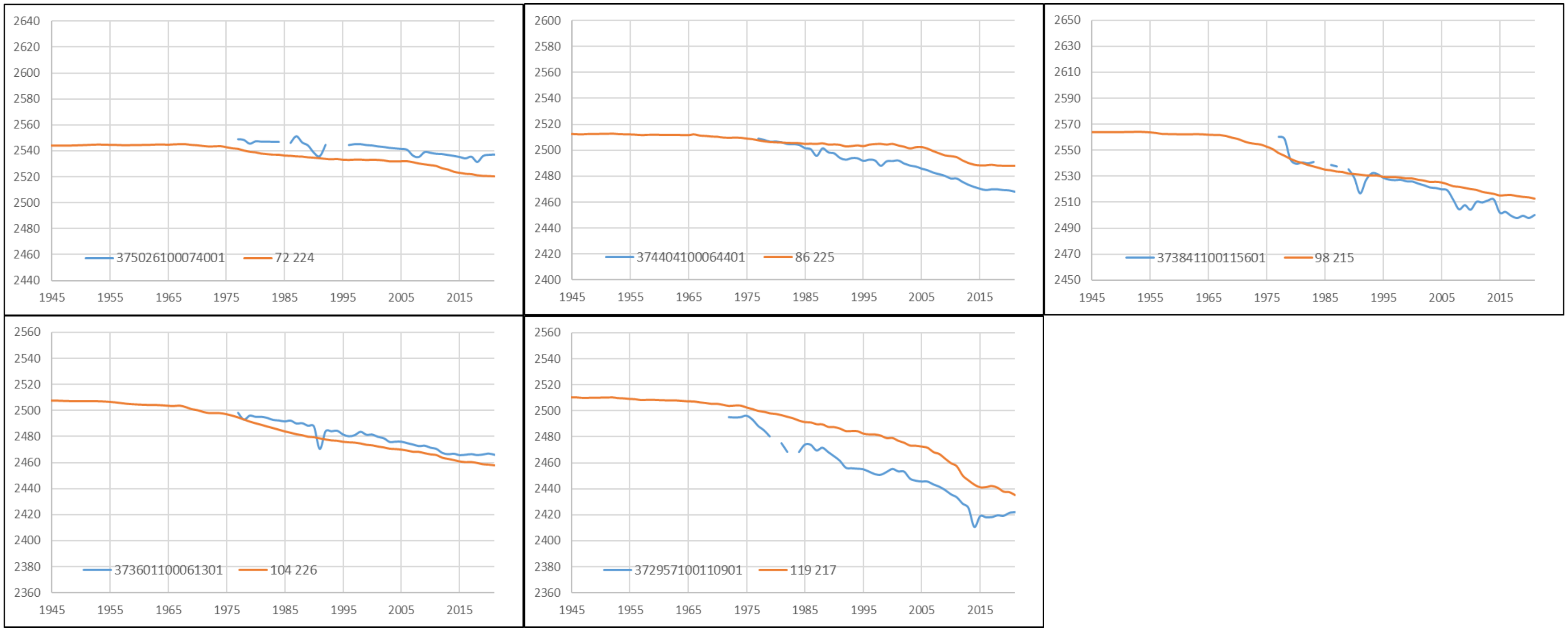

Figure 53. Simulated (orange line) versus observed (blue line) well hydrographs, western Ford County.

Figure 54. Simulated (orange line) versus observed (blue line) well hydrographs, central and eastern Ford County.

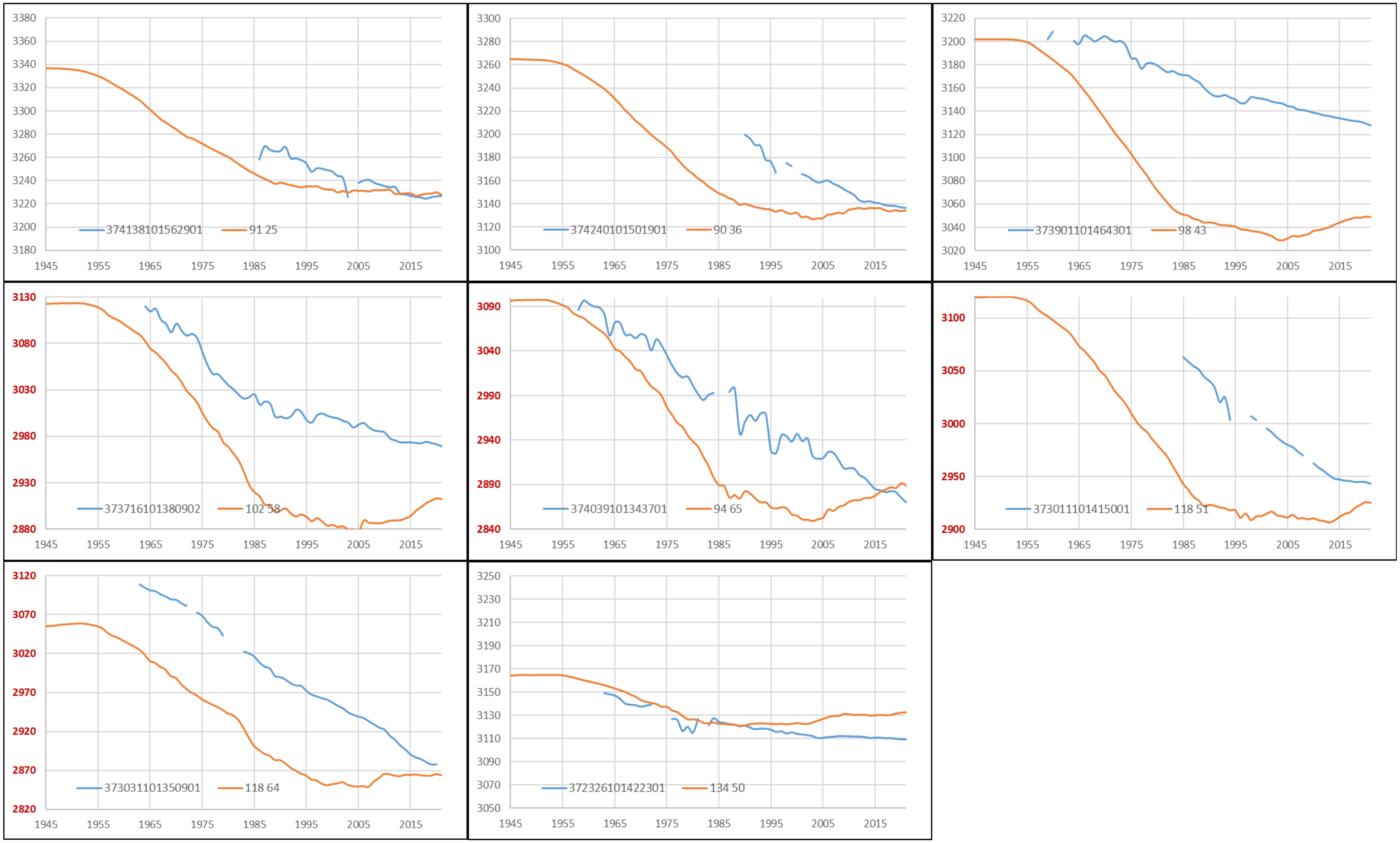

Figure 55. Simulated (orange line) versus observed (blue line) well hydrographs, Stanton County. All hydrographs are plotted to the same scale (20 ft intervals over 200-foot range) unless shown in red.

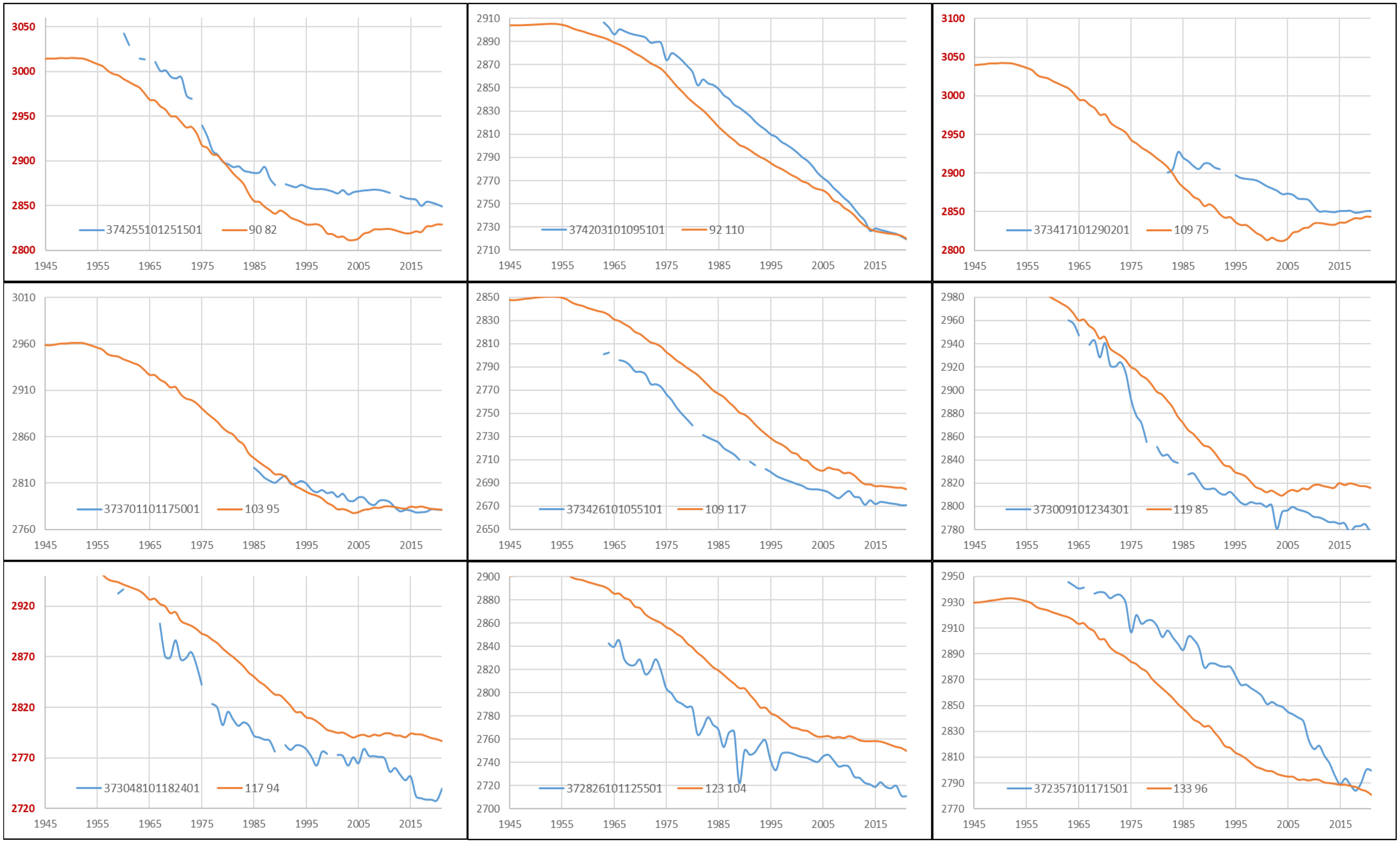

Figure 56. Simulated (orange line) versus observed (blue line) well hydrographs, Grant County. All hydrographs are plotted to the same scale (20 ft intervals over 200-foot range) unless shown in red.

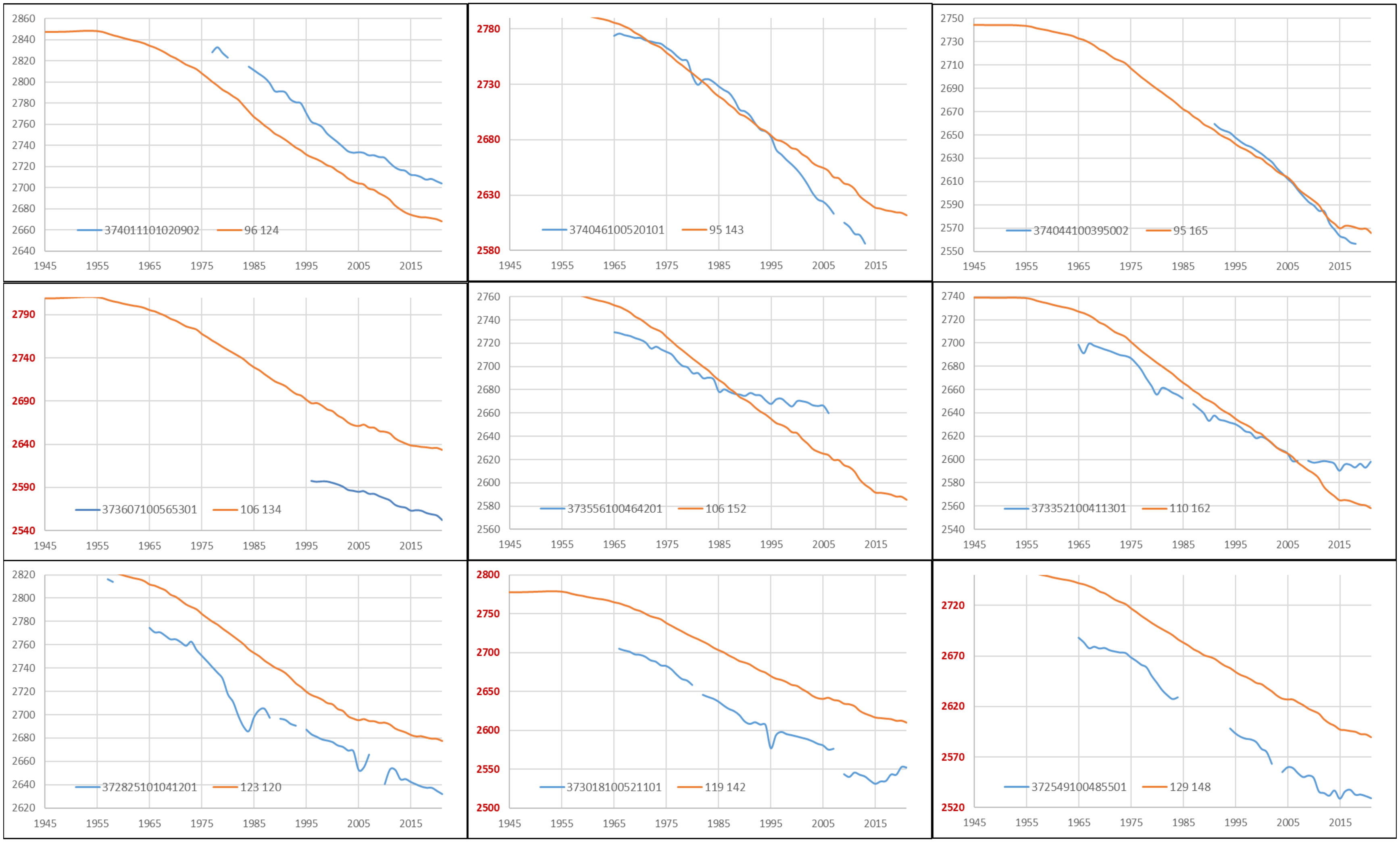

Figure 57. Simulated (orange line) versus observed (blue line) well hydrographs, Haskell County. All hydrographs are plotted to the same scale (20 ft intervals over 200-foot range) unless shown in red.

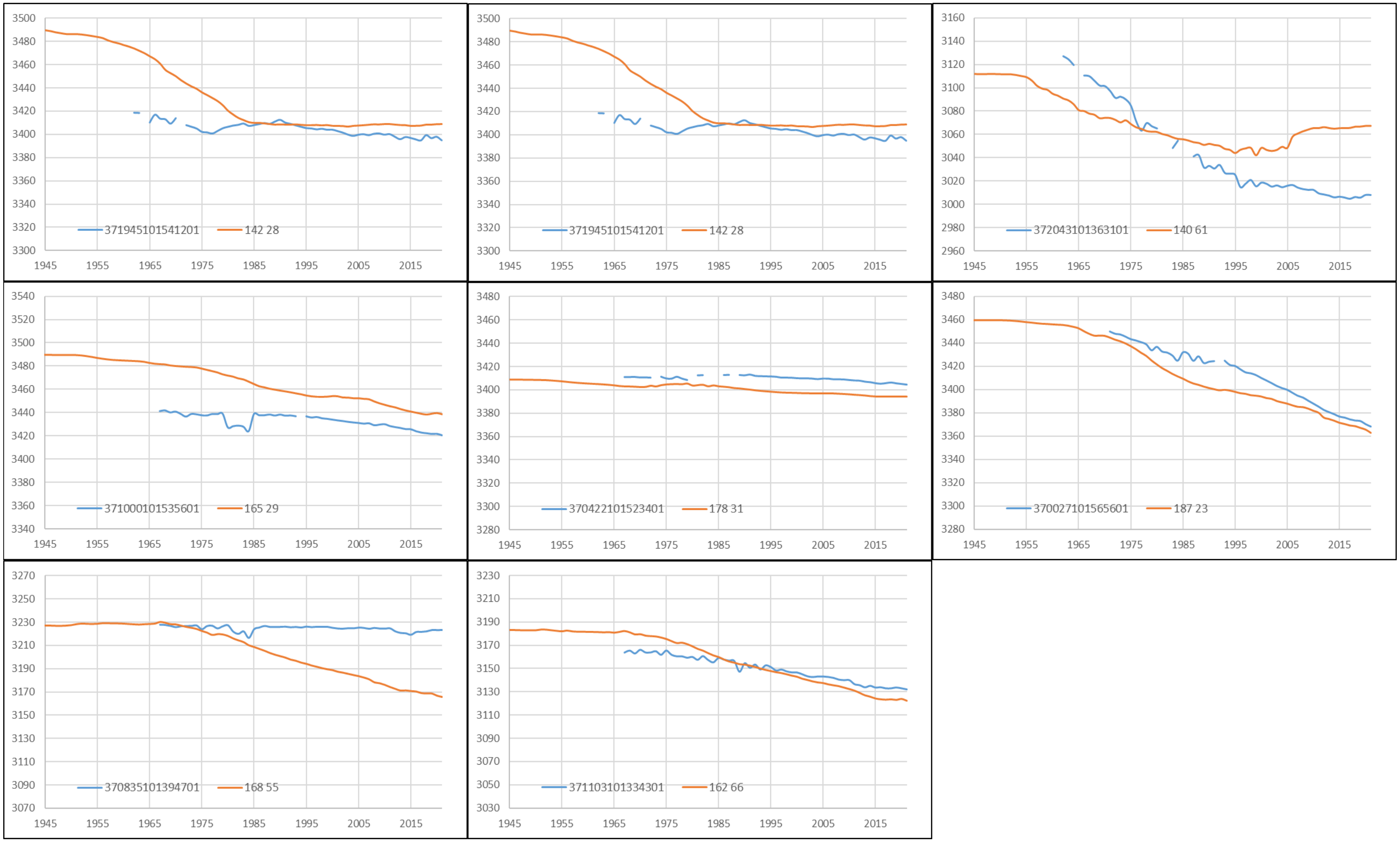

Figure 58. Simulated (orange line) versus observed (blue line) well hydrographs, Morton County.

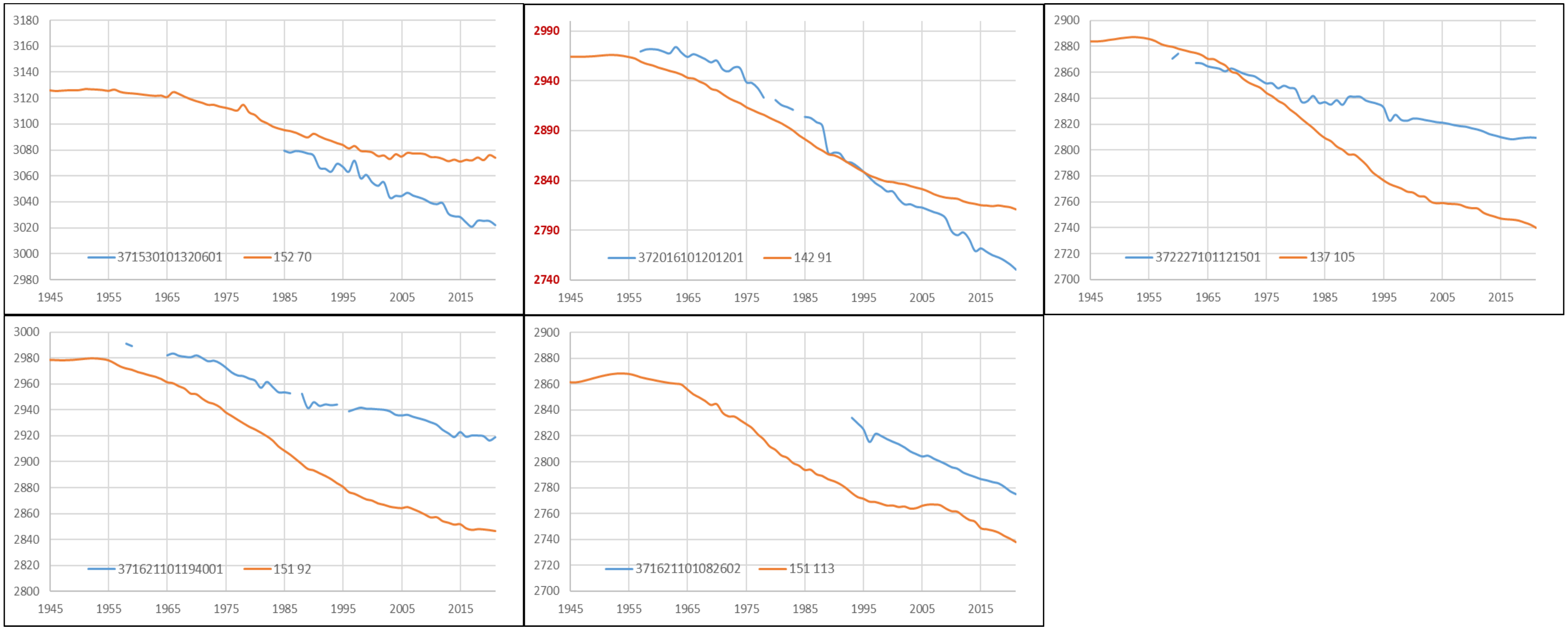

Figure 59. Simulated (orange line) versus observed (blue line) well hydrographs, northern Stevens County. All hydrographs are plotted to the same scale (20 ft intervals over 200-foot range) unless shown in red.

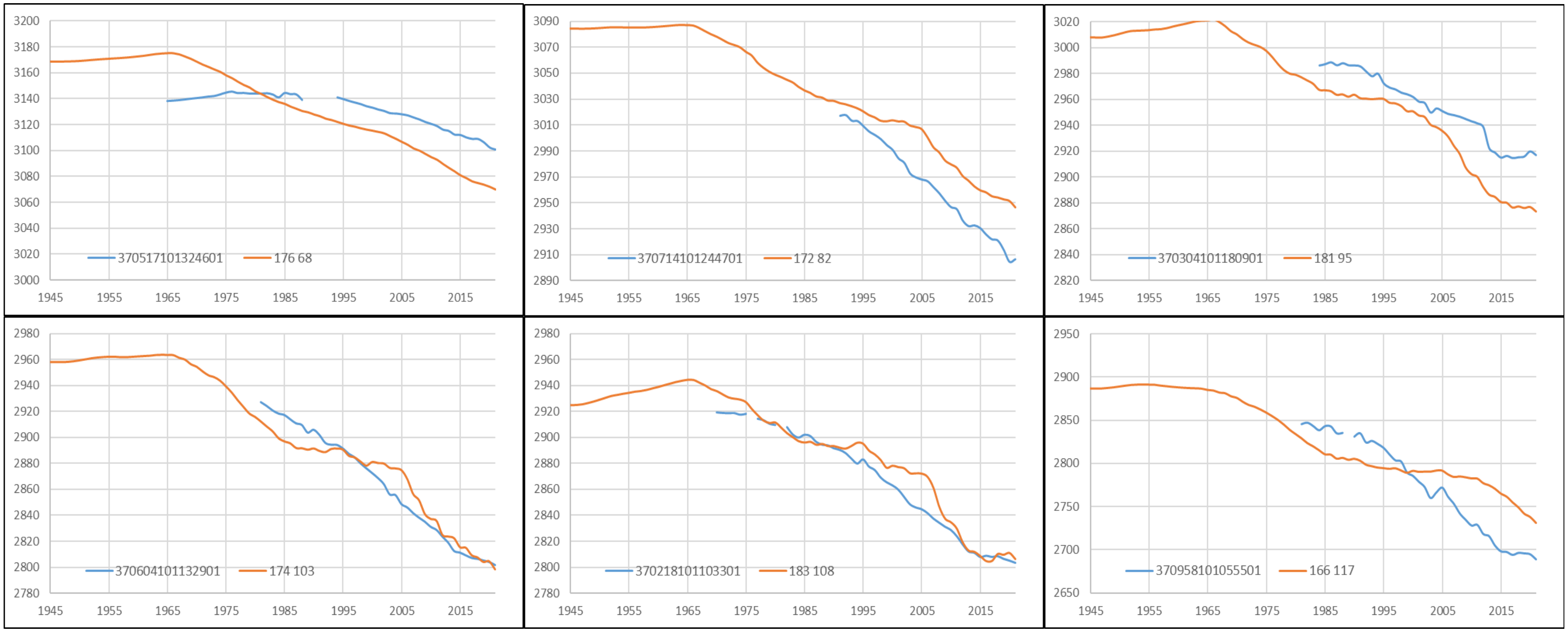

Figure 60. Simulated (orange line) versus observed (blue line) well hydrographs, southern Stevens County.

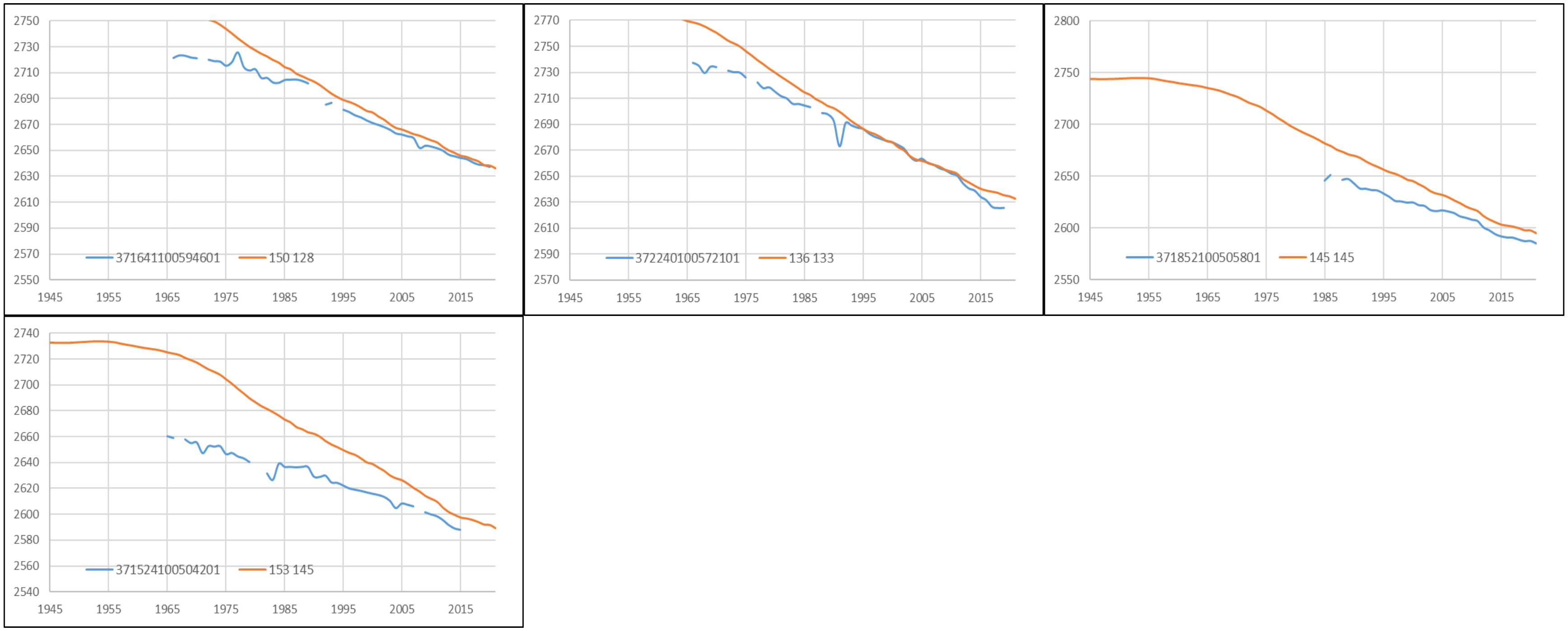

Figure 61. Simulated (orange line) versus observed (blue line) well hydrographs, northern Seward County.

Figure 62. Simulated (orange line) versus observed (blue line) well hydrographs, southern Seward County.

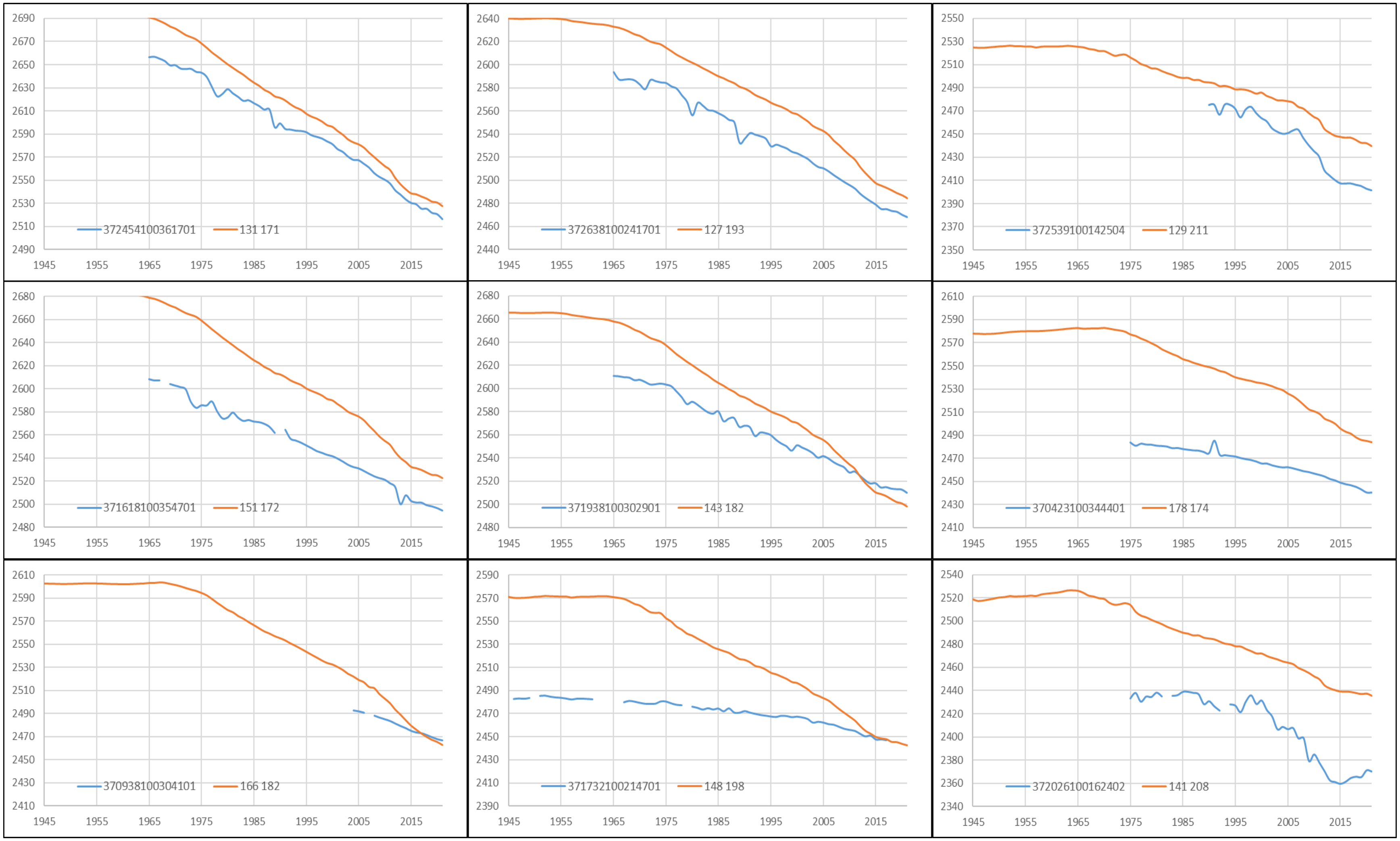

Figure 63. Simulated (orange line) versus observed (blue line) well hydrographs, Meade County.

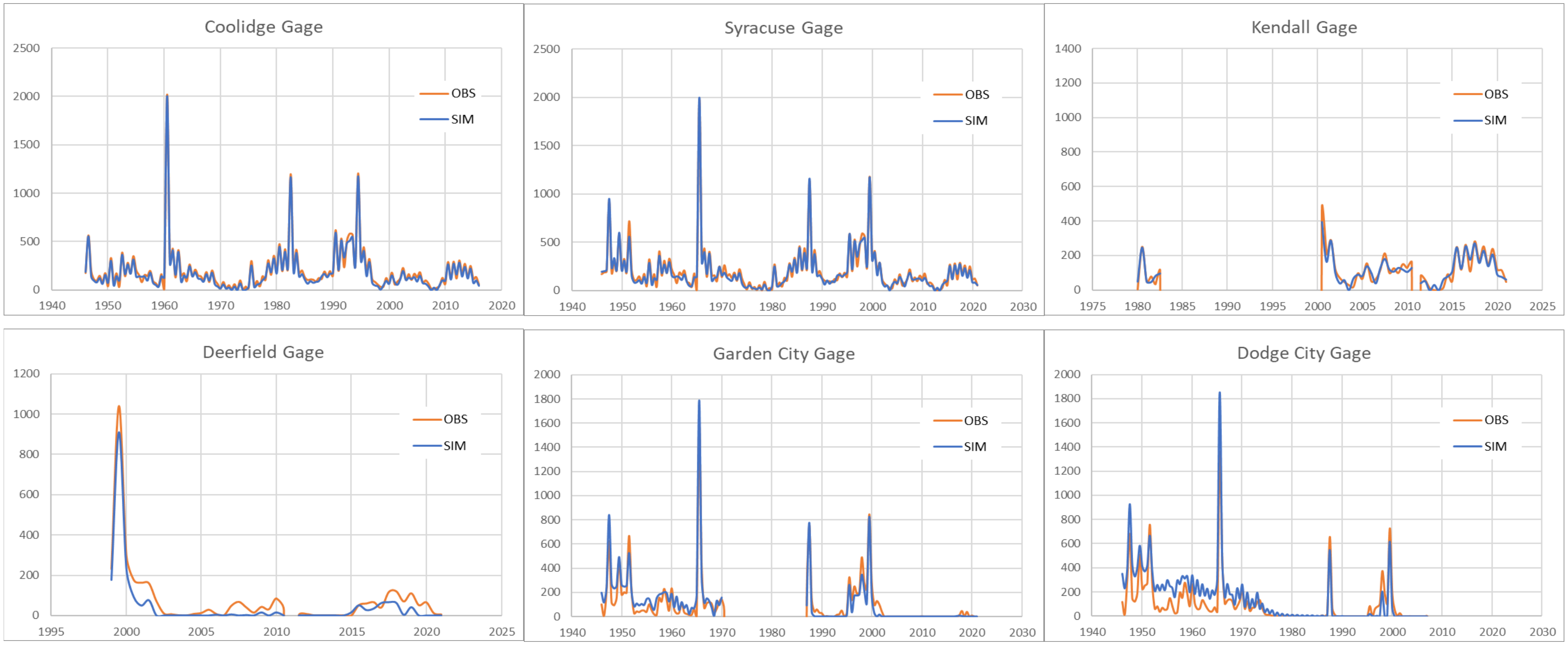

Figure 64. Simulated (blue line) versus observed (orange line) streamflow in cubic feet per second for stream gages along the Arkansas River.

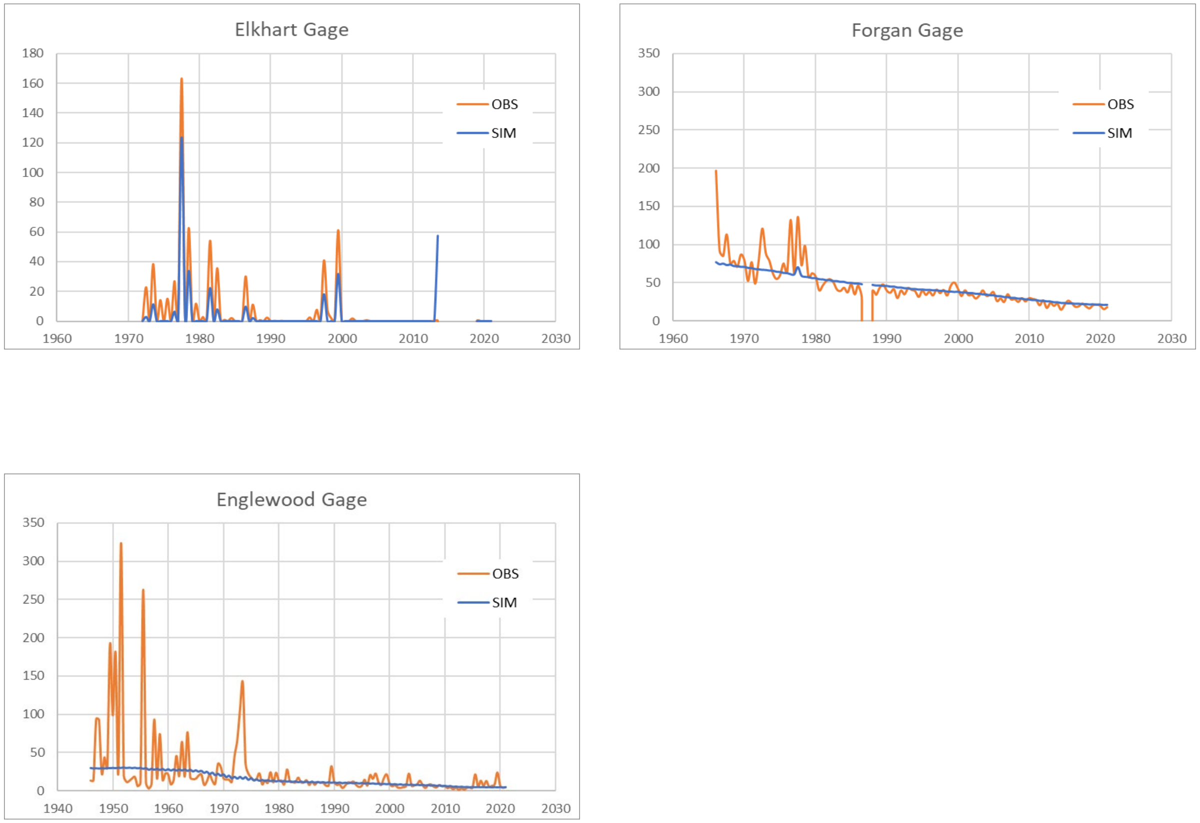

Figure 65. Simulated (blue line) versus observed (orange line) streamflow in cubic feet per second for stream gages along the Cimarron River (top) and Crooked Creek (bottom).

Model Budgets

Figure 66 shows the simulated groundwater budget for GMD3 over the transient period, including the net storage change, lateral flow across the GMD3 boundaries (lateral X and Y), well pumping, evapotranspiration (ET) loss, total areal recharge, and stream leakage. Positive values indicate inflows of water to the aquifer system and negative values reflect outflows from the aquifer.

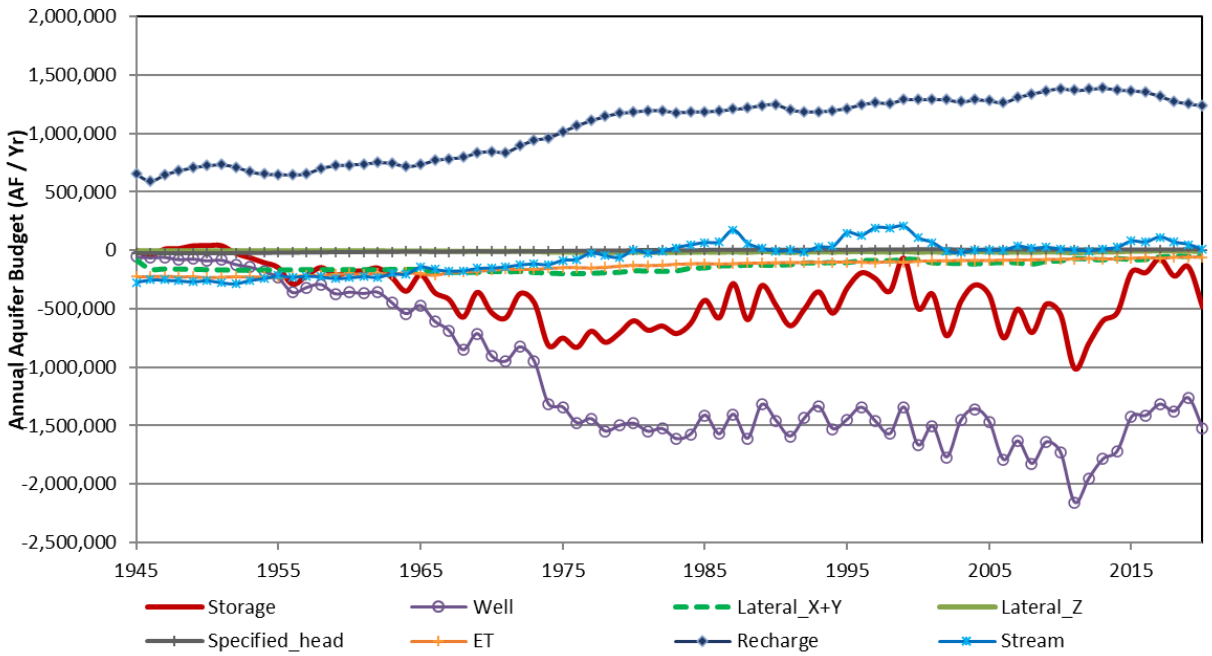

Figure 66. Annual aquifer budget for GMD3 from the calibrated model.

The largest inflows to the aquifer come from recharge, which represents the sum of all precipitation-based recharge, irrigation return flows, and lagged drainage by low-permeability units. The net lateral flow of groundwater in and out of GMD3 decreases slightly with time, which indicates the water-level decline within the district has caused some decrease in the groundwater outflow to aquifers down gradient. The largest volume of lateral flow enters the district from Colorado. Water flows laterally following a general gradient west to east and southwest where it exits the district along its eastern boundaries.

Groundwater pumping (identified as "Well" in fig. 66) represents the largest outflow from the aquifer. Annual groundwater usage has been relatively constant since the mid-1970s, with a shift to slightly less water usage in recent years after the drought years of 2011 and 2012. The amount of water loss from the aquifer to ET decreases slightly during the transient period in response to water levels that have been declining over time (when the water level is below the extinction depth, groundwater ET loss to plants and the atmosphere is no longer possible).

The aquifer loses water to streamflow in the form of baseflow from predevelopment until the early 1980s, at which time it gains water from stream/aquifer interactions. Periods of surface water flow induced recharge events, particularly in the Arkansas River in the mid-1990s and late 2010s, are clearly visible in the model's budget.

Changes in aquifer storage over time are computed as the difference between groundwater inflows and outflows. Prior to the 1950s, the aquifer gains slightly in storage. The aquifer begins to lose water from storage starting in the 1960s in response to increased pumping. It should be noted that the overall computed loss in storage is significantly lower in this updated model than was estimated by the older GMD3 groundwater model (Liu et al., 2010). This is a result of the current model's use of smaller Sy values, determined from the data-driven water-balance (i.e., Q Stable) and lithology approach to characterize aquifer conditions. To balance the outflows that were roughly the same as used in the old model, inflows in the current model had to be increased. However, simple increases to land-surface recharge rates do not work, since these result in simulated water table elevations that are too high in the early portion of the transient simulation, when pumping and water-level declines were not significant. Increasing inflows from lagged drainage of perched water through low-permeability sediments allows the model's budget to balance while adequately simulating observed water-level changes.

Figure 67 plots the various recharge components originating from the land surface. Precipitation recharge is generated by the precipitation-recharge curves described earlier in this report and represents the amount of new water entering the aquifer system from both the upland areas of the aquifer and the higher rates of recharge for stream channels. Precipitation recharge has a slight increasing trend over the transient period with an average of 1.18 inches per year. Recharge from irrigation return flows represents the amount of pumped irrigation water that infiltrates past the root zone of the irrigated crops, eventually reaching the water table. As the number of water rights and pumping volumes increase during the 1960s and 1970s, so does the amount of return flows. As water usage declines and irrigation systems become more and more efficient, the amount of return flow declines. Over the transient period, irrigation return flow averages 0.39 inches per year.

The final components are the amount of water coming from enhanced precipitation-based recharge occurring over irrigated fields and the ditch service areas. Compared to the precipitation recharge, the irrigation-enhanced precipitation recharge is relatively small because 1) irrigation enhancement to precipitation recharge occurs only during the growing season while precipitation recharge is calculated for both the growing and non-growing seasons and 2) the acreage of irrigated lands is much smaller than the active model area (fig. 28). Therefore, although irrigation doubles the precipitation recharge in the irrigated fields during the growing season, the amount of irrigation-enhanced precipitation recharge is small when compared to the overall precipitation recharge over the entire active model area. Enhanced recharge from the ditch service areas averages 0.11 inches a year and is the result of simulated leakage from the irrigation canals, primarily in areas west of Garden City.

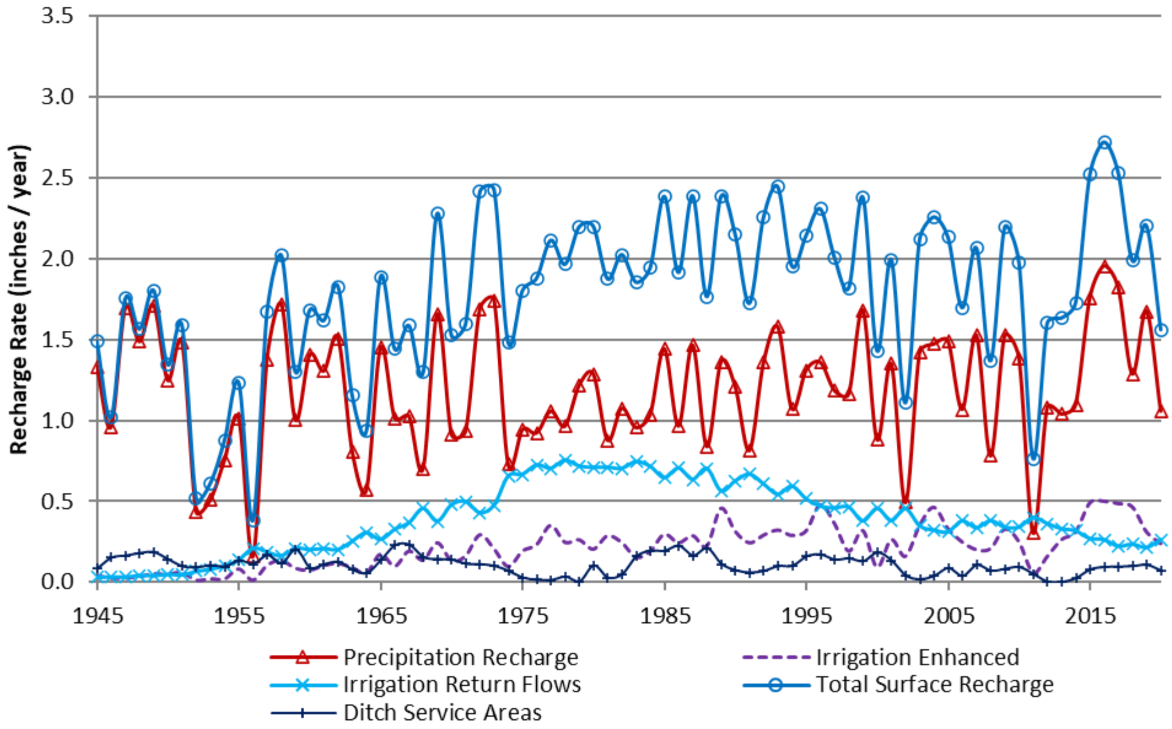

Figure 67. Recharge components originating from the land surface.

Each of the land-surface recharge components is subject to the model's vadose zone delay function, and the total amount of water delayed in the vadose zone in each time step is tracked. Figure 68 illustrates the total amount of water derived from surface recharge that actually reaches the ever-changing water table. Compared to surface recharge, which is directly driven by precipitation and fluctuates significantly from year to year, the delayed recharge at the water table is smoother as the delay in the vadose zone has removed much of the annual fluctuation. Prior to the 1970s, delayed recharge from the surface was primarily controlled by precipitation recharge. During the 1970s and 1980s, it increased as irrigation return flows increased. Between the 1980s and 1990s, the delayed recharge from the surface remained stable but it started to decline in the mid-2000s only to increase toward the end of the transient period, likely in response to an increase in precipitation events during those years.

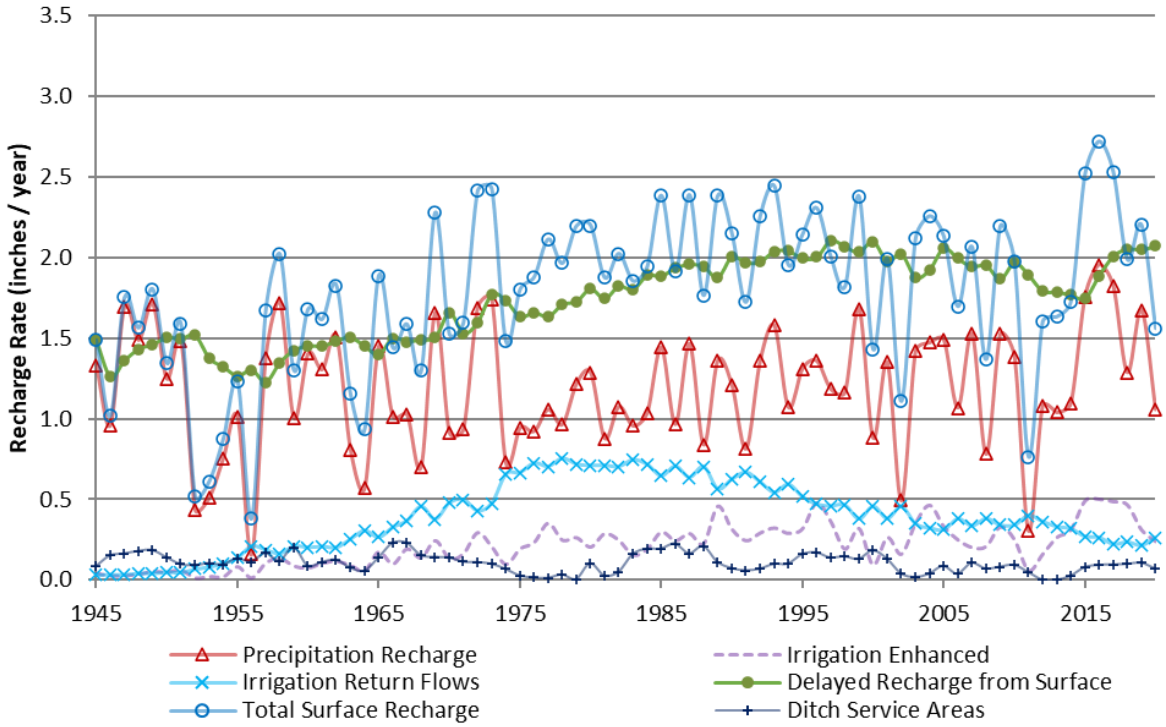

Figure 68. Total delayed recharge reaching the water table from the surface.

Figure 69 plots the amount of lagged drainage of perched water through low-permeability sediments. The total recharge to the water table is the sum of the lagged drainage and the delayed recharge from the surface. Given that lagged drainage occurs only when the water table declines, it does not start until the mid-1960s. Beginning in 1970, the amount of lagged drainage from the dewatered sediments averages 0.90 inches a year. The total inflows from all sources since 1980 average 2.69 inches a year, which is in line with the computed net inflows of 2.87 inches from the data-driven water-balance methods (Butler et al., 2016, 2018).

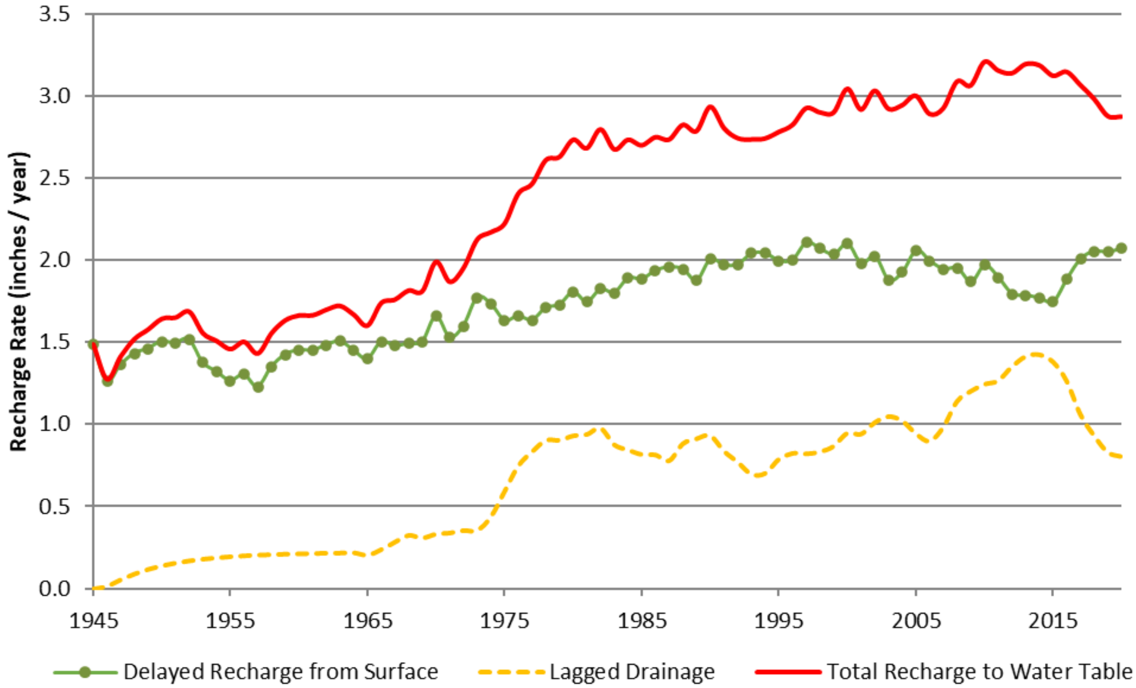

Figure 69. Lagged drainage and the total amount of recharge to the water table.

Figure 70 plots the cumulative change in the model's groundwater budget. Aquifer storage is calculated for each model step based on the simulated water levels and specific yield values for the different HyDRA lithology groups. The computed total predevelopment aquifer storage within GMD3 is estimated to be 91.6 million acre-ft. The net effect of the model components produces an estimated 391,504 acre-ft average annual loss of storage. The simulated cumulative storage loss in 2020 is 30% of the predevelopment value.

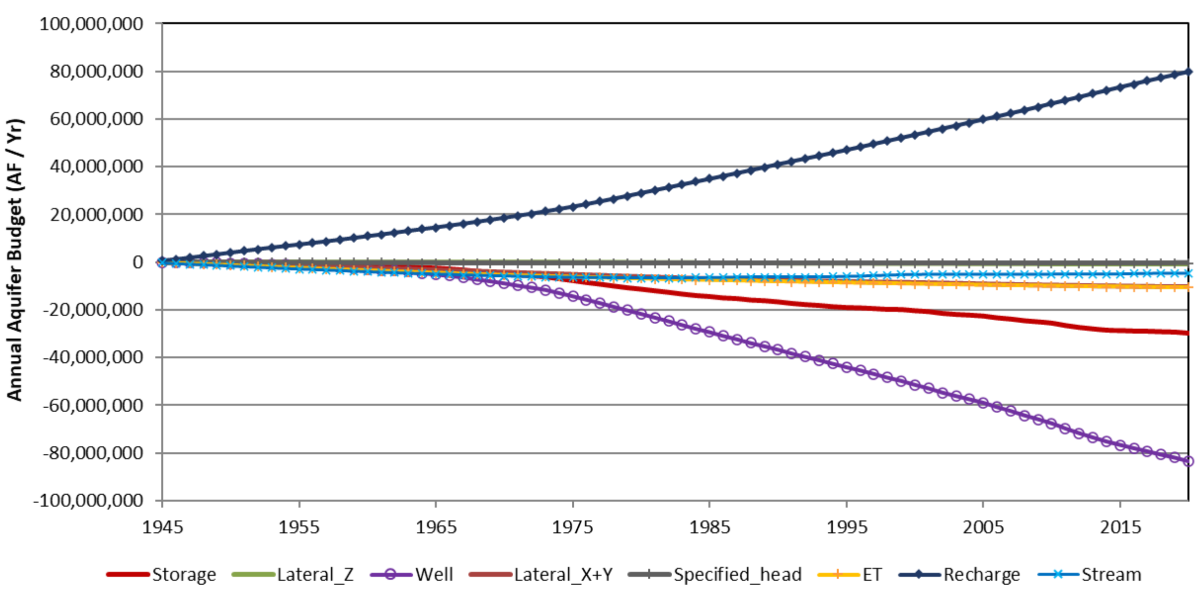

Figure 70. Accumulated groundwater budget, GMD3.

MODEL SCENARIOS

One of the valuable uses of a calibrated groundwater model is to assess the future responses of an aquifer to various water resources management and climatic scenarios. Three scenarios were considered in this study:

1) Status quo (no change in water-use policy).
2) Q stable.
3) Drought of record.

In all scenarios, the calibrated model is run from 2023 to 2083, with various repeats of past precipitation patterns. To better represent current conditions as the starting conditions of future simulations, calendar year 2022 is skipped between the historical and future simulations to insert water levels based on an interpolated surface generated from averaged 2021–2023 measured values. The model continues to track and apply its delayed recharge from land surface and lagged drainage from dewatered units, which runs through both the historical and future simulations (predevelopment to 2083). The irrigation system types at the end of the historical model (2021) are held constant. For the specified head boundaries, the average water-level change over the last 20 years is used to project future water levels on these boundaries until a minimum HPA saturated thickness of 10 ft is reached.

Model pumping over the historical period uses reported water use from 2005 to 2021 and regressed values based on the ratios of water use/authorized quantities versus precipitation over the same period to estimate pumping from 1945 to 2004 (fig. 21). For future simulations, the regression equation was shifted to characterize conditions from 2013 to 2022. This removes the influences of 2011 and 2012, a unique period of abnormally higher water usage permitted through the issuance of special term permits to help mitigate drought conditions. Like the historical model version, the adjusted regression equation used for future model runs is statistically significant ($P < 0.0087$) and highly correlated to variations in precipitation (R-squared value of 0.86) while providing a better match to conditions over the last 10 years (fig. 71).

Future pumping estimates in each scenario are reduced if the simulated water levels in the aquifer reach a point where the aquifer cannot yield enough water to support the projected demands. This adjustment is based on the transmissivity of each model cell, which is computed for each future year time step. As shown in fig. 72, a log function is used to reduce well yields at a larger rate as the water levels approach the bottom of the aquifer. This adjustment starts when the transmissivity is less than 2,000 ft^2/d (equivalent to a saturated sand layer of 20 ft with a hydraulic conductivity of 100 ft/d), the well pumping rate starts to decrease according to a log curve until is reaches 1,000 ft^2/d (equivalent to a saturated sand layer of 10 ft with a hydraulic conductivity of 100 ft/d) when all pumping from the cell is shut off. Any irrigation return flows are also adjusted accordingly.

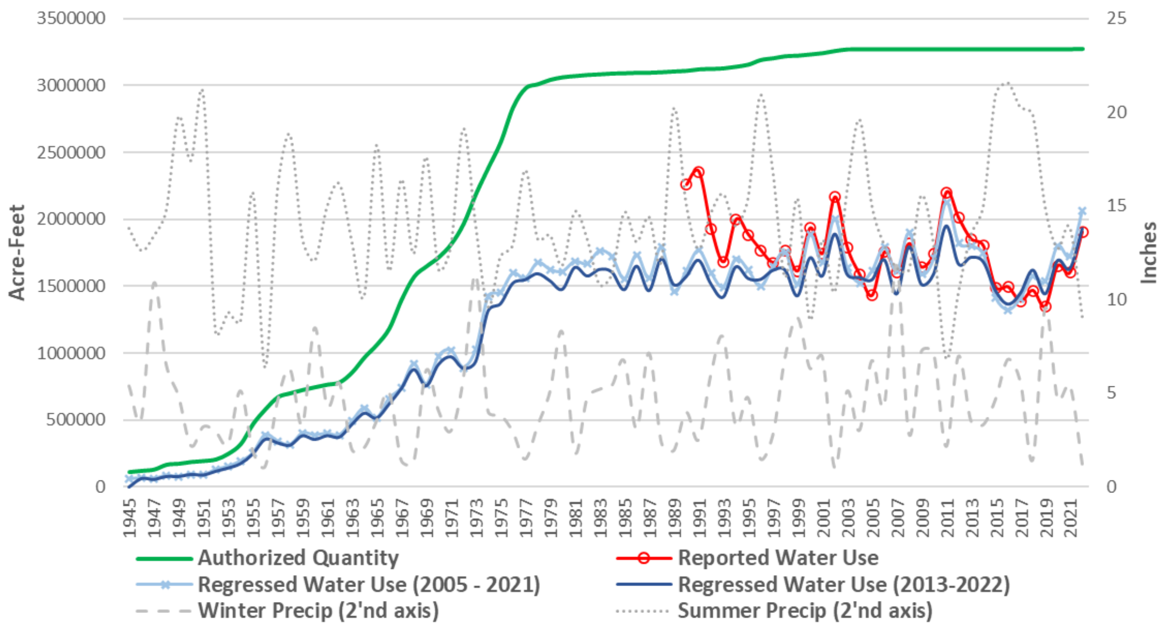

Figure 71. Total authorized quantity, regressed water use, summer precipitation, and reported water use for GMD3. The regression equation based on the 2013–2022 data (solid blue line) is used for pumping estimation in future simulations.

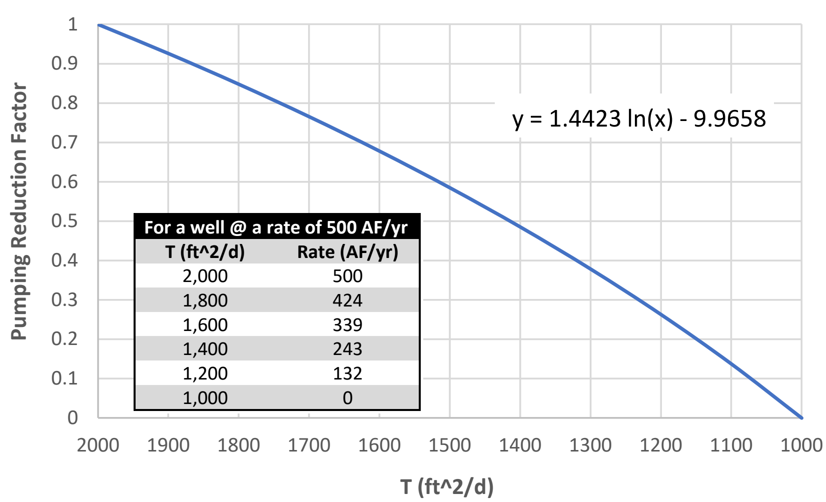

Figure 72. Pumping adjustment based on transmissivity during future scenario simulations.

Future diversion rates from ditches along the Arkansas River were held constant based on 2020 records, which roughly equal the average over the past two decades. Streamflow entering the model domain is based on a three-time repeat of historical conditions from 2003 to 2022. Ditch seepage was also treated as part of the aquifer recharge inputs at the land surface, which are then subject to the delayed recharge calculation through the vadose zone.

Status Quo (no change in water-use policy)

This scenario uses the updated regression equation (based on 2013 to 2022 conditions) to compute the ratio of water use/authorized quantity, assuming there is no change in future water-use policy. For a given future year, the ratio, which is dependent on summer and winter precipitation, is converted into the actual water-use demand by multiplying it by the present-day authorized quantity. Precipitation patterns from 2003 to 2022 are repeated three times to complete the 60-year simulation. Future pumping is not adjusted to account for any special water plans, such as water conservation areas, that might be put in place.

Figure 73 shows the annual aquifer budget for GMD3 based on the status quo scenario. Groundwater pumping continues to be the most significant outflow component of the aquifer budget. The total recharge, including both the delayed surface recharge (i.e., the water that has moved from surface recharge down to the water table) and lagged drainage release, is not sufficient to balance pumping, labeled as "Well" in the chart. As a result, the aquifer continues to lose water out of storage (annual storage budget is negative in most years). Water loss from ET and lateral flow across the district (the total from both horizontal and vertical flow paths) is relatively small and constant while the aquifer gains some water through stream loss. Despite year-to-year fluctuations, future pumping shows a gradual decrease in response to continuing losses in aquifer storage.

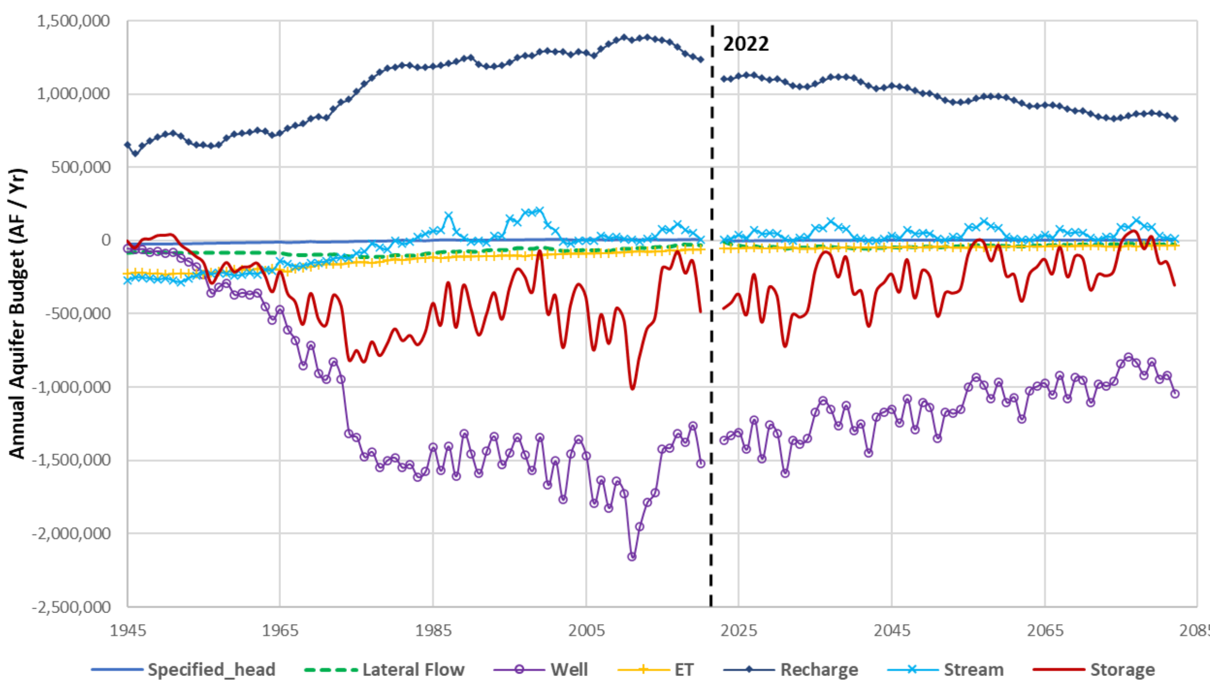

Figure 73. Annual aquifer budget (HPA) for GMD3 under the status quo scenario. The calibrated historical model budget (1945 to 2021) is also plotted for comparison.

Figure 74 shows the contributions of the water-table recharge from delayed surface recharge and lagged drainage from partially dewatered sediments after water-table decline. Delayed recharge from the land surface averages 1.8 inches over future simulation with a slight declining trend, caused by the reduction in return flows as the model reduces irrigation pumping in cells reaching the minimum transmissivity thresholds. The contributions from dewatered units are primarily a function of water level decline rate, which holds steady until roughly 2045, after which it begins a constant declining trend toward the end of the simulation. This is a result of reduced water-level declines as more areas of the aquifer reach the end of their usable lifetimes. The total average recharge (delayed recharge from surface plus lagged drainage from dewatered units) for the future scenario start at 2.6 inches a year and are projected to be 2.1 inches per year by the year 2083 with an overall average of 2.5 inches per year.

Figure 75 shows different surface recharge components. Consistent with the estimates in future pumping, irrigation return flows and enhanced recharge show slightly declining trends with annual fluctuations. Precipitation-based recharge, the largest source of inflow from the land surface, reflects the 20-year repeating pattern in precipitation observed from 2003 to 2022 and averages 1.3 inches per year over the simulation.

Figure 76 shows the simulated head changes for selected time intervals for the status quo / no change in future water use scenario. Most of the district will see a certain amount of water-level decline with the largest occurring in a band running from southwest Gray County into central portions of Haskell and Grant counties. Enhanced recharge coming from the ditch service and canals moderate water-level declines and in some cases can cause rises. Areas of less water usage, such as in the chloride areas of southern Meade County and eastern Ford County, have relatively stable projected water levels throughout the scenario simulation. The average water-level change across GMD3 over the next 10 (2023 to 2033) and 20 (2023 to 2043) years are projected to be -15.4 ft and -26.8 ft, respectively.

Figure 77 shows simulated future aquifer thickness maps for both the HPA and the HPA in combination with the unconfined Dakota, where it exists directly underneath the HPA. Thickness for the HPA is projected to thin across much of the core areas of the district relative to the thicker areas west of Crooked Creek and along the Oklahoma border. Water Levels in southern Hamilton and northwest Stanton counties are primarily in the Dakota as the HPA cells become dry (shown by the darker gray colors). Less is known about the well yields, water availability, and dynamics of water-level change in the Dakota system, but current estimates of the Dakota's thickness are significant, especially in those thinner areas of the HPA. It should be noted, however, that thickness can be a bit deceiving as large intervals of the Dakota aquifer often consist of less permeable shales. A future enhancement to the model is to better understand and simulate the interactions between the connected units of the Ogallala and the underlying Dakota systems in this and other model areas.

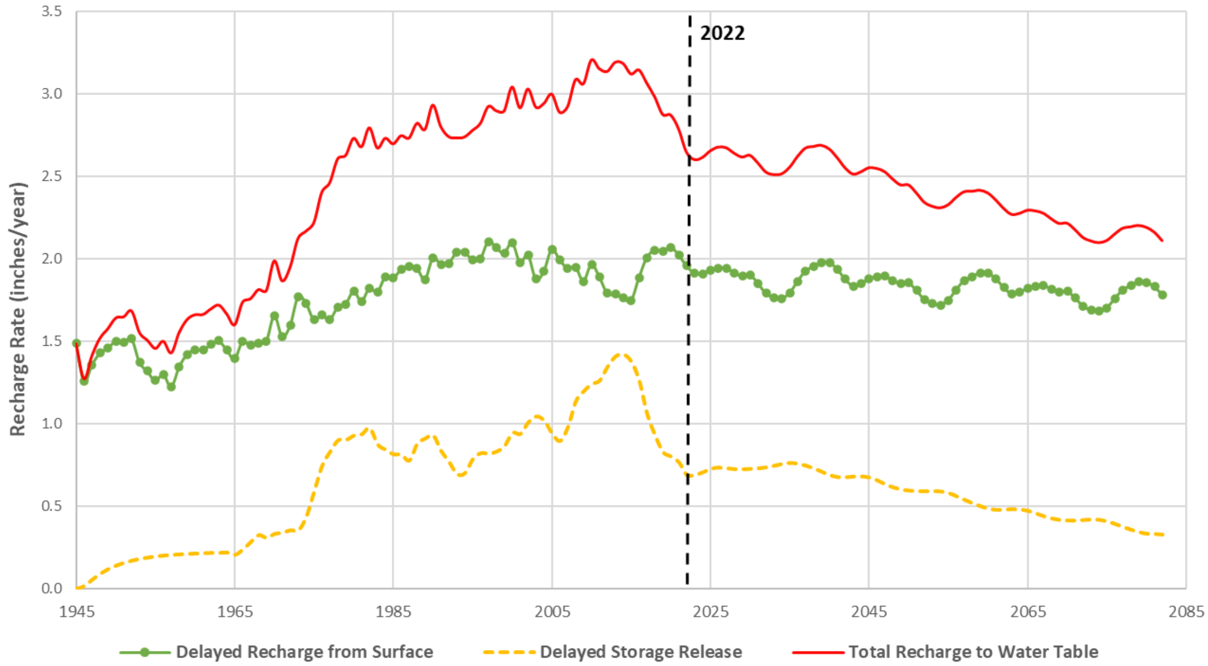

Figure 74. Water-table recharge in GMD3 under the status quo future water use scenario.

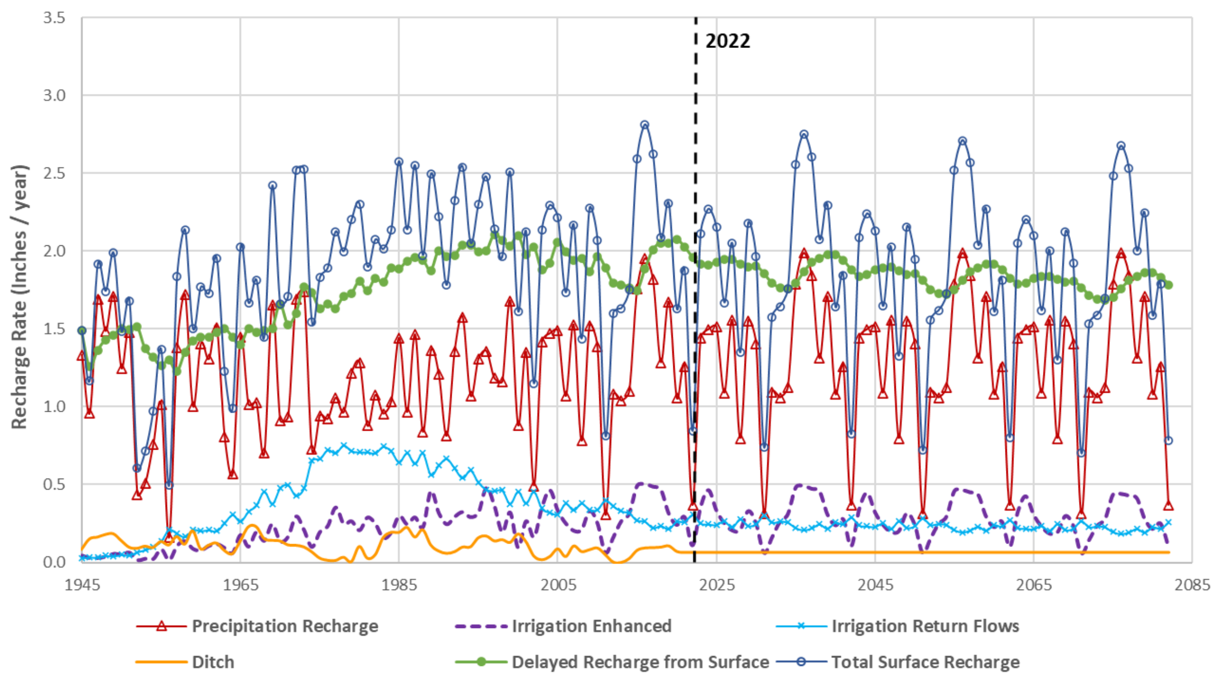

Figure 75. Different surface recharge components for GMD3 under the no change in future water use scenario. The delayed surface recharge (listed as “Delayed Recharge from Surface”) is also plotted for comparison.

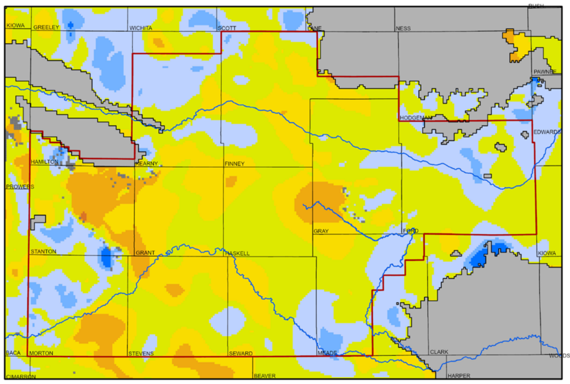

(a) 2023 to 2033

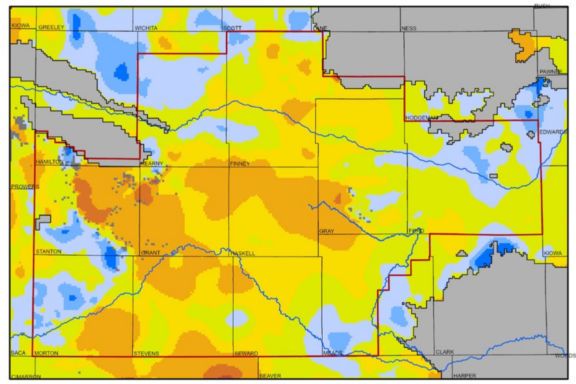

(b) 2023 to 2043

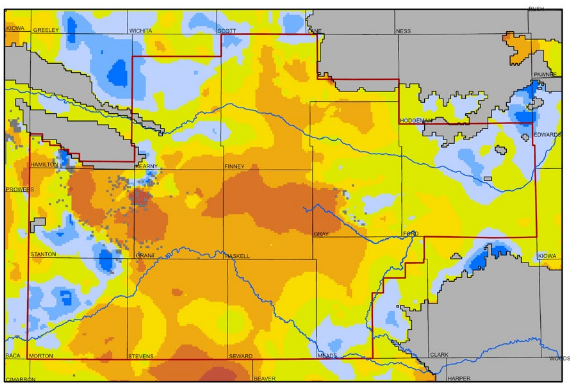

(c) 2023 to 2053

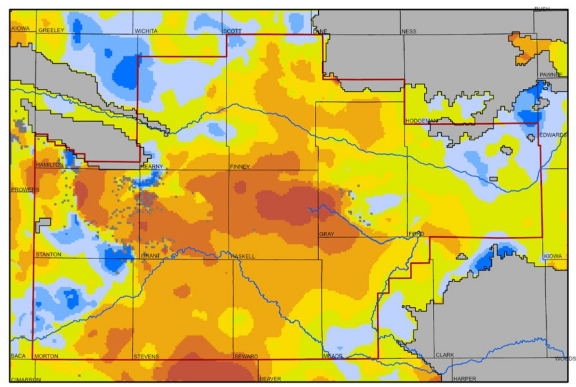

(d) 2023 to 2063

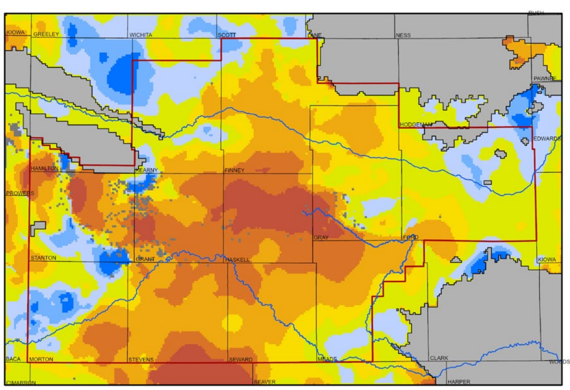

(e) 2023 to 2073

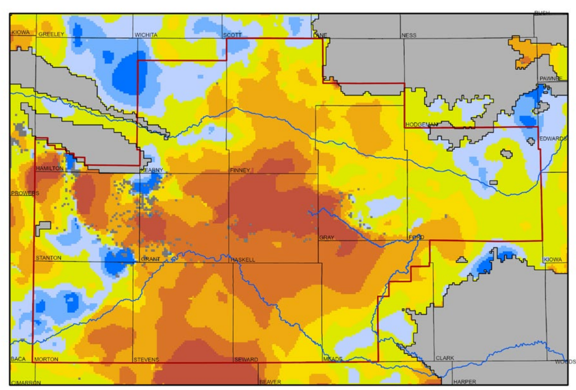

(f) 2023 to 2083

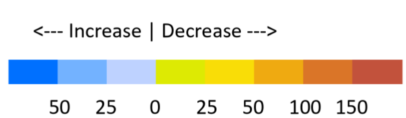

Figure 76. Simulated water-level change, in feet, for the status quo scenario.

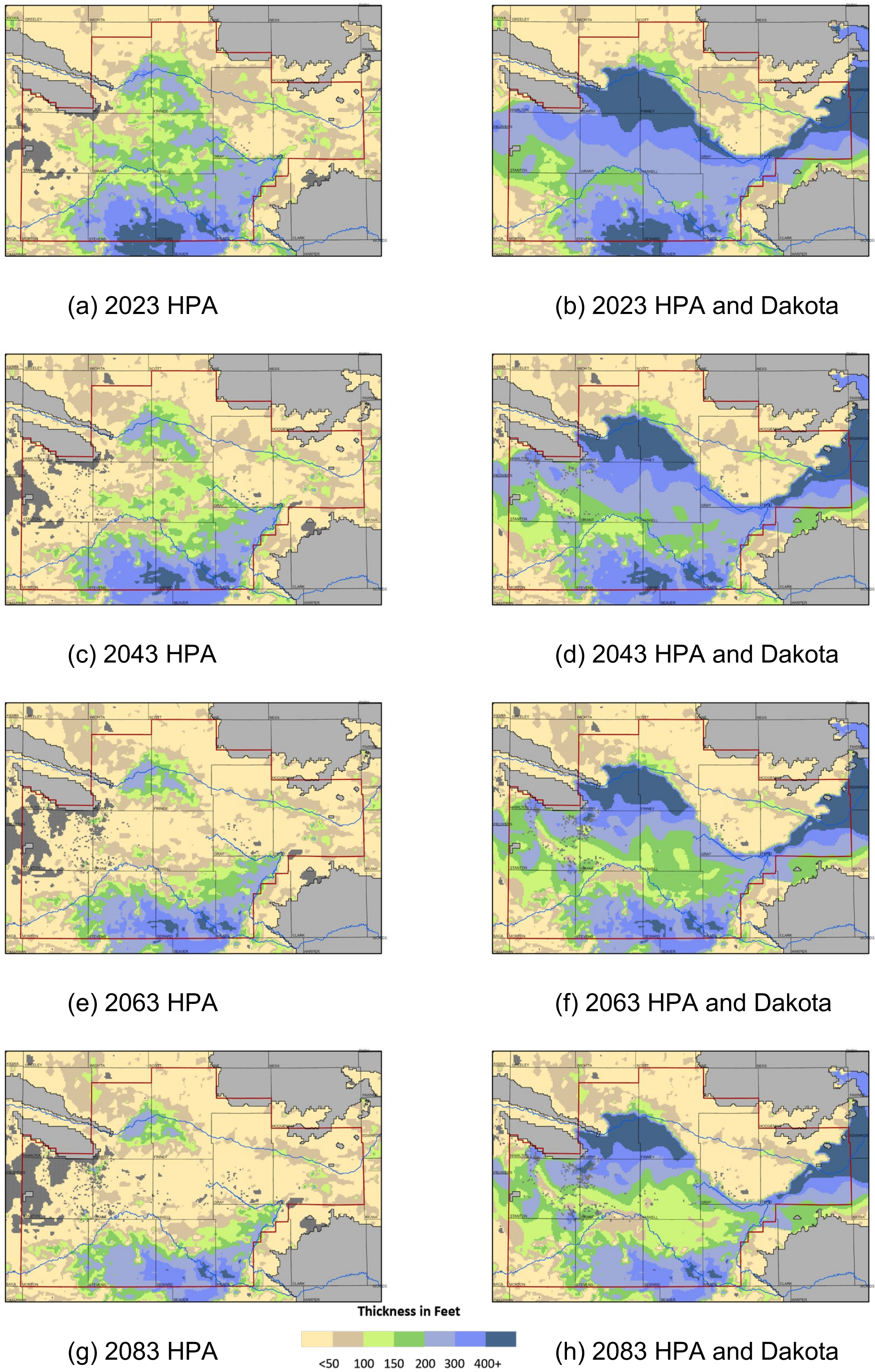

Figure 77. Simulated aquifer thickness, in feet, for the status quo scenario. The darker gray areas indicate dry cells.

The model's function by which future pumping is reduced based on lower yields from the aquifer can be used to determine the estimated usable lifetime of the aquifer (EUL). In areas of groundwater declines, the number of years until a model cell reached transmissivity values of 2,000 ft^2/day (the equivalent of a 20 ft sand layer with a hydraulic conductivity of 100 ft/d) were measured and mapped. Results were then compared to a second method published in KGS public information circular (PIC) no. 18 by Buchanan et al. (2023). The PIC's version of the EUL map is based on projecting past water-level trends into the future until the present-day aquifer thickness reaches a point where 200 gallons per minute well yields over the summer become impractical.

Figure 78 shows the different EUL maps based on the PIC and status quo scenario. The PIC version (fig. 78a) focused solely on the HPA and does not account for any contributions from the Dakota aquifer system. Areas in the southern half of Gray County and northern extents of Stanton and Stevens counties are projected to have less than 20 years until the projected water level reaches the minimum threshold. Areas of northern Haskell, Grant, and southern Finney counties are projected to have a range of 20 to 60 years. In comparison, the model's projections based on the status quo scenario, focused solely on the HPA layer (fig. 78b), show similar patterns, albeit not as large. When taking into account the unconfined portions of the Dakota aquifer system (fig. 78c), the lifetime estimates in these areas increase noticeably in response to the added storage from the underlying sandstones. Areas identified as already being at the minimum threshold are very similar between all the EUL maps, which should be expected given they all reference the same starting aquifer thickness, roughly centered on 2022.

.

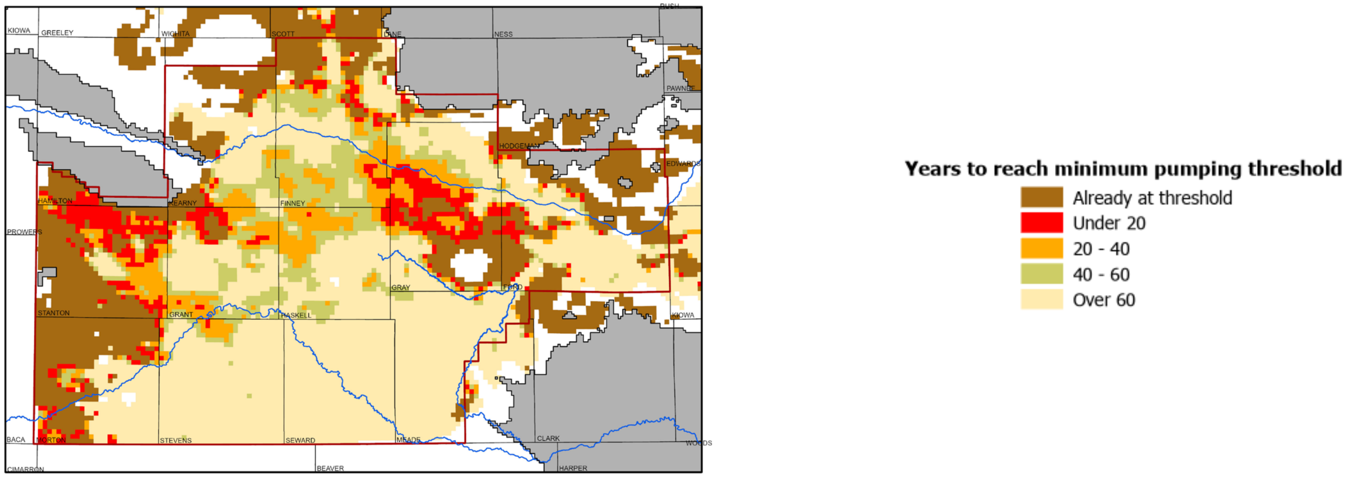

(a) KGS PIC No. 18, HPA

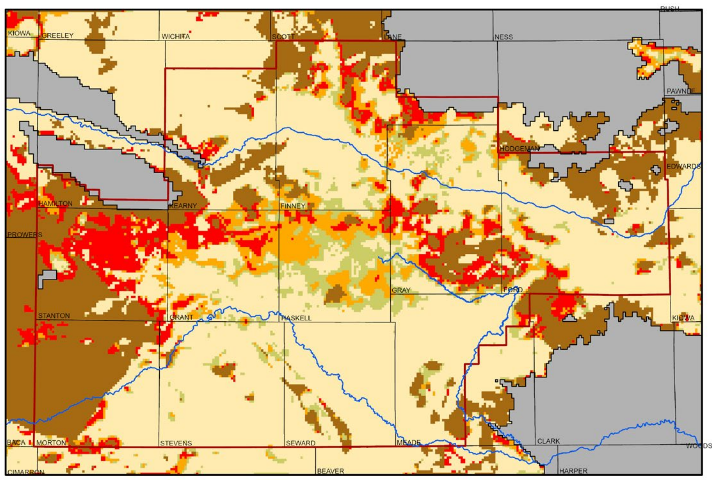

(b) Modeled 2,000 ft^2/day, HPA

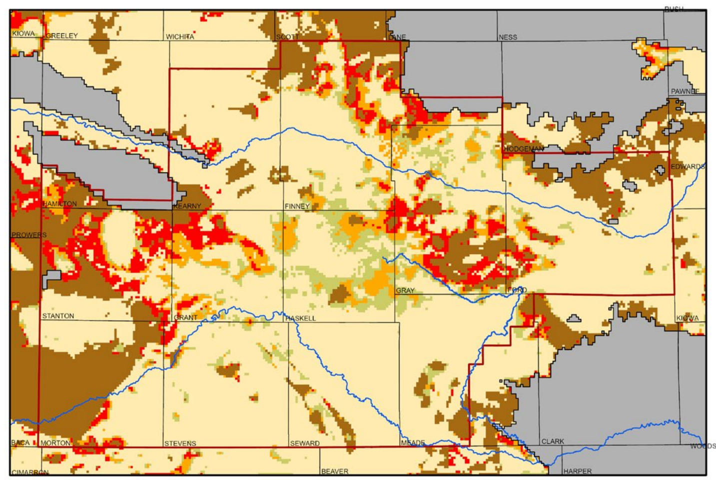

(c) Modeled 2,000 ft^2/day, HPA and Dakota

Figure 78. Comparison of estimated usable lifetime maps, KGS PIC no. 18 and status quo scenario.

Q Stable

The KGS developed a data-driven water-balance approach (Butler et al., 2016, 2018), often referred to as "Q stable," that identifies the relationship between water-level change and groundwater use to determine the reductions in pumping needed to stabilize water levels for the short term (i.e., one to two or more decades). This scenario uses Q stable values originating from GMD3's I-CARE reports, mailings sent to water right holders, which compared their historic water use to other peer wells in the area. A portion of each I-CARE mailing displayed aquifer conditions and Q stable numbers for 17 areas, each uniquely defining some element of aquifer conditions or geologic features (fig. 79). This scenario applies the Q stable percentage reduction by I-CARE region to the regressed pumping estimated in the status quo scenario. Note, this simulation is to test the model's capabilities of replicating conditions specified by the Q stable analysis and should not be interpreted as a proposed management plan.

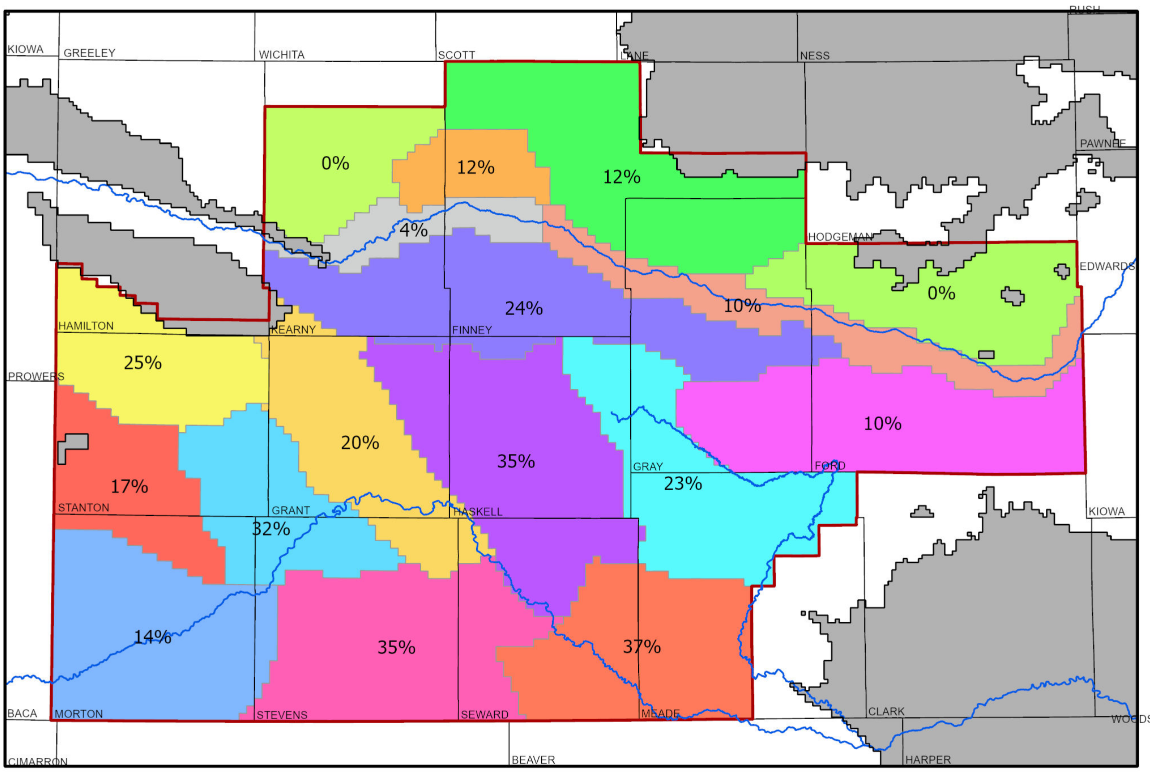

Figure 79. GMD3 I-CARE regions. The values listed within each region are the percent reduction in pumping needed to stabilize water levels based on the Q stable assessment.

Figure 80 shows the annual aquifer budget for GMD3 based on the Q stable scenario. Compared to the status quo scenario, the overall aquifer pumping is reduced; it is still projected to decline in time, but at a much slower rate. As pumping is decreased, aquifer storage depletion is slowed across the simulation. Figure 81 shows the contributions of lagged drainage and delayed surface recharge for this scenario, and fig. 82 displays the different surface recharge components. As the pumping is reduced, so are the rates of irrigation return flows. In addition, contributions from dewatered units are reduced in response to the moderated water-level declines. The total average recharge (delayed recharge from surface plus lagged drainage from dewatered units) over the Q stable scenario are projected to be 2.3 inches per year.

Figure 83 shows the simulated head changes for selected time intervals for the Q stable simulation, and fig. 84 shows the simulated thickness of the aquifer units. Early in the simulation, water levels across much of GMD3 are projected to get close to stable conditions, especially through the center of the district and in counties along the Oklahoma border, with some areas showing rises. However, declines are still projected to occur in smaller pockets, such as in southwest Gray and southeast Morton counties. Despite some areas achieving stable conditions, the average water-level changes across the whole of GMD3 over the next 10 (2023 to 2033) and 20 (2023 to 2043) years are projected to be -6.7 ft and -12.4 ft, respectively, much smaller than the projected values in the status-quo scenario (-15.4 ft and -26.8 ft). Figure 85 shows the EUL maps under this simulation. Given the reduced storage loss from the aquifer and reduced pumping rates, the EUL maps all extend the number of years until the I-CARE regions reach their various threshold amounts.

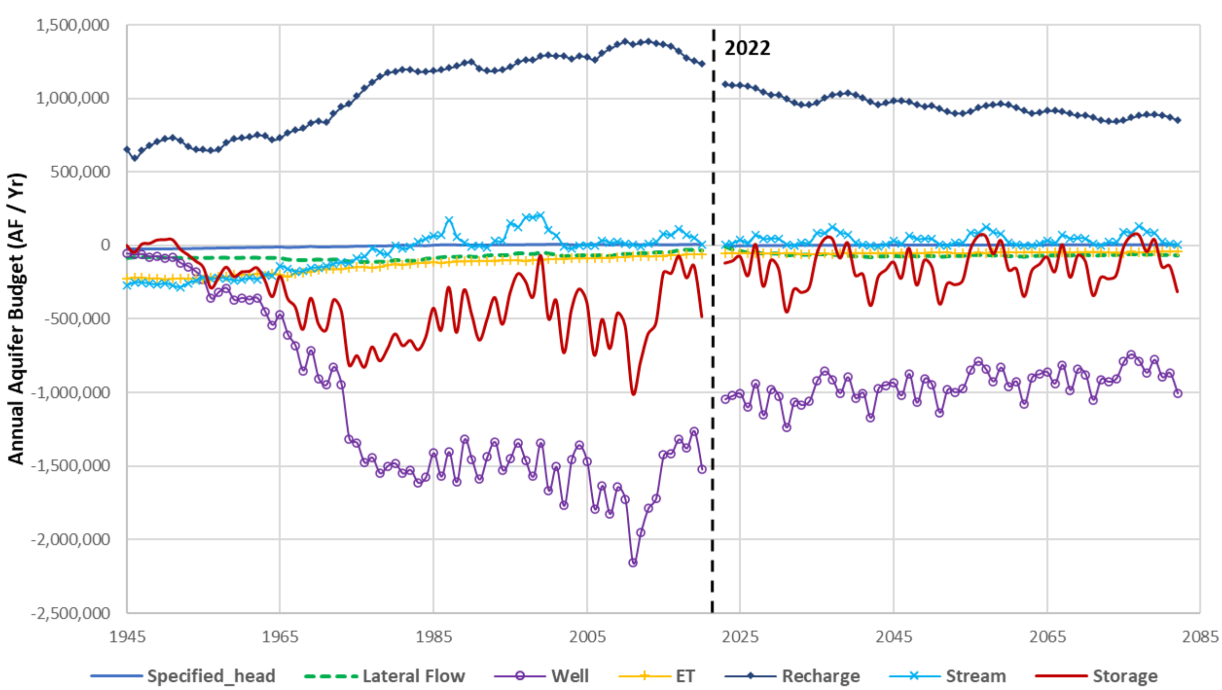

Figure 80. Annual HPA aquifer budget for GMD3 under the Q stable scenario. The calibrated historical model budget (1945 to 2021) is also plotted for comparison.

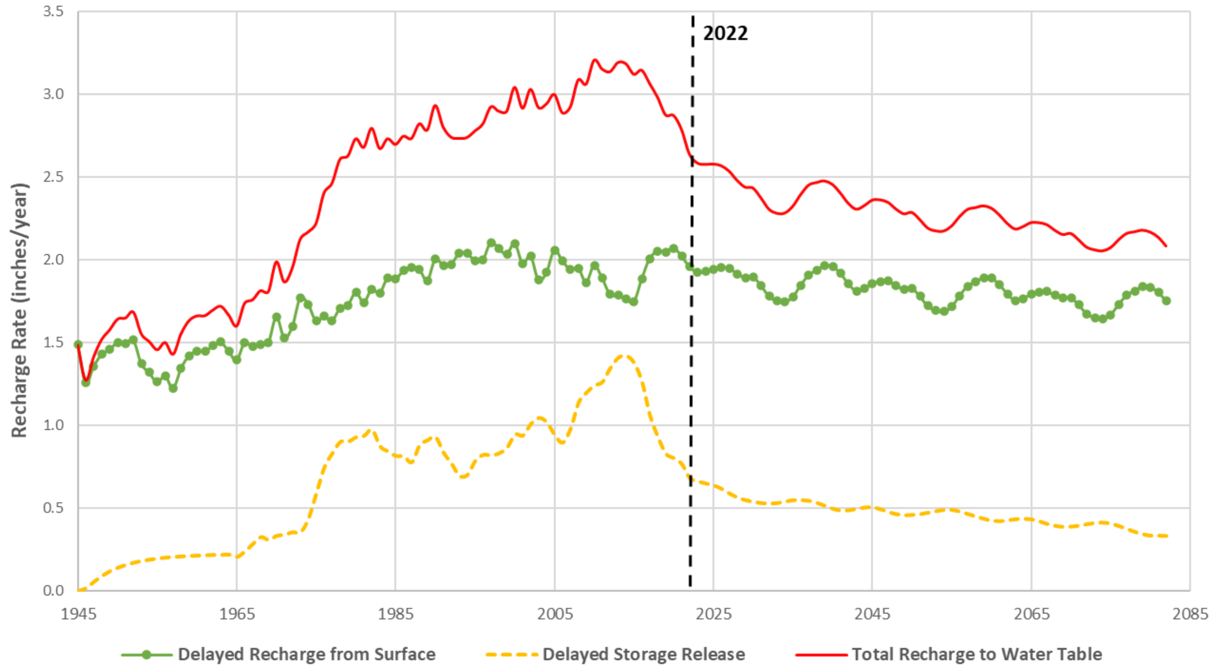

Figure 81. Water-table recharge in GMD3 under the Q stable scenario.

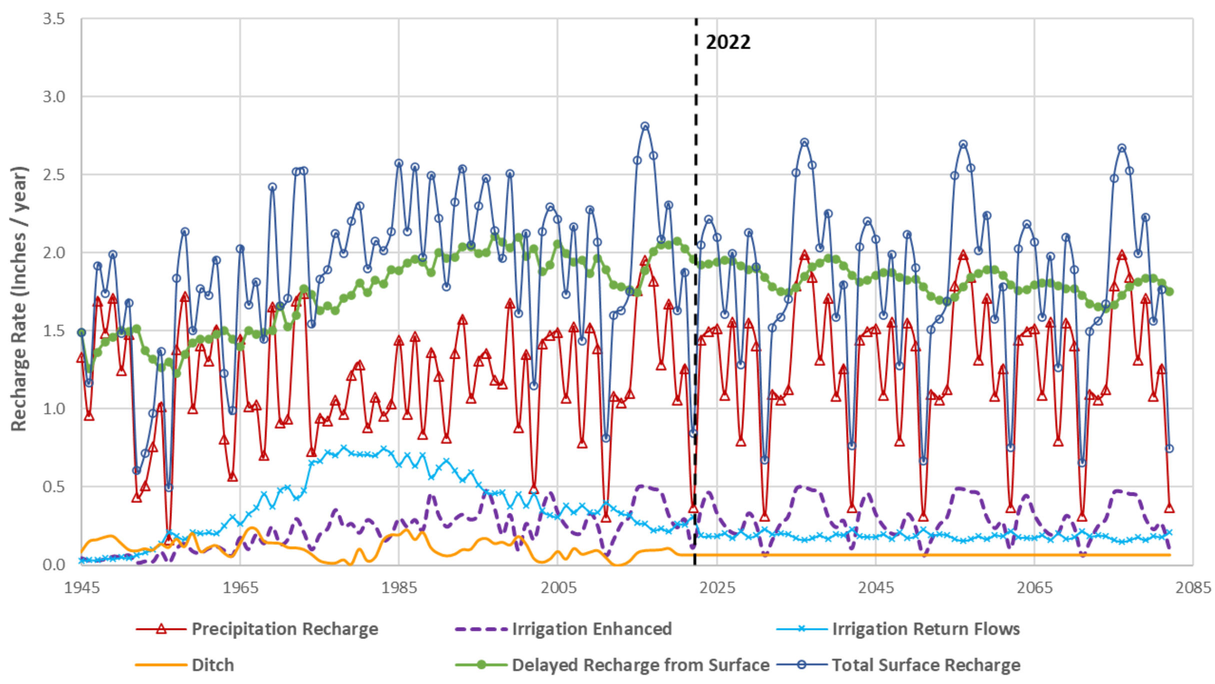

Figure 82. Different surface recharge components for GMD3 under the Q stable scenario.

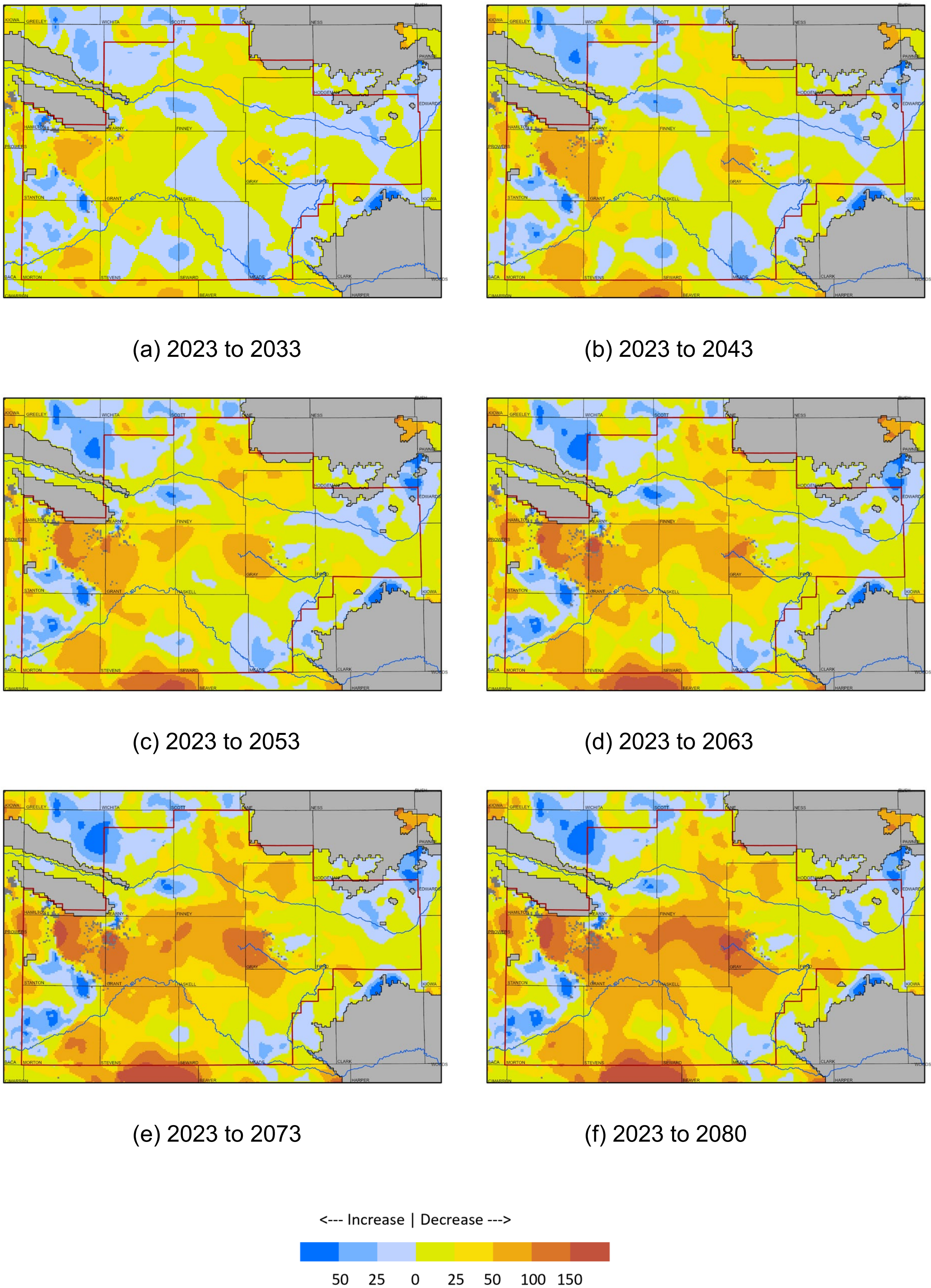

Figure 83. Simulated water-level change, in feet, for the Q stable scenario.

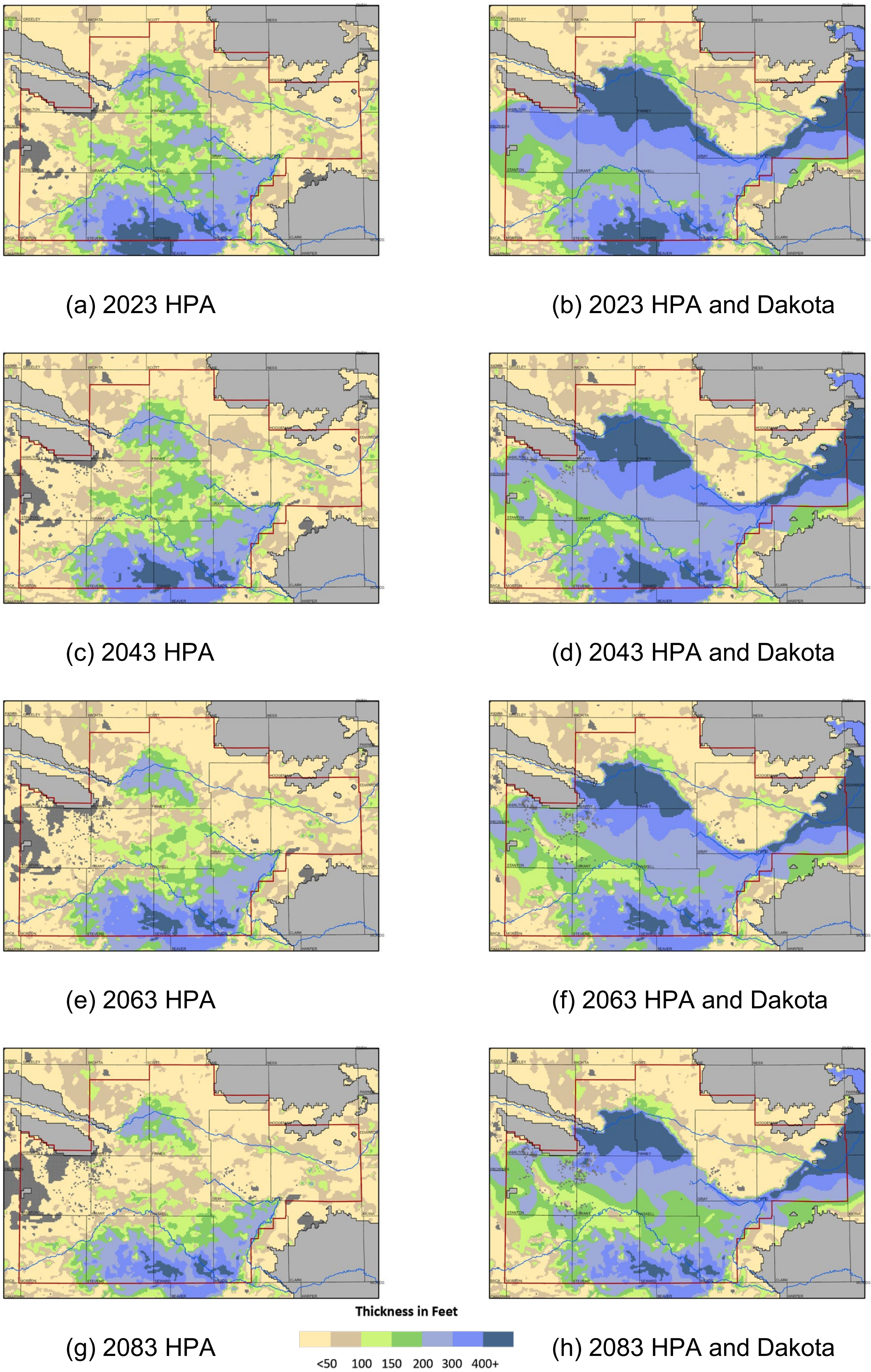

(a) 2023 HPA

(b) 2023 HPA and Dakota

(c) 2043 HPA

(d) 2043 HPA and Dakota

(e) 2063 HPA

(f) 2063 HPA and Dakota

(g) 2083 HPA

(h) 2083 HPA and Dakota

Figure 84. Simulated aquifer thickness, in feet, for the Q stable scenario.

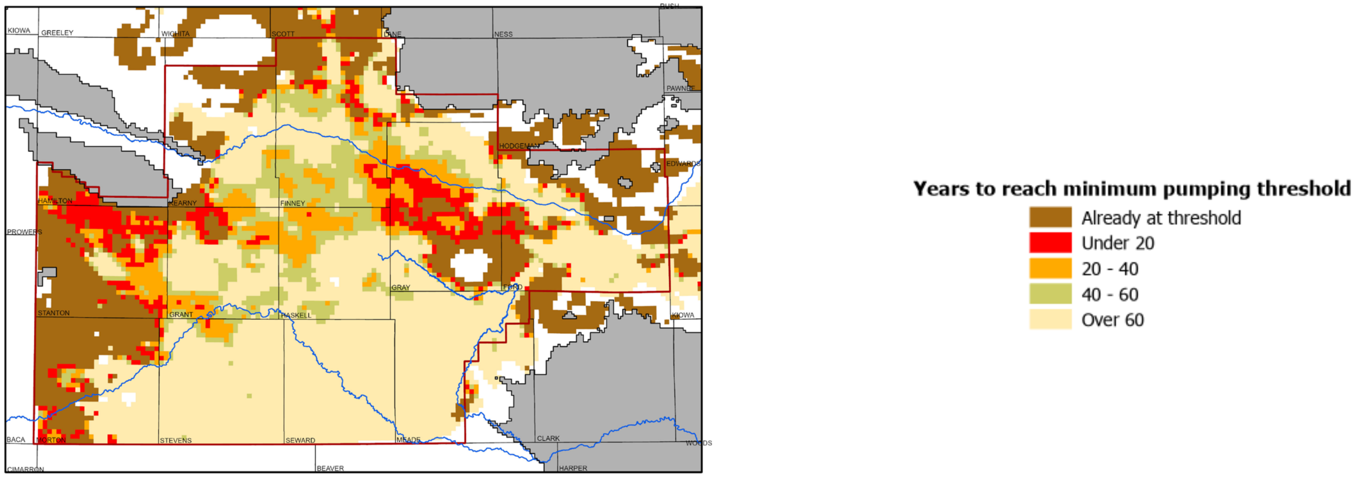

(a) KGS PIC No. 18, HPA

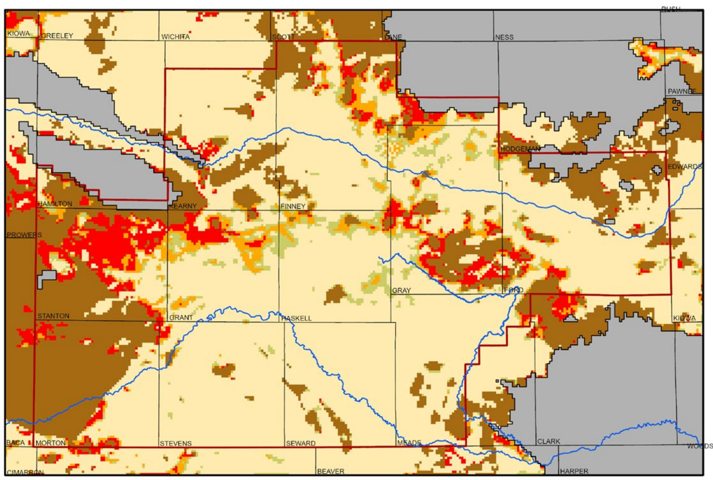

(b) Modeled 2,000 ft^2/day, HPA

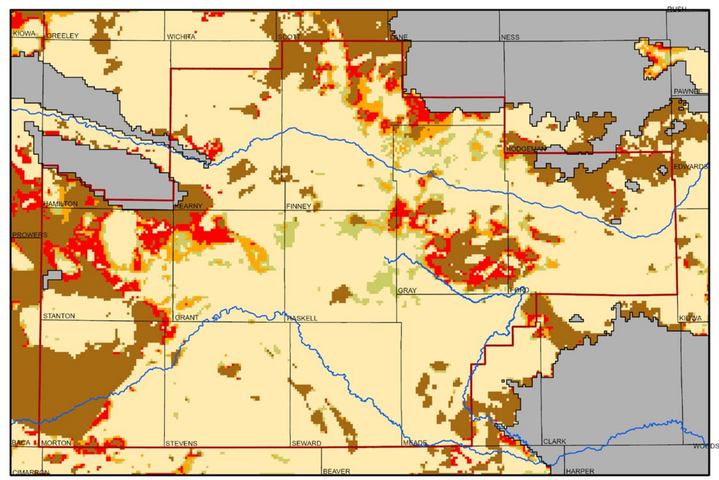

(c) Modeled 2,000 ft^2/day, HPA and Dakota

Figure 85. Comparison of estimated usable lifetime maps, KGS PIC no. 18 and Q stable scenario.

Drought of Record

The dry conditions over most of the state in the 1950s are considered the drought of record for several Kansas water management policies and programs. This scenario simulates those conditions by replacing the first 20 years of precipitation used in the status quo scenario with those from 1950 to 1969.

Figure 86 shows the annual aquifer budget for GMD3 based on the drought scenario. Compared to the status quo scenario, the overall aquifer pumping increases in the first 20 years in response to the dry conditions, which also causes aquifer storage loss to increase. Both return to similar levels and trends shown in the status quo scenario by 2053. Figure 87 shows the contributions of lagged drainage to increase in response to greater water-level declines while the overall recharge to the surface is slightly lower in the first 20 years of the simulation. This is caused by drought-induced reductions in precipitation-based recharge rates as shown in fig. 88. The total average recharge (delayed recharge from surface plus lagged drainage from dewatered units) over the drought scenario are projected to be 2.4 inches per year.

Figure 89 shows the simulated head changes for selected time intervals for the drought simulation, and fig. 90 shows the simulated thickness of the aquifer units. As would be expected, water levels are projected to decline at a slightly faster rate during the drought period but by 2063 will reflect many of the same patterns and trends as the status quo scenario. Under the drought scenario, the average water-level changes for GMD3 over the next 10 (2023 to 2033) and 20 (2023 to 2043) years are projected to be -18.6 ft and -32.1 ft, respectively. Figure 91 shows the EUL maps under this simulation.

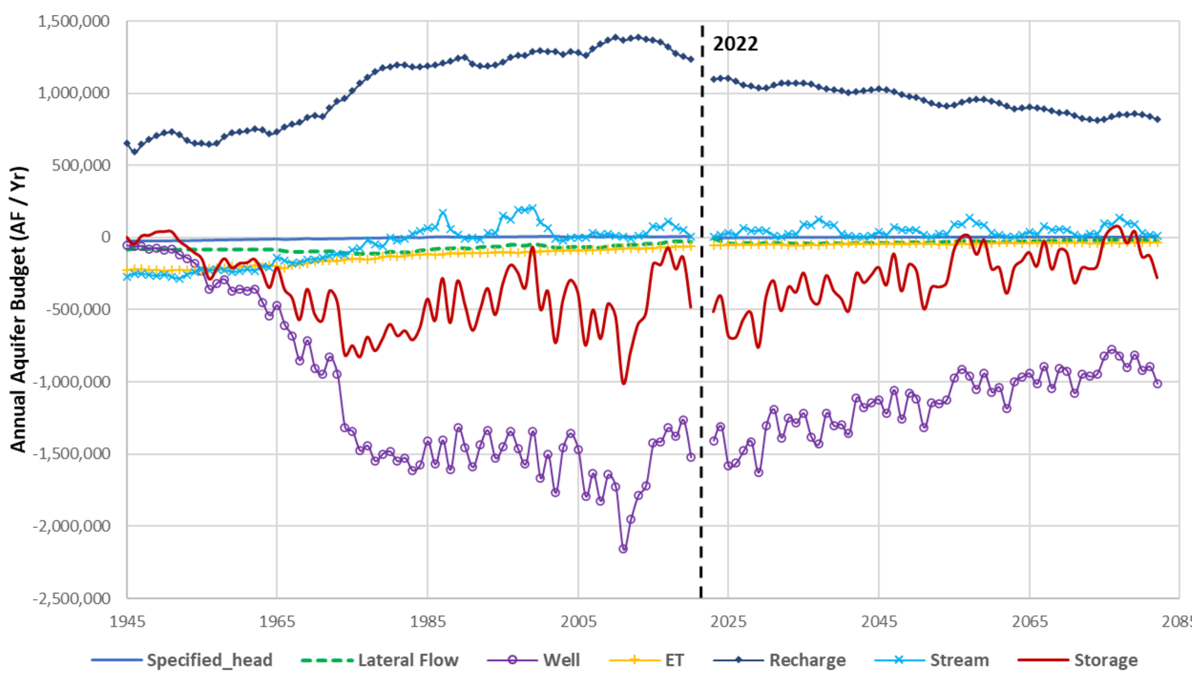

Figure 86. Annual aquifer budget for GMD3 under the drought scenario. The calibrated historical model budget (1945 to 2021) is also plotted for comparison.

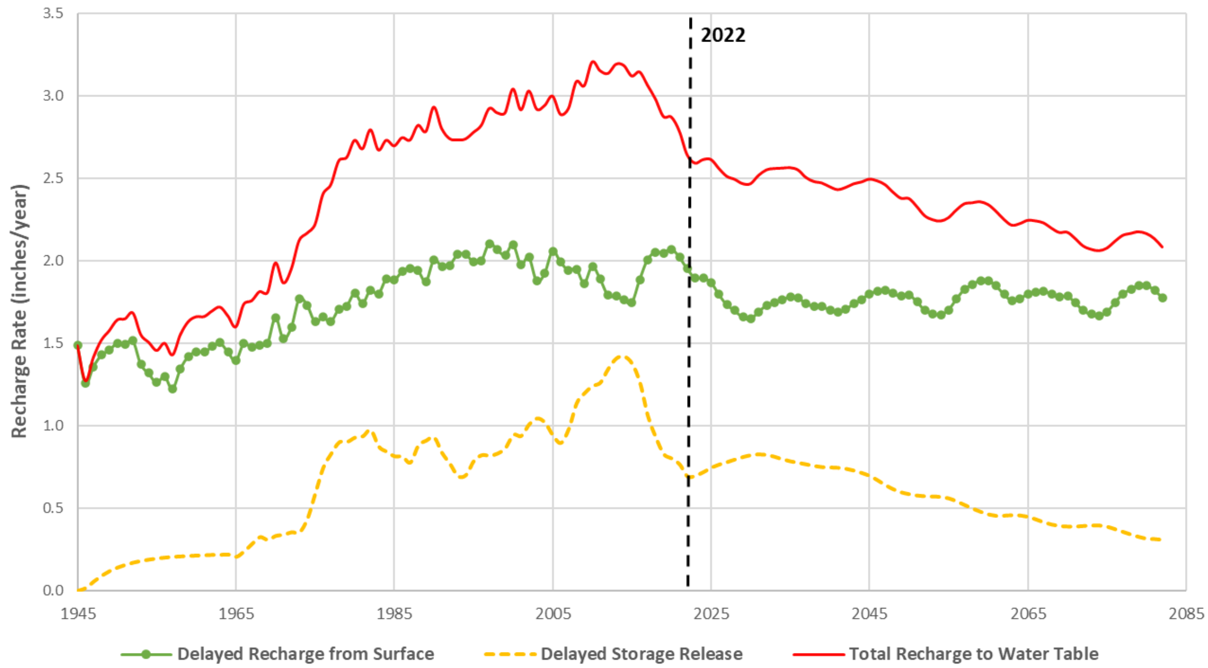

Figure 87. Water-table recharge in GMD3 under the drought scenario.

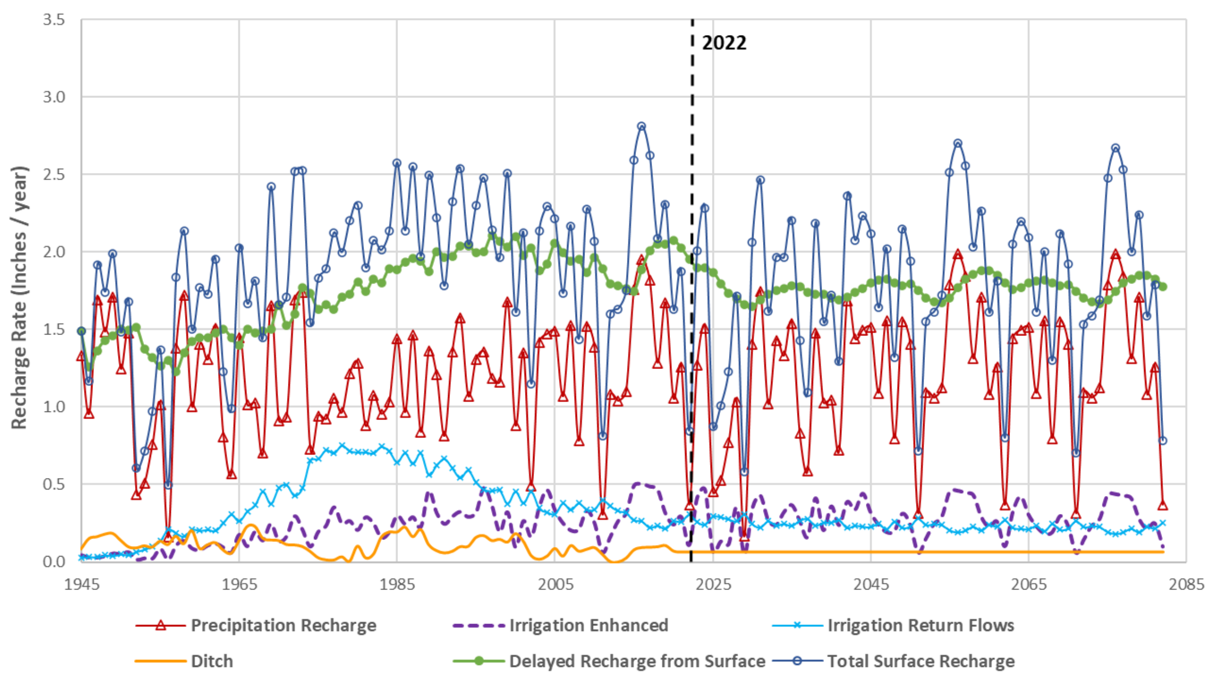

Figure 88. Different surface recharge components for GMD3 under the drought scenario.

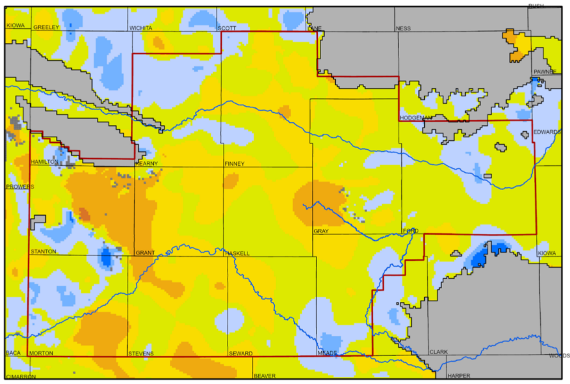

(a) 2023 to 2033

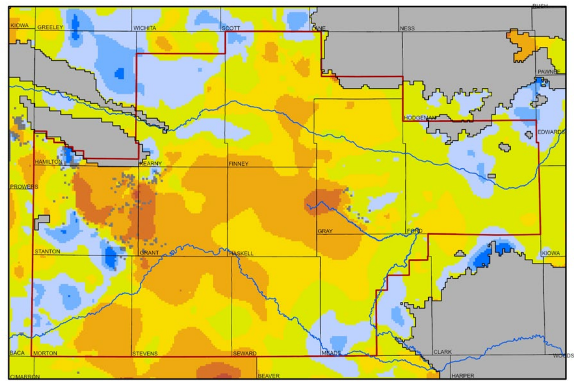

(b) 2023 to 2043

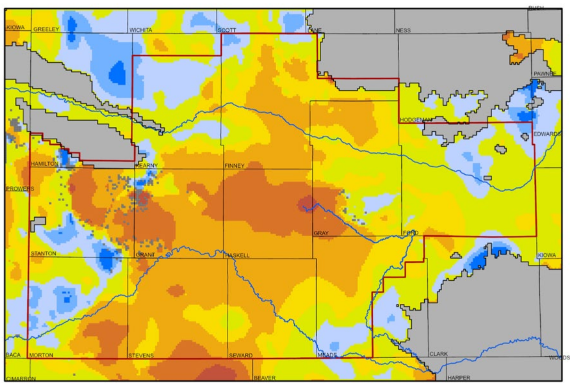

(c) 2023 to 2053

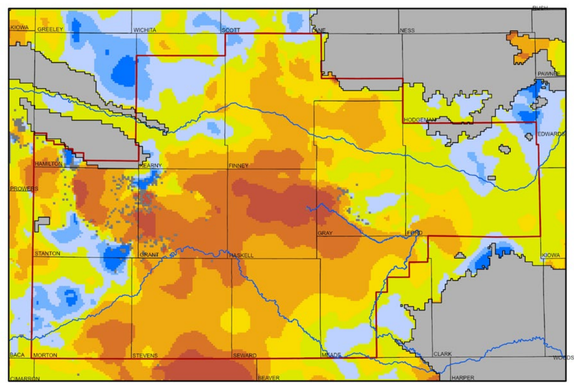

(d) 2023 to 2063

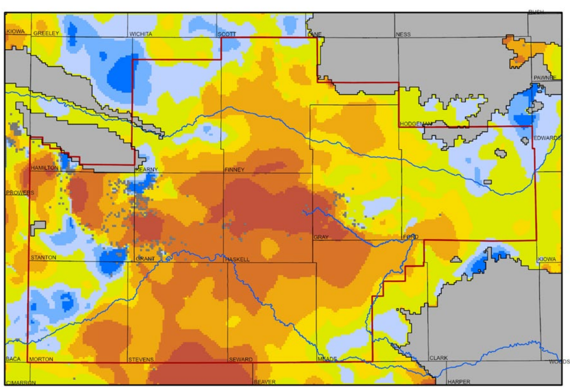

(e) 2023 to 2073

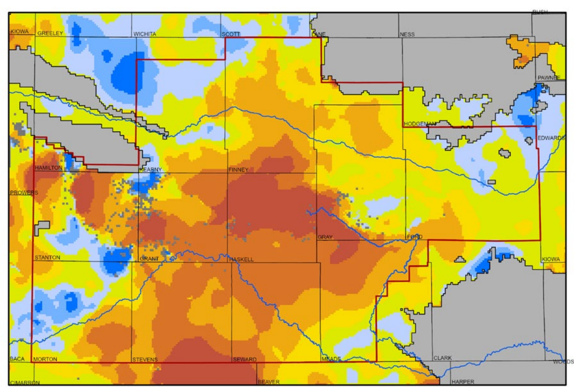

(f) 2023 to 2080

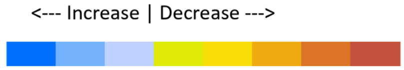

Figure 89. Simulated water-level change, in feet, for the drought scenario.

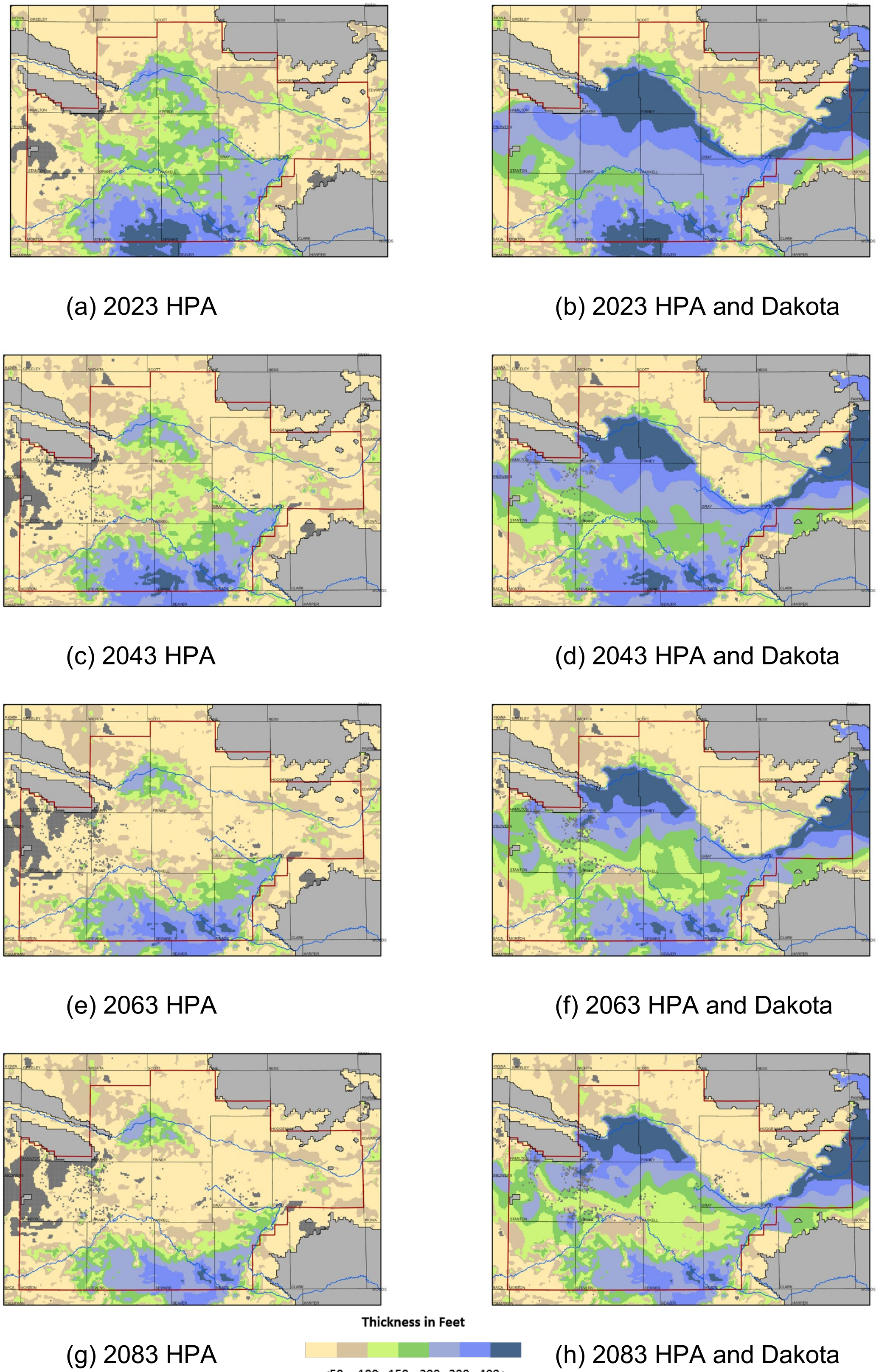

Figure 90. Simulated aquifer thickness, in feet, for the drought scenario.

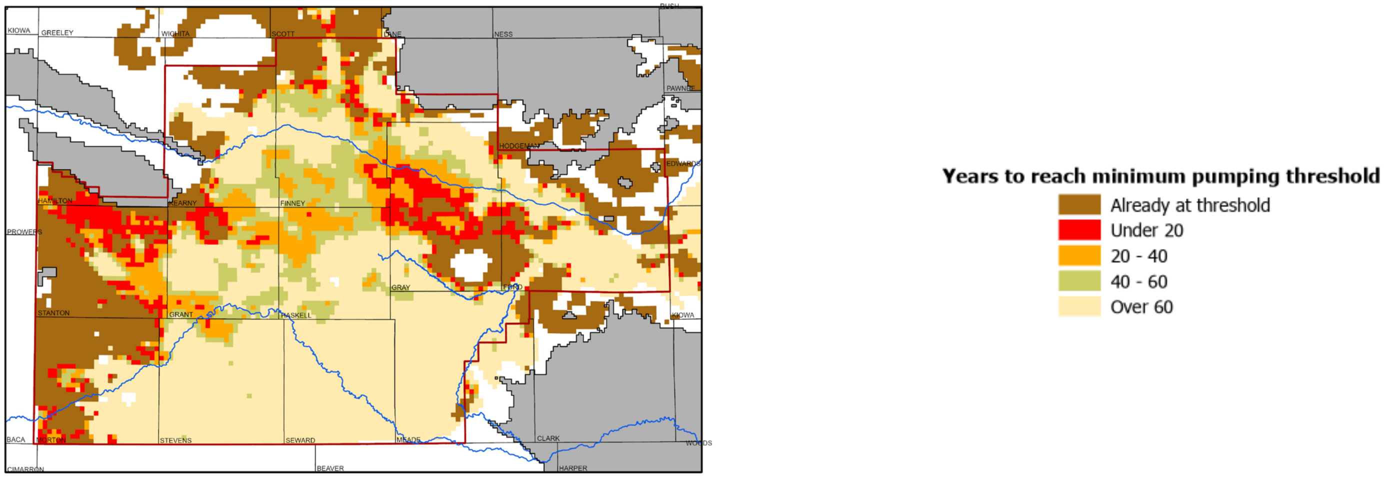

(a) KGS PIC No. 18, HPA

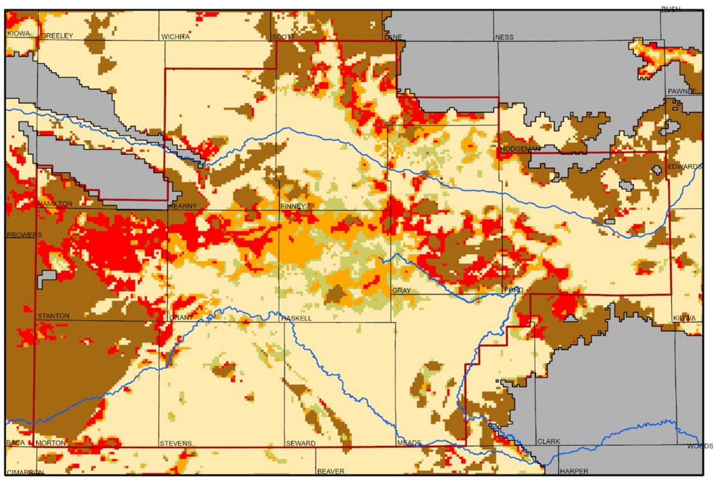

(b) Modeled 2,000 ft^2/day, HPA

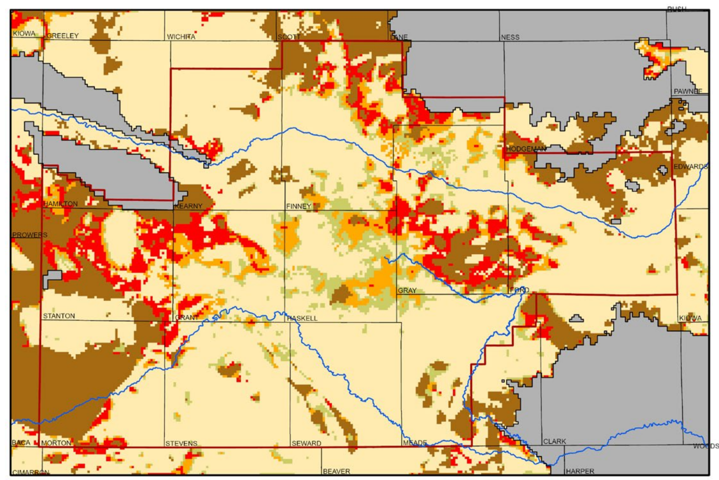

(c) Modeled 2,000 ft^2/day, HPA and Dakota

Figure 91. Comparison of estimated usable lifetime maps, KGS PIC no. 18 and drought scenario.

Comparison of All Scenarios

Figure 92 shows the annual and cumulative change in storage for GMD3 under all modeled scenarios. From the status quo scenario, the district, as a whole, is projected to consistently lose water from the aquifer going into the future. The Q stable scenario did not stabilize aquifer conditions across all of GMD3 in the first 10 years but greatly reduced storage loss. Eventually the components of the water budget adjust to the new pumping levels, and storage loss approaches rates similar to the status quo scenario. The reduced pumping starting in 2023 for the Q stable scenario greatly slows water-level declines, especially in the first two decades, which leaves more water in storage. This in turn slows the rate that future water demands are reduced due to limited water availability from the aquifer.

Storage losses are the greatest in the first 20 years of the drought scenario as the repeat of the 1950s drought stresses the system. At year 2043, both the status quo and drought scenarios use the same precipitation and pumping patterns, which causes the annual storage loss to be the same from that point forward and the accumulated change for the two scenarios mirror each other throughout the rest of their simulations. At the end of the 60-year simulation, the drought scenario produces an 8% increase in storage loss relative to the status quo run. This is an indication that the district, as a whole, can generally withstand a repeat of the 1950s drought occurring in the first 20 years, so long as precipitation returns to a more “normal” pattern going forward. However, if the frequency of severe droughts increases, the impact on the aquifer would be considerably greater.

Storage loss from both the status quo scenario and drought scenarios are much greater at the start of the simulation, but as pumping is reduced, the annual rates of loss slow and eventually mirror those in the Q stable scenario at the end of period. However, the accumulated loss of storage from the Q stable simulation is 44% and 48% less than that shown in the status quo and drought runs, respectively.

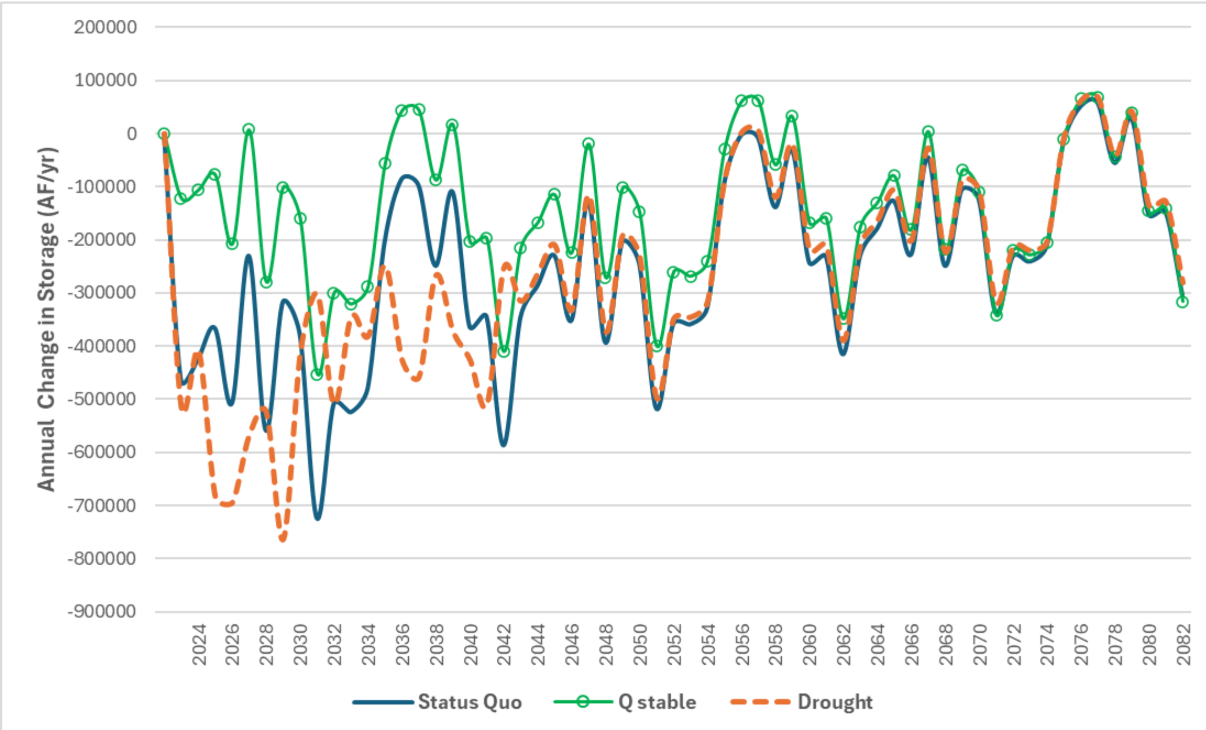

a) Annual

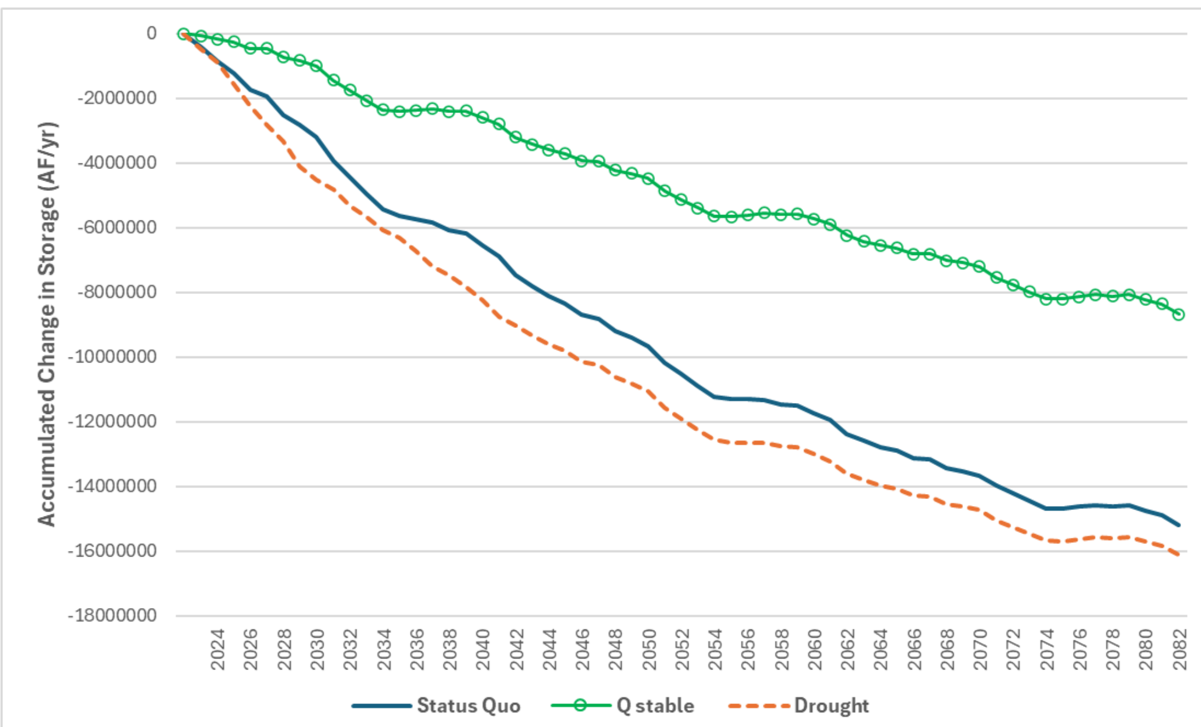

b) Accumulated

Figure 92. Change in GMD3 aquifer storage for the future scenarios.

Acknowledgments

The KGS modeling team acknowledges the funding support of the Kansas Water Office (and the State Water Plan Fund) and Southwest Kansas GMD3 for this project. The authors thank Josh Olson of the KWO and Mark Rude of GMD3, who served as the primary contacts. In addition, we thank the GMD3 board members, who helped review the model's development. We also acknowledge KGS staff who contributed to this report. John Woods spent a substantial amount of time identifying stream elevations along the selected stream courses used in the project. We also thank Julie Tollefson, KGS editor, who reviewed the final report.

REFERENCES

Becker, M. F., 1999, Digital map of predevelopment water levels for the High Plains aquifer in parts of Colorado, Kansas, Nebraska, New Mexico, Oklahoma, South Dakota, Texas, and Wyoming: U.S. Geological Survey, Open-File Report 99-264.

Bohling, G. G., 2016, User's Guide to Hydra_translate.xlsm: An Excel Workbook for Quantification of Water Well Driller's Logs. Kansas Geological Survey, Open-File Report 2016-30, 26p.

Bohling, G. G., B.B. Wilson, and D. Adkins-Heljeson, 2020, Explanation of Quantitatively Interpreted Logs in the Kansas Geological Survey's WWC5 Database, Open-File Report 2020-13, 14p.

Buchanan R. C., Wilson, B. B., and Butler, J. J., Jr., 2023, The High Plains Aquifer: Kansas Geological Survey Public Information Circular 18 (revised Jan. 2023). https://kgs.ku.edu/high-plains-aquifer

Butler, J. J., Jr., Bohling, G. C., Perkins, S.P., Whittemore, D. O., and Wilson, B. B., 2023, Net inflow: An important target on the path to aquifer sustainability: Groundwater, v. 61, no. 1, doi: 10.1111/gwat.13233.

Butler, J. J., Jr., Bohling, G. C., Whittemore, D. O., and Wilson, B. B., 2020, A roadblock on the path to aquifer sustainability: Underestimating the impact of pumping reductions: Environmental Research Letters, v. 15, 014003, doi:10.1088/1748-9326/ab6002.

Butler, J. J., Jr., Whittemore, D. O., Wilson, B. B., and Bohling, G. C., 2016, A new approach for assessing the future of aquifers supporting irrigated agriculture: Geophysical Research Letters, v. 43, no. 5, p. 2,004–2,010.

Butler, J. J., Jr., Whittemore, D. O., Wilson, B. B., and Bohling, G. C., 2018, Sustainability of aquifers supporting irrigated agriculture: A case study of the High Plains aquifer in Kansas: Water International, v. 43, no. 6, p. 815–828.

Byrne, F. E., and McLaughlin, T. G., 1948, Geology and ground-water resources of Seward County Kansas: Kansas Geological Survey Bulletin, no. 69, 140 p.

Doherty, J., 2004, PEST—Model-Independent Parameter Estimation. User Manual, 5th Edition. Watermark Numerical Computing, 333 p.

Frye, J. C., with analyses by Hess, R. H., and Homes, E. O., 1942, Geology and ground-water resources of Meade County, Kansas: Kansas Geological Survey Bulletin, no. 45, 152 p.

Harbaugh, A. W., Banta, E. R., Hill, M. C., and McDonald, M. G., 2000, MODFLOW-2000, the U.S. Geological Survey modular ground-water model—User guide to modularization concepts and the Ground-Water Flow Process: U.S. Geological Survey, Open-File Report 00-92, 121 p.

Homer, C.H., Fry, J.A., and Barnes C.A., 2012, The National Land Cover Database, U.S. Geological Survey Fact Sheet 2012-3020, 4 p.

Latta, B. F., 1941, Geology and ground-water resources of Stanton County, Kansas: Kansas Geological Survey Bulletin, no. 37, 119 p.

Latta, B. F., with analyses by Holmes, E. O., 1944, Geology and ground-water resources of Finney and Gray counties, Kansas: Kansas Geological Survey Bulletin, no. 55, 272 p.

Liu, G., Wilson, B. B., Bohling, G. C., Whittemore, D. O., and Butler, J. J., Jr., 2021, Estimation of Specific Yield for Regional Groundwater Models: Pitfalls, Ramifications, and a Promising Path Forward: Water Resources Research, 14 p., https://doi.org/10.1029/2021WR030761.

Liu, G., Wilson, B. B., Whittemore, D. O., Wei Jin, W., and Butler, J. J., Jr., 2010, Ground-water model for Southwest Kansas Groundwater Management District No. 3: Kansas Geological Survey, Open-File Report 2010-18, 106 p.

Ludvigson, G. A., Sawin, R. S., Franseen, E. K., Watney, W. L., West, R. R., and Smith, J. J, 2009, A review of the stratigraphy of the Ogallala Formation and revision of Neogene ("Tertiary") nomenclature in Kansas; *in*, Current Research in Earth Sciences: Kansas Geological Survey, Bulletin 256, part 2.

Macfarlane, P. A., Jayatillake, H., and Yoder, S., 1995, Bottom configuration of the Dakota aquifer: Large regional maps of the Dakota aquifer: Kansas Geological Survey, https://www.kgs.ku.edu/Dakota/vol3/bigmaps/index.htm.

Macfarlane, P. A., and Wilson, B. B., 2006, Enhancement of the bedrock-surface map beneath the Ogallala portion of the High Plains aquifer, western Kansas: Kansas Geological Survey, Technical Series Report 20, 28 p.

McLaughlin, T. G., with analyses by Hess, R. H., 1942, Geology and ground-water resources of Morton County, Kansas: Kansas Geological Survey Bulletin, no. 40, 126 p.

McLaughlin, T. G., with analyses by Holmes, E. O., 1943, Geology and ground-water resources of Hamilton and Kearny counties, Kansas: Kansas Geological Survey Bulletin, no. 49, 220 p.

McLaughlin, T. G., with analyses by Stoltenberg, H. A., 1946, Geology and ground-water resources of Grant, Haskell, and Stevens counties, Kansas: Kansas Geological Survey Bulletin, no. 61, 221 p.

Peterson, D., 2018, Kansas Land Cover Patterns Phase II: Final Report. Kansas Biological Survey Technical Report.

Prudic, D.E., Konikow, L.F., Banta, E.R., 2004, A New Streamflow-Routing (SFR1) Package to Simulate Stream-Aquifer Interaction with MODLFOW-2000; U.S. Geological Survey, Open-File Report 2004-1042, 104 p.

Waite, H. A., with analyses by Herbert, A. W., 1942, Geology and ground-water resources of Ford County, Kansas: Kansas Geological Survey Bulletin, no. 43, 250 p.

Whittemore, D. O., Butler, J. J., Jr., and Wilson, B. B., 2016, Assessing the major drivers of water-level declines: New insights into the future of heavily stressed aquifers: Hydrological Sciences Journal, v. 61, no. 1, p. 134–145.

Whittemore, D. O., Butler, J. J., Jr., and Wilson, B. B., 2023, Status of the High Plains aquifer in Kansas: Kansas Geological Survey, Technical Series 25, 22 p.

Whittemore, D. O., Grieve, E. R., Young, D. P., and Wilson, B. B., 2005, Water quality in the High Plains aquifer and the Cimarron River in Seward and Meade counties, KS: Kansas Geological Survey, Open-File Report 2005-27, 36 p.

Whittemore, D. O., Macfarlane, P. A., and Wilson, B. B., 2014, Water resources of the Dakota aquifer in Kansas: Kansas Geological Survey, Bulletin 260, 68 p.

Whittemore, D. O., Seybold, E. E., Wilson, B. B., Woods, J. J., and Butler, J. J., Jr., 2023, Assessment of groundwater mineralization in the Upper Arkansas River Corridor: Kansas Geological Survey, Open-File Report 2023-21, 56 p.

Wilson, B. B., Ahring, T., and Dick S., 2023, Southwest Kansas GMD3 I-CARE Project: ArcGIS Story Map, https://storymaps.arcgis.com/stories/f422d10893f8419395f0f095c11219e3

Wilson, B. B., and Bohling, G. C., 2003, Assessment of reported water use and total annual precipitation, state of Kansas: Kansas Geological Survey, Open-File Report 2003-55C, 39 p.

Wilson, B. B., Liu, G., Bohling, G. C., Whittemore, D. O., and Butler, J. J., Jr., 2015, West Central Kansas GMD1 Model: Kansas Geological Survey, Open-File Report 2015-33, 137 p.

Wilson, B. B., Liu, G., Whittemore, D. O., Butler, J. J., 2008, Smoky Hill River ground-water model: Kansas Geological Survey, Open-File Report 2008-20, 99 p

Wilson, B. B., Liu, G., Bohling, G. C., Whittemore, D. O., and Butler, J. J., Jr., 2020, GMD2 Groundwater Flow Model: Kansas Geological Survey, Open-File Report 2020-1, 93 p.

Wilson, B. B., Liu, G., Bohling, G. C., and Butler, J. J., Jr., 2021, GMD4 Groundwater Flow Model: Kansas Geological Survey, Open-File Report 2021-6, 106 p.